EXPERIMENTAL STUDY OF MASONRY-INFILLED STEEL FRAMES
SUBJECTED TO COMBINED AXIAL AND IN-PLANE LATERAL LOADING

by

Pouria Behnam Manesh

Submitted in partial fulfilment of the requirements
for the degree of Master of Applied Science

at

Dalhousie University
Halifax, Nova Scotia
October 2013

TABLE OF CONTENTS

LIST OF TABLES

LIST OF FIGURES

ABSTRACT

An experimental program was conducted to investigate some aspects of in-plane behaviour of masonry infilled steel frames. Eight concrete masonry infilled steel frames, consisting of three fully grouted and five partially grouted infills, were tested under combined lateral and axial loading. All specimens were constructed using one-third scale concrete masonry units. The in-plane lateral load was gradually increased at the frame top beam level until the failure of the specimen while an axial load was applied to the top beam and held constant. The parameters of the study included axial load, extent of grouting, opening, and aspect ratio of the infill. The experimental results were used, along with other test results from the literature, to evaluate the efficacy of stiffness and strength predictions by some theoretical methods with a focus on Canadian and American design codes. Cracking pattern, stiffness, failure mode, crack strength, and ultimate strength of the specimens were monitored and reported.

Presence of axial load was found to increase the ultimate strength of the infilled frame but had no marked effect on its stiffness. Two specimens exhibited "splitting failure" due to axial load. Partially grouted specimens developed extensive diagonal cracking prior to failure whereas fully grouted specimens showed little or no cracking prior to failure. An increase in grouting increased the ultimate strength of the frame system but reduced its ductility. Presence of opening reduced the ultimate strength of the infilled frame and increased its ductility but its effect on the stiffness of the frame system was not significant. A review of current Canadian and American design codes showed that the Canadian code significantly overestimates the stiffness of infilled frames whereas the American code provides improved predictions for stiffness of these frame systems. Both design codes underestimate the strength of masonry infilled steel frames but grossly overestimate the strength of masonry infilled RC frames.

LIST OF ABBREVIATIONS AND SYMBOLS USED

Symbols

A_d	Area of the diagonal strut
E_f	Modulus of elasticity of frame
E_m	Modulus of elasticity of masonry
f'_m	Compressive strength of masonry
h	Height of infill
h'	Height of frame
H_I	Nominal strength of infill
I_b	Second moment of area of beam
I_c	Second moment of area of column
k	Stiffness
l	Length of infill
L_d	Diagonal length
M_d	Dry mass
M_i	Initial mass
M_{pb}	Plastic moment capacity of beam
M_{pc}	Plastic moment capacity of column
M_{pj}	Plastic moment capacity of the joint
M_s	Saturated mass
P_{fc}	Cracking strength of infilled frame
P_{ult}	Ultimate strength of infilled frame
R'_c	Nominal diagonal load on infill
t	Thickness of infill
t_e	Effective thickness of infill
w	Width of the diagonal strut
α_b, α_l	Contact length between the beam and the infill
α_c, α_h	Contact length between the column and the infill
γ_{xy}	Shear strain
ε_1	Maximum principal strain
ε_x	Normal strain in the x-direction
ε_y	Normal Strain in the y-direction
θ	Angle of diagonal and horizontal
λ	Characteristic of the system
ω_n	Natural frequency of the structure

Abbreviations

ASTM	American Society for Testing and Materials
CMU	Concrete Masonry Unit
CSA	Canadian Standards Association
FG	Fully Grouted

LVDT	Linear Variable Differential Transformer
MISF	Masonry-Infilled Steel Frame
MSJC	Masonry Society Joint Committee
NBCC	National Building Code of Canada
PG	Partially Grouted
RC	Reinforced Concrete
SCT	Structural Clay Tile

ACKNOWLEDGEMENTS

First and foremost, I would like to thank Dr. Yi Liu for her guidance and her valuable advice throughout the project. I am very grateful for her support in carrying out the research program and preparation of this thesis.

I would like to express my gratitude to Dr. John Newhook and Dr. Gordon Fenton for reviewing this thesis.

The complex experimental program would not have been possible to carry out without the help of departmental technicians Mr. Brian Kennedy, Mr. Brian Liekens, Mr. Blair Nickerson, and the mason Mr. Gerry Hubley. I am grateful to them for their assistance.

Lastly, I would like to thank my parents for their never-ending support and encouragement.

CHAPTER 1   INTRODUCTION

1.1 BACKGROUND

Masonry is one of the oldest building materials and has been popular for thousands of years. Ancient civilizations chose masonry for its durability and aesthetic reasons. In addition, fire and heat resistance, price, and versatility make masonry, to this day, an appealing building material. Despite the rich history of masonry construction, analytical techniques and rational design methods developed much later for masonry structures compared to more modern construction materials. The application of structural engineering principle to the design of masonry structures since the second half of the 20th century has, once again, made masonry a competitive construction material.

Masonry walls are commonly used as interior partitions as well as exterior walls infilled in either steel or reinforced concrete (RC) frames in building construction. Masonry infilled frames are inexpensive and easy to construct. In the past, infills were identified as a contributing factor to structural failures in earthquakes. Frame-infill interaction can induce brittle failure in RC frames by creating the short column effect. They can also create a soft-storey ground floor by over-strengthening the upper floors in a multi-storey building. However, there is strong evidence that infilled frames can improve seismic behaviour of a frame system if properly designed (Dawe & Seah 1989, Shing & Mehrabi 2002, and Tucker 2007).

Due to a lack of universally accepted design guidelines in assessing the extent of composite action between infill and frame, the infill is often treated as a non-structural element and the surrounding frame is designed as the principal load-carrying element. The contribution of the masonry infill wall to lateral resistance of the frame system is essentially ignored. However, ignoring the interaction between the infill and the surrounding frame does not necessarily result in a safe design, and in fact may have a detrimental effect to the frame and ultimately to the structure (Drysdale & Hamid, 2005). Infill walls significantly stiffen the frame system while reducing overall ductility.

1

Increased stiffness caused by the infill wall attracts larger forces to the frame system and the frame has to be designed in recognition of this effect.

A review of the literature shows that experimental and theoretical research on in-plane lateral behaviour of masonry infilled frames has continually increased in the past 60 years. Despite the effort, uncertainties remain in assessing the behaviour of these frame systems due to their complexity. Numerous factors such as material properties, type of loading, dimensions, infill openings, infill and frame properties, gaps between the frame and the infill, and construction details contribute to this complex behaviour.

Most of the research available in the literature has focused on masonry infilled frames subjected to lateral loading only. As a result, the current design methods specified in the various standards deal only with the infill capacity under lateral load. This research investigates a scenario where the frame systems are subjected to a combination of lateral and axial loading. This is a common occurrence in practice where the frame is used to support gravity loads. Furthermore, most of the research in the literature is on frames with infills constructed using hollow concrete masonry units (CMUs). This study investigates the effects and merits of grouting by comparative examination of partially grouted (PG) and fully grouted (FG) masonry infills. Additionally, infill opening and aspect ratio are studied in this research.

1.2 CONSTRUCTION OF MASONRY INFILLED FRAMES

The most common method of construction of masonry infilled frames is to, first, build the bounding frame (steel or RC) and, later, build the masonry wall which infills the frame. This is a relatively convenient method of construction as it provides a supporting system for the masonry wall during construction. The other alternative which is used with RC frames is to build and cure the masonry wall before casting the beam and the columns to form a RC frame. Although the second method provides for a better fit of the infill into the frame, it is more difficult to carry out as it requires a temporary support system for the

infill during construction. In this research, the steel bounding frame will be fabricated first and the infill will be built inside the frame to minimize the potential gap issues.

1.3 OBJECTIVES AND SCOPE OF THE RESEARCH

This research is focused on obtaining experimental results on infilled frames subjected to combined axial and lateral loading and using the test results to assess the efficacy of current theoretical methods, especially the current design codes in design of infills. The theoretical methods are evaluated based on their ability to predict the stiffness and strength of masonry infilled frames. The emphasis is also given to the behaviour of concrete masonry infilled steel frames using a parametric study. The objectives of this research can be summarized as follows.

    a. To conduct an extensive literature review on the relevant research in the area of masonry infilled frames

    b. To carry out an experimental program examining the effects of axial load

    c. To evaluate the efficacy of current theoretical methods focusing on Canadian and American design standards

    d. To discuss possible adjustments to design equations as appropriate.

1.4 OUTLINE OF THE RESEARCH

This research includes a review of available literature, laboratory testing of 8 concrete masonry infilled steel frames, and comparison and evaluation of theoretical methods and design standards regarding stiffness and strength of masonry infilled frames.

Literature review is presented in Chapter 2. Chapter 3 includes a detailed description of the experimental program designed to investigate the behaviour of masonry infilled steel

frames using one-third scale CMUs. The experimental results and the parametric study are presented and discussed in Chapter 4.

Chapter 5 presents the comparison and evaluation of some of the theoretical methods focusing on the Canadian Standard for Design of Masonry Structures CSA S304.1 (2004), and Building Code Requirements and Specification for Masonry Structures MSJC (2011). The merits and limitations of the aforementioned methods are also discussed in Chapter 5. Finally, Chapter 6 presents a summary and conclusion.

CHAPTER 2   LITERATURE REVIEW

2.1 BACKGROUND

Most of the research in the literature has focused on the behaviour of infilled frames subjected to lateral loading only. The following literature survey contains information on analytical and experimental studies as well as practice codes and guidelines.

2.2 ANALYTICAL STUDIES

Polyakov (1960) and Holmes (1961) were among the first who proposed the diagonal strut concept for the analysis of infilled frames. The former observed that applying a lateral load causes the separation of the infill and the frame over a significant length on each side leaving a limited contact area at the compression corners. The latter suggested that the geometry of the diagonal strut is a function of dimensions and physical properties of the infill. It has the same thickness and modulus of elasticity as the infill and the width of the diagonal strut can be taken as one-third of the diagonal length.

Stafford-Smith & Carter (1969) were the first to develop a theoretical framework to calculate the width of the equivalent diagonal strut based on earlier studies by Stafford-Smith (1967) and Stafford-Smith (1968). This method is the foundation work for the provisions of the Canadian standard for design of masonry structures, CSA S304.1 (2004). They suggested that the diagonal stiffness of an infill is not only a function of its dimensions and physical properties but also depends on the length of contact between the frame and the infill which can be approximated by Equation [2.1].

$$\frac{\alpha}{h'} = \frac{\pi}{2\lambda h'} \qquad [2.1]$$

where $\lambda h'$ is a non-dimensional parameter expressing the relative stiffness of the column to the infill and h' is height of the column, in which

$$\lambda = \sqrt[4]{\frac{E_m t \sin 2\theta}{4 E_f I_c h}} \qquad [2.2]$$

where E_m, t and h are Young's modulus, thickness, and height of the infill, respectively; E_f and I_c are the Young's modulus and moment of inertia of the column, and θ is the slope of the infill diagonal to the horizontal axis. They considered the contact length between the infill and the beam to be half the span of the beam based on observation. Therefore, the width of the diagonal strut can be calculated using Equation [2.3].

$$w = \sqrt{\alpha^2 + \left(\frac{l}{2}\right)^2} \qquad [2.3]$$

where l is the span of the top beam.

Mainstone (1971) adopted the equivalent strut model for steel frames and conducted a series of tests on small scale micro-concrete and brick infills. He proposed Equation [2.4] for brick infills and Equation [2.5] for concrete infills to calculate the width of the diagonal strut utilizing $\lambda h'$ by Stafford-Smith & Carter (1969).

$$\frac{w}{L_d} = 0.175(\lambda h')^{-0.4} \qquad [2.4]$$

$$\frac{w}{L_d} = 0.115(\lambda h')^{-0.4} \qquad [2.5]$$

where w is the width of the diagonal strut and L_d is the diagonal length of the infill. He suggested that the infill strength can be calculated as the horizontal component of the diagonal strut strength as shown in the following equations.

$$H_I = R'_c \cos\theta \qquad [2.6]$$

$$R'_c = f'_m \, w.t \qquad [2.7]$$

where H_I is the nominal strength of the infill; R'_c is the nominal diagonal load on the infill; w is the effective width of the diagonal strut; f'_m is the compressive strength of the infill material; θ and t are defined in Equation [2.2].

Wood (1978) categorized four different collapse modes by observing previous full-scale and model tests by Simms (1967); Thomas (1953); and Wood (1958). The failure modes included composite shear mode (strong frame, weak wall), shear rotation mode (medium strength wall), diagonal compression mode (strong panel, weak frame) and corner crushing mode (very strong panel and very weak frame). He introduced a reduction factor for compressive strength of masonry f'_m in the model to achieve a reasonable agreement with the experimental results. However, Liauw & Kwan (1983) suggested that the Wood's theory led to overestimation of the strength as the excessive friction was assumed at the structural interface and neglecting the separation of infill wall and frame. They in turn proposed a plastic theory which identified three major collapse modes including corner crushing with failure in columns, corner crushing with failure in beams and diagonal crushing. This method neglected the shear force at the areas of contact of the frame and the infill. Liauw and Kwan (1983) proposed Equation [2.8] to calculate the width of diagonal strut for stiffness prediction.

$$w = \frac{0.95h\cos\theta}{\sqrt{\lambda h}} \qquad [2.8]$$

El-Dakhakhni et al. (2003) proposed the "Three-Strut Model" as shown in Figure 2.1. They suggested that it is more logical to consider that the panel consists of two diagonal regions rather than one diagonal strut based on a suggestion by Saneinejad and Hobbs (1995). The three struts in this model do not fail simultaneously which is the case in actual infill panels. Neglecting the friction between the steel frame and the concrete masonry panel, the total diagonal strut area is given by Equation [2.9].

$$A_d = \frac{(1-\alpha_c)\alpha_c ht}{\cos\theta} \qquad [2.9]$$

7

where α_c is given in Equation [2.10] and θ is defined in Equation [2.2].
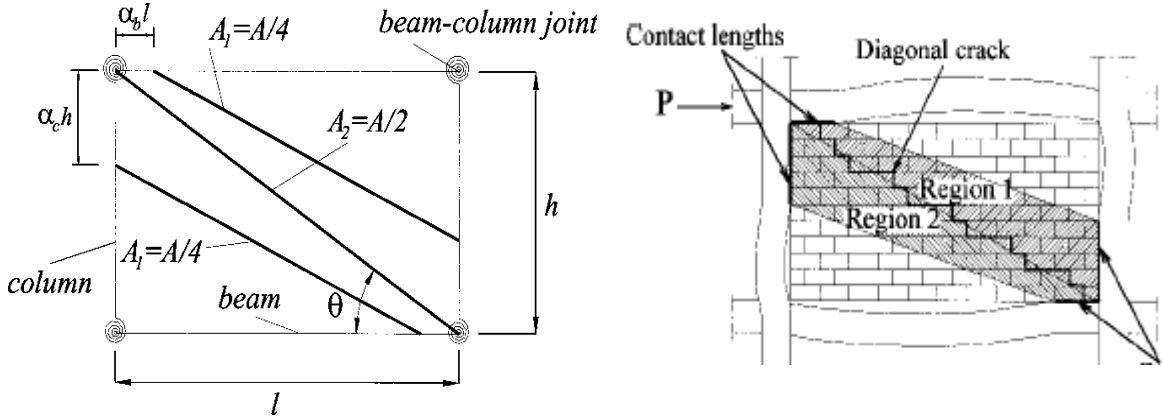
Figure 2.1. Masonry infilled steel frame model proposed by El-Dakhakhni et al. (2003)

Adapted from El-Dakhakhni et al. (2003)

They proposed the following equations for the contact lengths:

$$\alpha_c h = \sqrt{\frac{2M_{pj} + 0.2M_{pc}}{tf'_{m-0}}} \leq 0.4\,h \qquad [2.10]$$

$$\alpha_b l = \sqrt{\frac{2M_{pj} + 0.2M_{pb}}{tf'_{m-90}}} \leq 0.4\,l \qquad [2.11]$$

where f'_{m-0} and f'_{m-90} are the compressive strength of the masonry panel parallel and normal to the bed joint; M_{pj} is the plastic moment capacity of the joint, taken as the lesser of plastic moment capacity of the column, the beam and the connection; M_{pc} and M_{pb} are column and beam plastic moment capacities, respectively.

Flanagan & Bennett (1999) adopted the equivalent strut concept and suggested the area of the diagonal strut to be calculated by Equation [2.12].

$$A = \frac{\pi.t}{C\lambda\cos\theta} \qquad [2.12]$$

8

where *C* is an empirical constant that depends on the displacement of the infill and the type of damage to the infill and λ, *t* and θ are defined in Equation [2.2]. Flanagan & Bennett (2001) provided a table for values of *C* for different infill and frame materials. This method is the basis of Building Code Requirements and Specification for Masonry Structures MSJC (2011). Flanagan & Bennett (1999) also presented Equation [2.13] for corner crushing strength of masonry infills.

$$H_{ult} = K_{ult}.t.f'_m \qquad [2.13]$$

where K_{ult} is an empirical constants with value of 264 mm for SCT, 191 mm for brick, and 259 mm for CMU infills; f'_m is the compressive strength of masonry; *l* and *t* are the length and thickness of the infill, respectively.

By comparing the analytical methods to the available experimental data, Tucker (2007) proposed Equation [2.14] to the diagonal strut width for the calculation of the stiffness of the infilled frame system.

$$w = 0.25L_d(\lambda h)^{-1.15} \qquad [2.14]$$

where L_d is the diagonal length; *h* is the height of the infill and λ is defined in Equation [2.2]. Tucker (2007) also proposed three sets of equations for predicting the crack load and ultimate strength of different types of masonry infilled frames. Equations [2.15] and [2.16] predict the crack load and ultimate strength of CMU infilled frames, respectively.

$$P_{fc} = 0.6f'_m \, wt \cos\theta \qquad [2.15]$$

$$P_{ult} = 1.05f'_m \, wt \cos\theta \qquad [2.16]$$

Equations [2.17] and [2.18] predict the crack load and ultimate strength of structural clay tile (SCT) infilled frames.

$$P_{fc} = 1.05 f'_m \, wt \cos \theta \qquad\qquad [2.17]$$

$$P_{ult} = 2.4 f'_m \, wt \cos \theta \qquad\qquad [2.18]$$

Equations [2.19] and [2.20] predict the crack load and ultimate strength of brick infilled frames. The methods proposed by Tucker (2007) are further discussed in Chapter 5.

$$P_{fc} = f'_m \, wt \cos \theta \qquad\qquad [2.19]$$

$$P_{ult} = 1.9 f'_m \, wt \cos \theta \qquad\qquad [2.20]$$

2.3 EXPERIMENTAL STUDIES

Dawe & Seah (1989) presented the experimental results of full scale concrete masonry infilled steel frames tested by several graduate students at University of New Brunswick (McBride 1984, Yong 1984, Amos 1985, and Richardson 1986). They tested 28 large-scale (3600 mm long by 2800 mm high frame filled with 200 mm standard concrete blocks) specimens by applying a lateral load at roof level as shown in Figure 2.2. Columns were oriented to bend about the weak axis and beams were oriented for strong axis bending.
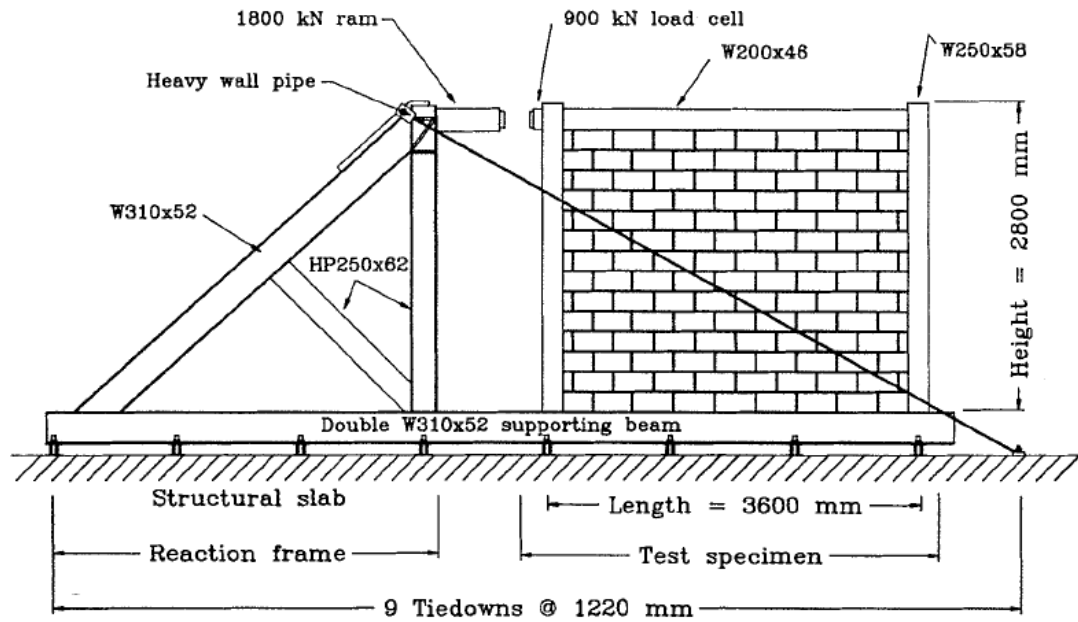
Figure 2.2. Experimental setup from Dawe & Seah (1989)

Adapted from Dawe & Seah (1989)

They found that interface conditions between panel edges and frame significantly affect the strength and behaviour of the system. A 20 mm gap between the roof beam and the panel was found to be detrimental to the shear capacity of the system. The gap caused 50% reduction in crack load and 60% reduction in stiffness and ultimate strength. Horizontal joint reinforcement limits the extent of cracking after appearance of major diagonal crack patterns but without contributing to the overall strength of the infilled frame. The door opening that constituted 18% of surface area of the infill reduced the ultimate strength by about 40%. Comparison of the results of selected test specimens with theoretical methods is presented in Chapter 5.

Flanagan (1994) tested eleven steel frames infilled with SCT. The walls had a height of 2.2 m and three height-to-length aspect ratios of 1:1, 1:1.3, and 1:1.5 were used. A typical test setup is shown in Figure 2.3. The frame with the lowest aspect ratio (1:1.5) had the highest ultimate strength and the highest crack load, while the other two specimens had similar strengths. He found no correlation between aspect ratio and stiffness of infilled frames.
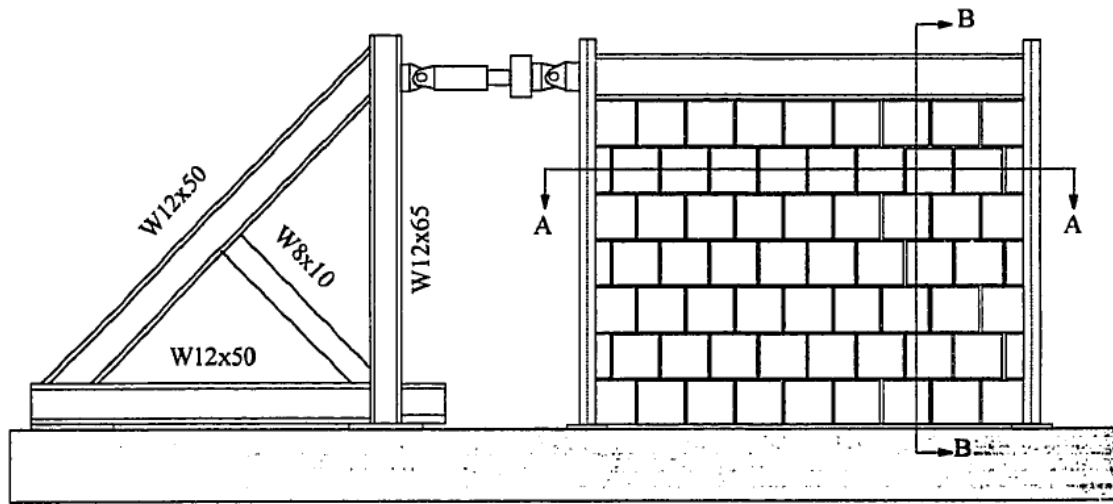
Figure 2.3. Typical test setup from Flanagan (1994)

Adapted from Flanagan (1994)

Mehrabi et al. (1996) investigated the influence of masonry infill panels on the seismic performance of RC frames. Twelve half-scale single-storey, single-bay, frame specimens were tested. The non-linear behaviour was usually initiated by the cracking of the infill. The cracks were inclined with approximately a 45° angle and developed around the compression corners. In specimens with weak frame and strong panel, brittle shear failure was observed in the columns. They concluded that for a frame that is properly designed for earthquake forces, masonry panels will most likely have a beneficial influence on its performance. They also suggested that the infill panels can be potentially used to improve the performance of existing non-ductile frames.

Mosalam et al. (1997) tested 5 specimens to study the response of unreinforced masonry infilled steel frames to gradually applied cyclic lateral loads. The experimental setup consisted of a bolted framed beam connections and quarter-scale concrete masonry blocks were used. The weak blocks had compressive strength of about 13 MPa and the strong blocks were of about 30 MPa strength. The following conclusions were made.

- Solid panels cause the infilled frame to be more brittle than the panel with openings.

- The presence of openings reduces the stiffness by about 40% for lateral loads below the cracking load and causes the ultimate load to be significantly higher than the cracking load.
- Solid infills and infills with windows had similar ultimate load capacities while the presence of door opening reduced the ultimate load capacity by 20%.
- The relative strength of concrete blocks and the mortar joints significantly affects the mode of failure. Weak blocks ($f < 14$ MPa) cause corner crushing while stronger blocks ($f > 19$ MPa) lead to diagonal cracking.

Fiorato et al. (1970) performed scaled tests on masonry infilled RC frames using brick masonry to investigate the effect of some parameters such as infill opening and number of stories. They concluded that the presence of opening slightly reduced the stiffness of the frame system. Three of these tests are compared with the selected analytical methods in Chapter 5.

Angel (1994) tested seven large-scale RC frames infilled with brick and CMU infill to investigate the loss of out-of-plane strength of unreinforced masonry infilled frames due to in-plane cracking. Figure 2.4 shows the test setup. He concluded that in-plane stiffness of the infilled frame was directly proportional to the masonry compressive strength. He proposed that the stiffness can be approximated using an equivalent diagonal strut with a width equal to one eighth the diagonal length of the infill. Angel also observed that the out-of-plane strength was reduced to half as the result of extensive in-plane cracking. The experimental results provided by Angel (1994) are used for comparison with theoretical methods in Chapter 5.
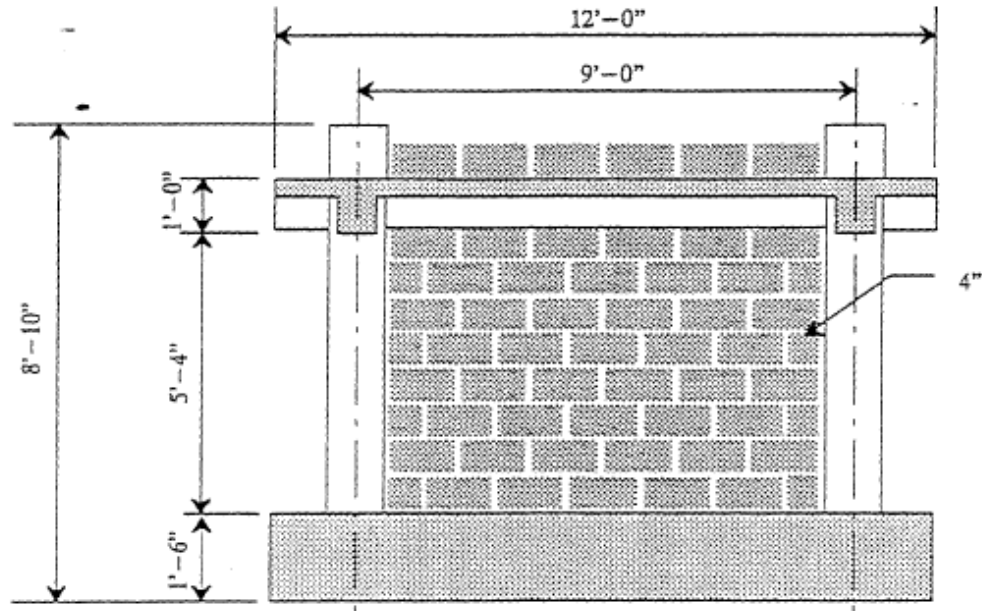
Figure 2.4. A typical test setup of Angel (1994)

Adapted from Angel (1994)

Crisafulli (1997) tested a concrete masonry infilled RC frame using solid concrete units 230×90×75 mm. Figure 2.5 shows the test setup. He observed that shear and axial forces on the columns can cause a sliding shear failure of the columns. Considering the fact that a sliding shear failure of the columns is a highly destructive mode of failure, he recommended the use of additional longitudinal reinforcement in the columns to control sliding shear especially when tensile axial forces are expected. The result of this test is further discussed in Chapter 5.
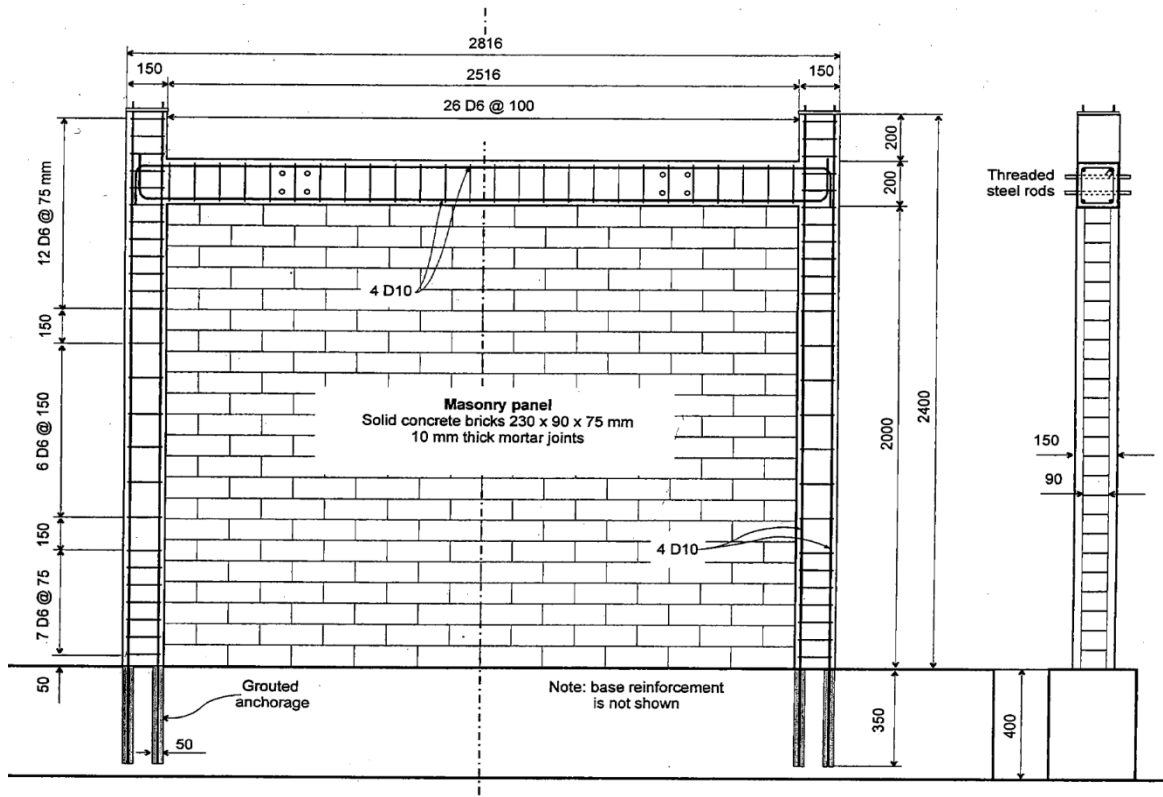
Figure 2.5. Experimental setup of Crisafulli (1997)

Adapted from Crisafulli (1997)

Al-Chaar (1998) carried out an experimental program to examine the behaviour of non-ductile RC frames infilled with masonry. By comparing a bare frame with an infilled frame with similar properties, he observed that the initial lateral stiffness of the infilled frame is 15 times higher than that of the bare frame. Two of these tests on single bay infilled frames are chosen and discussed in Chapter 5.

Chiou et al. (1999) conducted scaled tests to study the behaviour of framed masonry walls subjected to in-plane monotonic loading. They used three specimens: (1) an RC frame; (2) a partially infilled RC frame (infilled up to the mid-height); and (3) a completely infilled RC frame. Masonry walls were built using brittle brick and mortar. They concluded that the characteristics of the masonry infilled frame are highly influenced by failure of mortar. In addition, the partially infilled frame creates a short column effect that can cause severe failure of the column. On the other hand, the

15

completely infill wall increased the stiffness of the structure and the adjacent column failed with nearly uniform cracks.

Ng'andu et al. (2005) investigated the response of calcium silicate infilled steel frames subjected to in-plane monotonic loading. They studied the influence of frame to wall stiffness ratio, a gap between the wall and the roof beam, and the use of a corner bearing wedge on the response in terms of overall stiffness, stress-strain distributions, and cracking loads and patterns. They concluded that the top gap increases the deflection range and delays interlocking of the frame and the panel. However, introducing bearing wedges at the top corners significantly reduces the influence of the top gap. Also, using a stiffer frame increases the diagonal tension cracking capacity.

2.4 DESIGN CODES AND GUIDELINES

2.4.1 Canadian Code

Canadian masonry design standard, CSA S304.1 (2004) adopts a semi-empirical approach using the diagonal strut concept initially used by Stafford-Smith and Carter (1969) to calculate the stiffness of the infill. Detailed explanation of this method is presented in Chapter 5.

2.4.2 American Code

The Masonry Standards Joint Committee (MSJC) introduced provisions for the design of masonry infills in the latest edition of the Building Code Requirements and Specification for Masonry Structures (2011). The equations proposed by MSJC (2011) are a modification of Equations [2.12] and [2.13] by Flanagan & Bennett (1999) and are explained in detail in Chapter 5. MSJC (2011) is the only design code that accounts for the existence of top gaps. According to MSJC existence of a gap up to 9.5 mm between the top beam and the infill is acceptable and the infill is considered a participating infill. However, the stiffness and strength of such infill shall be multiplied by a factor of 0.5. If

the gap is larger than 9.5 mm, the infill is considered a partial infill. Concrete columns with partial infills are vulnerable to shear failure due to "short column effect" and are undesirable in seismic events.

2.5 CONCLUDING REMARKS

Although there is a large body of literature on masonry infilled frames in the past six decades, the lack of a universally accepted method for design of masonry infilled frames is evident. While much research dealt with in-plane behaviour of infills subjected to lateral loading, the effect of axial load on the lateral resistance of the infill has not been studied. The infill design provisions contained in the current Canadian masonry standard were based on the method developed 40 years ago and their efficacy needs to be evaluated with the current masonry products and construction practice. The design guideline in the American standard are based on more recent research results but its performance has not been thoroughly examined.

CHAPTER 3   EXPERIMENTAL PROGRAM

3.1   INTRODUCTION

The experimental program was divided into two parts: (a) auxiliary tests to determine material properties of masonry components including blocks, mortar, grout, and reinforcing steel; and (b) testing of eight concrete masonry infilled steel frame specimens under combined in-plane lateral and axial loading. Detailed descriptions of test specimens, experimental setup, testing procedures and auxiliary tests are given in the following sections. A parallel experimental study conducted by a colleague (Soon, 2011) was focused on specimens under in-plane lateral loading only. Some results of the parallel study are compared with results of this study in later chapters. For ease of reference, specimens used in the parallel experimental program are also described in the following section.

3.2   TEST SPECIMENS

A summary of test specimens is listed in Table 3.1 for specimens under combined lateral and axial loading and in Table 3.2 for specimens under lateral loading only.

Table 3.1. Description of test specimens under combined lateral and axial loading

No.	Specimen Designation	Grouting	Aspect Ratio	Opening	Loading Condition (Lateral+Axial)
1	CF-1-1.3	FG	1:1.3	No	Axial (1)
2	CF-2-1.3	FG	1:1.3	No	Axial (2)
3	CF-3-1.3	FG	1:1.3	No	Axial (3)
4	CP-1-1	PG	1:1	No	Axial (1)
5	CP-1-1.3	PG	1:1.3	No	Axial (1)
6	CP-1-1.6	PG	1:1.6	No	Axial (1)
7	CPW-1-1.3	PG	1:1.3	Window	Axial (1)
8	CPD-1-1.3	PG	1:1.3	Door	Axial (1)

Table 3.2. Description of test specimens under lateral loading only (Soon 2011)

No.	Specimen Designation	Grouting	Aspect Ratio	Opening
9	LF-1.3	FG	1:1.3	No
10	LP-1	PG	1:1	No
11	LP-1.3	PG	1:1.3	No
12	LP-1.6	PG	1:1.6	No
13	LPW-1.3	PG	1:1.3	Window
14	LPD-1.3	PG	1:1.3	Door

A total of fourteen concrete masonry infilled steel frames were tested with eight of them under various combinations of in-plane lateral and axial loading. The axial load of a pre-determined magnitude was applied first through the frame beam and was held constant while the lateral loading applied at the beam level was increased gradually to the failure of the specimen. Parameters considered in this study included the aspect ratio, extent of grouting, opening in the infill panel, and axial load. For all specimens, the web of the steel column was oriented in the plane of the infill and thus the bending of columns under the lateral loading was with respect to its strong axis. The labelling scheme of the specimen is described as follows. "CF" designates a fully grouted wall whereas "CP" designates a partially grouted wall. Letters "W" and "D" imply the presence of a window or a door opening respectively. The first number indicates the axial load level and the second number is length to height ratio. Axial (1), (2) and (3) indicate a load level of 25,000 pounds (111.2 kN), 18,000 pounds (80.1 kN), and 11,000 pounds (48.9 kN), respectively. The axial load resistance of a fully grouted infill, $P_{r(max)}$, with 1:1.3 aspect ratio was calculated to be 528 kN based on CSA S304.1 (2004). The three axial load levels were then taken as approximately 20%, 15%, and 10% of $P_{r(max)}$, respectively.

The masonry infill walls were constructed using one-third scale of standard 200 mm CMUs. The efficacy of using scaled CMUs for masonry infills has been confirmed by past tests (Mehrabi et al. 1996, Mosalam 1996, Maleki et al. 2007). All the wall specimens were longitudinally reinforced with 6 mm threaded rebars. A smaller size rebar would be more desirable in the construction of this scale; however, this size was the smallest available on the market at the time of testing. Grouting and reinforcement

patterns of walls with three different height-to-length aspect ratios are illustrated in Figure 3.1. For the specimen with window opening (Figure 3.2) the reinforcing location was adjusted accordingly as shown in Figure 3.1c. The specimen with door opening had similar reinforcing pattern as the solid walls as shown in Figure 3.1b. The course above the opening was made into a lintel beam with horizontal reinforcement. The door and window openings reduced the surface area of the walls by 18% and 10%, respectively. The fully grouted walls had the same reinforcement patterns as their partially grouted counterparts.

a) Aspect ratio: 1:1

b) Aspect ratio: 1:1.3

c) Aspect ratio: 1:1.3 with window opening

d) Aspect ratio: 1:1.6
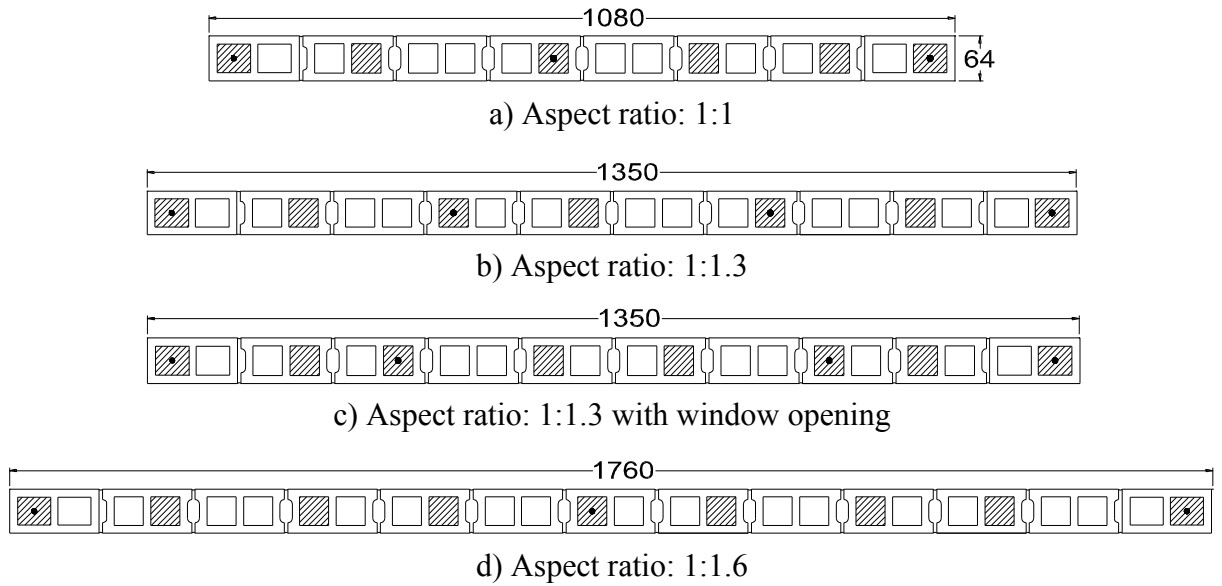
Figure 3.1. Grouting and reinforcement patterns of the partially grouted walls
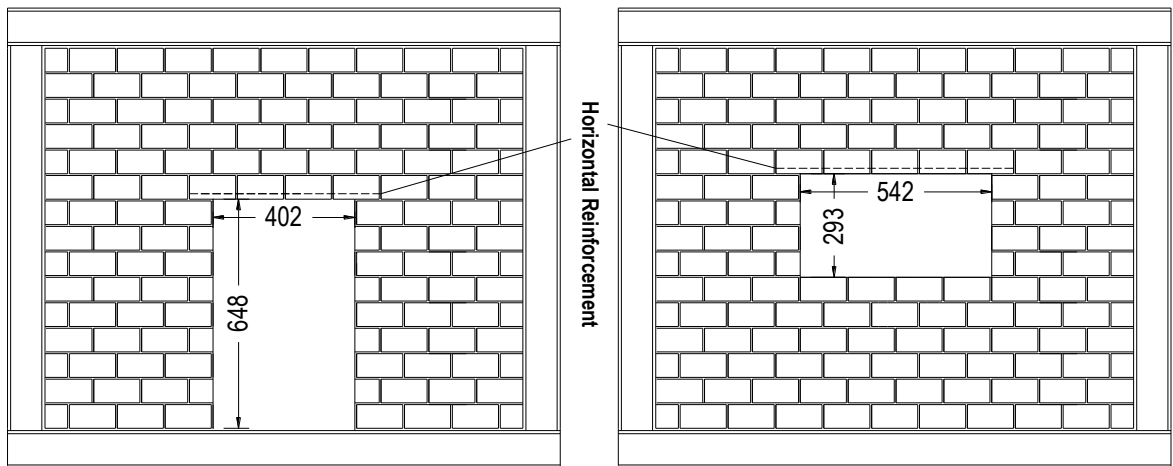
Figure 3.2. Schematic of specimens with door and window openings

3.2.1   Fabrication of Wall Specimens

Wall specimens and corresponding prisms were constructed and moist-cured for 7 days followed by air-curing for additional 21 days. All the specimens were constructed by an experienced certified mason under supervision to the standard of practice. The ambient temperature variation in the laboratory ranged from 10°C to 25°C while the humidity was 60 to 80%. Two methods were used in the construction of wall specimens. Specimens 1, 2 and 5 were built outside the bounding frame. As shown in Figure 3.3a, temporary support frames made of 2×4 lumber and plywood were built to support the wall during the construction and curing phases. The first course was laid on a strip of plywood. A horizontal line and level were used to keep the wall faces in alignment. Mortar was placed on both bed-joint and head-joint. Grouting took place after the wall was constructed to full height. Consequently, the reinforcing steel bars were placed in designated locations. After the curing, the wall was transported to the test location and positioned in the bounding frame at the time of testing. For the remaining specimens, the infill walls were constructed and cured directly inside the pre-fabricated bounding frames (Figure 3.3.b) to facilitate the transporting and testing procedure. Building infills inside the frame also reduced the possibility of gaps between the frame and the infill. The roof beam was welded on top of the columns after the curing period of 28 days and the whole frame specimen was lifted to testing location and set in the testing position.

a) First stage of construction	b) Second stage of construction

Figure 3.3. Construction of wall specimens

3.2.2   Steel Frames and Connections

The steel frame was constructed using W100x19 steel section for both the beam and the columns. For specimens1, 2 and 5, each column was welded to a 4 mm bearing plate that was subsequently bolted to a floor beam using eight 13 mm diameter, 50 mm long bolts (Figure 3.4.a). For the remaining five specimens, the columns were welded to a bottom beam which was in turn bolted to the floor beam (Figure 3.4.b). The roof beam was welded to the top of the columns using fillet welds (Figure 3.5).

a) First stage   b) Second stage

Figure 3.4. Details of connections of test frames to the floor beam

Figure 3.5. Roof beam connection detail

3.2.3   Infilled Frame Specimen Test Setup

A schematic view of a typical setup is illustrated in Figure 3.6 and a picture is shown in Figure 3.7. The loading arrangement and the infilled frame specimen were supported on a W200x46 steel section which was in turn connected to the strong floor through twelve 40 mm diameter threaded steel bars. The beam was stiffened using web stiffeners at four locations along its length. Lateral load was applied through a hydraulic actuator with a capacity of 250 kN. Axial load was applied using a manually operated hydraulic jack and it was kept constant as the lateral load applied till the failure of the specimen.

A skewed A-frame consisting of two W150x30 columns was provided as a reaction support for the load. The frame member and its connections were designed to withstand at least 250 kN of lateral load. As shown in Figure 3.8, the reaction column was braced in the out-of-plane direction with two W150x30 leaning columns to limit any potential out-of-plane movement of the loading frame.
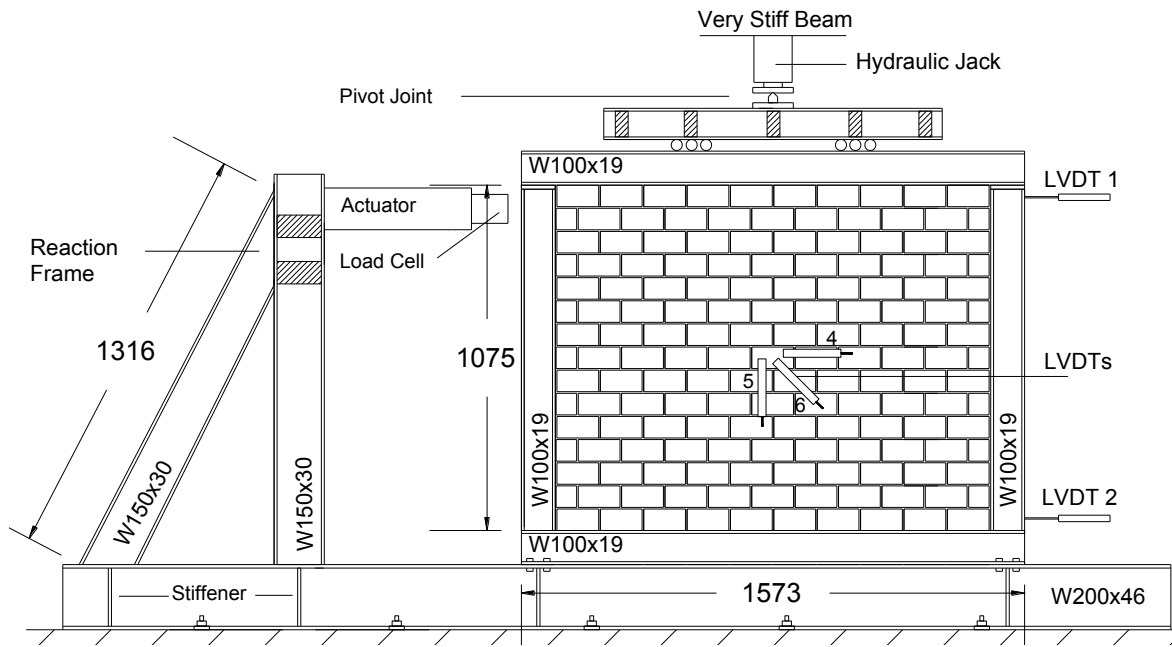
Figure 3.6. Schematic of the test setup (dimensions in mm)
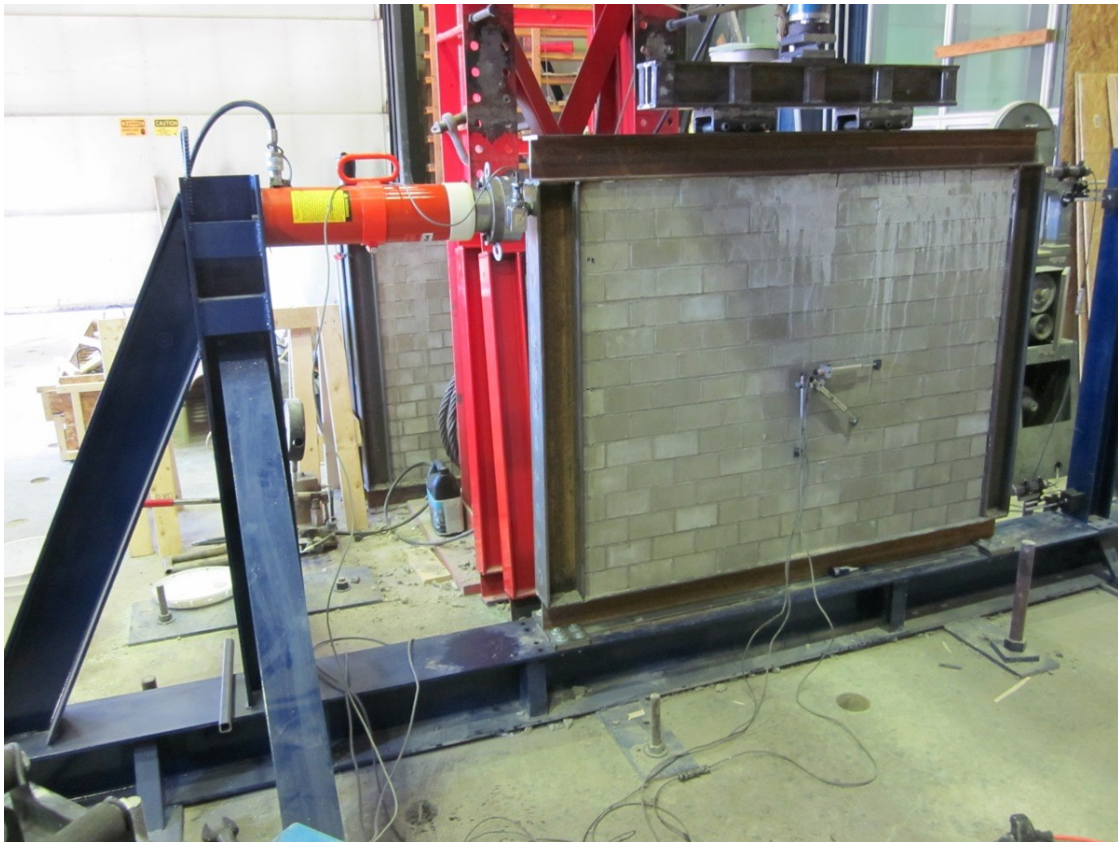
Figure 3.7. Test setup
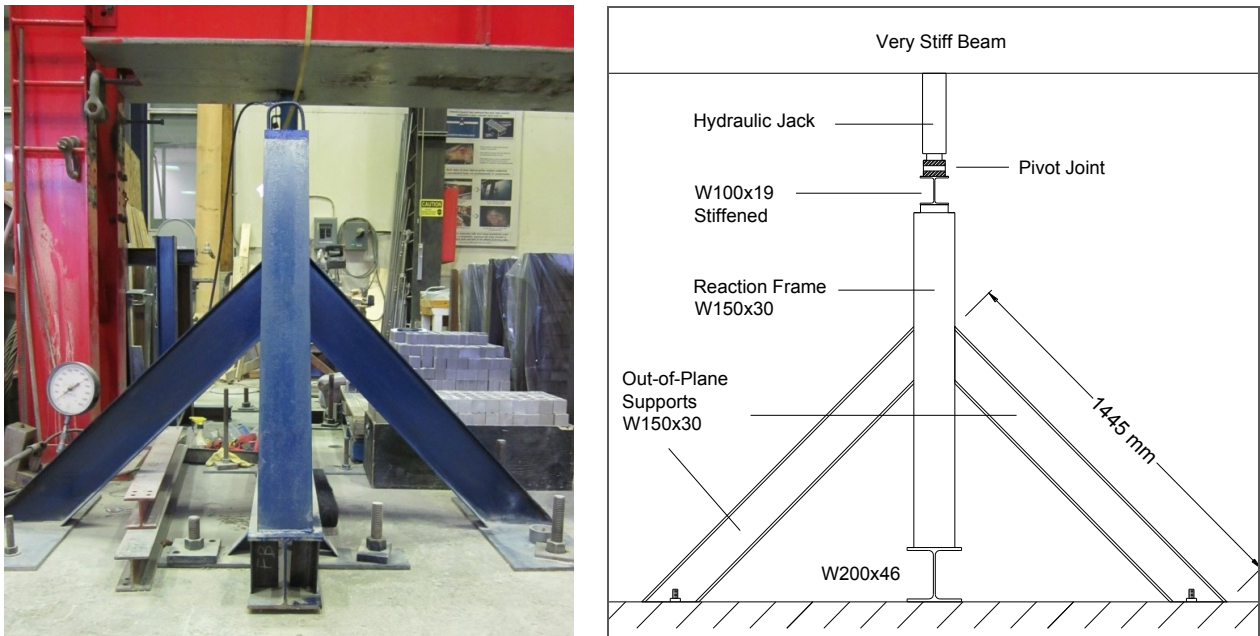
Figure 3.8. Out of plane support frame

3.2.3.1 Lateral Loading Arrangement

In-plane lateral loading was applied to each specimen using a 250 kN hydraulic actuator. The hydraulic actuator was fastened to the reaction frame as shown in Figure 3.9 using two 12 mm diameter bolts. A load cell was placed between the actuator and the frame to measure the load. The reaction column was stiffened with web stiffeners at the location where the load was applied.
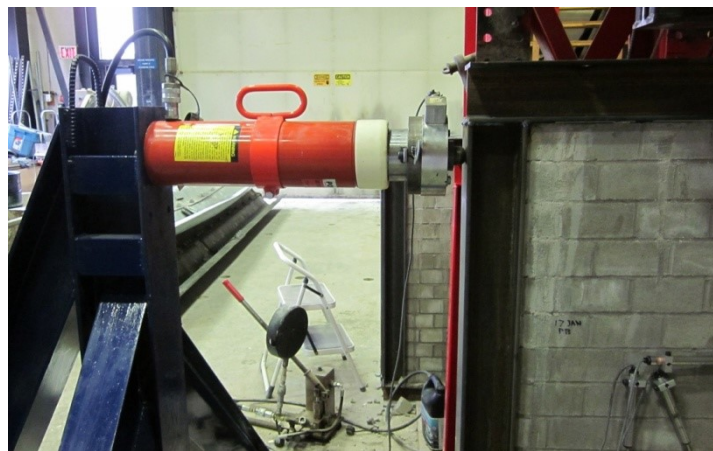
Figure 3.9. Lateral loading arrangement

3.2.3.2 Axial Loading Arrangement

The axial load was applied using a hydraulic jack through a spreader beam as shown in Figure 3.10. The jack was manually operated and was equipped with a release valve to keep the axial load constant during each test. A stiffened W100x19 beam supported on two roller assembly supports was used to distribute the axial load onto the top beam to simulate a four-point loading scheme. Each roller assembly consists of three rollers (Figure 3.11) at the load application point to accommodate the lateral movement of the top beam. The load was applied through a pivot joint onto the spreader beam. The pivot knife edge support was used to allow for slight in-plane rotation of the test specimen (Figure 3.12).
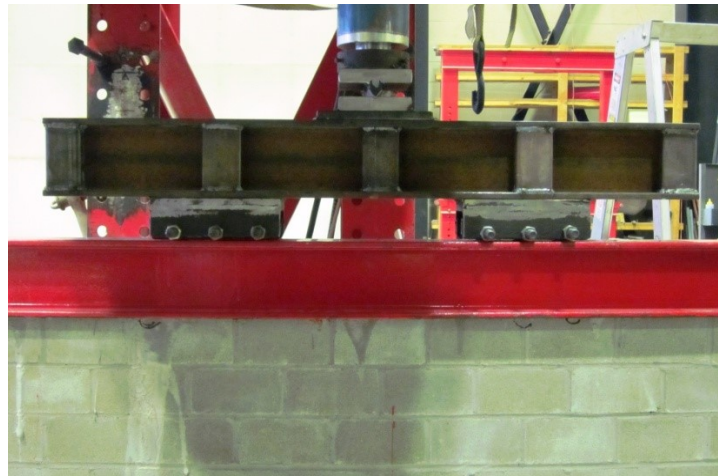
Figure 3.10. Axial loading arrangement

Figure 3.11. Roller assembly

Figure 3.12. Pivot knife edge support

3.2.3.3 Instrumentation and Data Acquisition

Two linear variable differential transformers (LVDTs) (LVDT 1 and 2) were used to measure in-plane lateral deflection at the top beam and the bottom beam as shown in Figure 3.6. One LVDT (LVDT3) was used to monitor any possible out-of-plane movement at about half height of the wall on the back side. LVDTs 4, 5, and 6 were mounted on the wall at the central region to measure the lateral, vertical and diagonal deformations as shown in Figure 3.13. The gauge length for LVDTs 4, 5 and 6 were kept at approximately 200 mm for each test.

Figure 3.13. LVDTs 4, 5 and 6 for strain measurements

3.2.4 Testing Procedure

A 10-ton ceiling crane was used to carry the test specimen from the fabrication area to the testing area. For specimens 1, 2 and 5, the wall was detached from the temporary wooden support after it was cured and lifted using heavy duty straps attached to the crane. The wall was then placed on the floor beam in between the two erected columns and it was carefully centered in both in-plane and out-of-plane direction. The roof beam was last attached to the columns. Extra care was taken to reduce gaps, if any, between the wall and the surrounding frame members. In some cases, cement and shims were used to fill gaps. For the remaining specimens, the entire infilled frame was lifted after curing by attaching two U-shaped hooks to the top flange of the roof beam. The frame was then

placed on the floor beam and it was centred and aligned properly. After securing the specimen in place, the six LVDTs were mounted at their designated locations and all readings were checked to make sure that they function properly before the test began. The load cell was placed over and around the tip of the actuator using a custom-made ring that was welded to the load cell.

Axial load was applied first gradually to the pre-determined level and held. The movement of the wall was closely monitored. The lateral load was then applied at a rate of 8 kN/min until the specimen lost capacity to sustain any additional load. In many cases, the test was stopped after the specimen experienced large lateral deflection accompanied with a decrease in the load. The load, deflections and deformations were monitored and recorded at an interval of 0.1 second throughout the loading history for each test. Appearance of cracks and signs of failure were noted and recorded next to registered load. Each test was continued well beyond failure of the wall. After removal of the loads, the cracking pattern was photographed and sketched and the specimen was disposed of.

3.3 AUXILIARY TESTS

Masonry components used in the experiments were one-third scale of standard 200 mm concrete masonry blocks, mortar, grout, and steel reinforcement bars. Physical and mechanical properties of these materials were determined by a number of auxiliary tests described below.

3.3.1 Physical Properties

Physical properties including dimensions, net and gross areas, density, and 24-hour percentage absorption were evaluated for the three different shapes of CMUs (Figure 3.14). In every case, a minimum of three samples were tested as required by ASTM C140 (2007). The 24-hour absorption test was done by determining the absorption of a unit when submerged in water at room temperature for 24 hours. The average surface area of

a stretcher block was around 4,200 mm^2. The average density of a concrete masonry block was 2,030 kg/m^3 which is comparable to the density of a standard 200 mm block. The average length, width, and height of a stretcher block were 131, 64, and 67 mm, respectively.

a) Stretcher block   b) End block

c) Half block   d) Three different types of 1/3 scale blocks
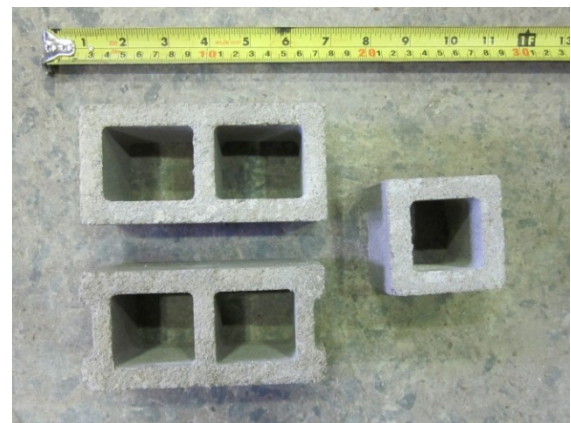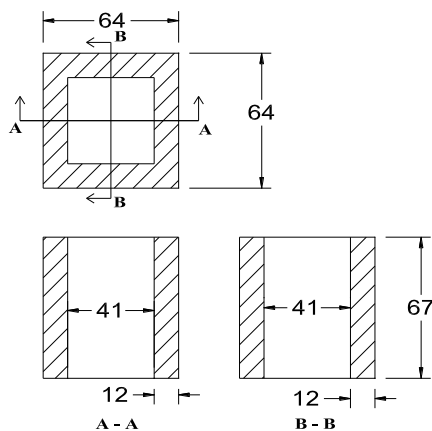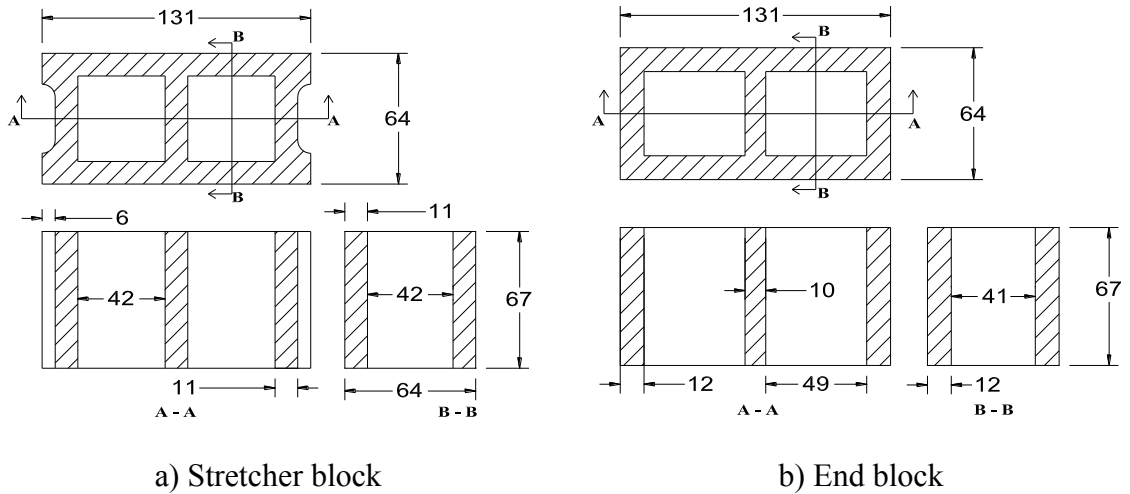
Figure 3.14. Details of the scaled blocks (dimensions in mm).

3.3.2 Mechanical Properties

Mechanical properties of concrete blocks, mortar, grout, three-high prisms, four-high square prisms, and reinforcing steel were determined as described in the following sections.

3.3.2.1 Masonry blocks

Five stretcher hollow concrete blocks, five end blocks and five half blocks were tested in axial compression using Instron universal testing machine according to ASTM C140 (2007) as shown in Figure 3.15. The randomly chosen block was measured and placed in the machine with two pieces of fiberboard on the loading surfaces. The block was carefully centered and aligned. The compressive load was then applied through a self-levelling metal piece to ensure a concentric load. The block was loaded beyond failure and the peak load was used to determine the compressive strength.

Figure 3.15. Universal Testing Machine test setup for concrete blocks

3.3.2.2 Mortar and Grout

A total of fifteen 50 mm mortar cubes were sampled (Figure 3.16) and tested according to CSA A179-04 (2009). Type S mortar was used. Proportions by volume for mortar were 1 portion Portland cement, 1/2 portion type N masonry cement, and 4 portions of loose sand in accordance with ASTM C270 (2008). Mortar samples were cured in a moisture room for 7 days and tested after 28 days. Grout consisted of sand to cement ratio of 5:1 and sufficient water to ensure workability. Ten 65 mm grout cubes were sampled using the configuration shown in Figure 3.17 according to CSA A179-04 (2009). Grout samples were air-cured for 48 hours and subsequently moist-cured until tested at 28 days. A concrete mixer was used to mix mortar and grout.

| Figure 3.16. Mortar cubes in mold | Figure 3.17. A typical grout mold |
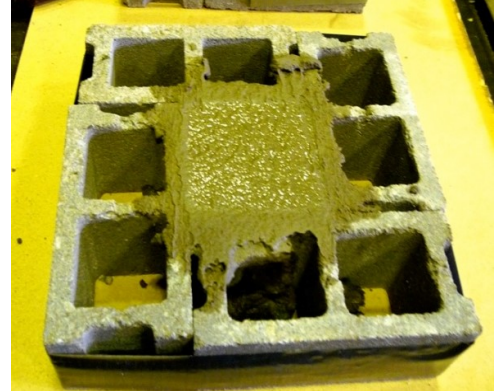
3.3.2.3 Masonry Prisms

Two types of masonry prisms (Figure 3.18) were cast, cured and tested as described below. Ten grouted and three hollow three-high full block prisms were cast and cured alongside the construction of the walls. The three-high prisms were tested according to ASTM C1314 (2009) to determine the compressive strength of masonry in compression (Figure 3.19a). Similar to the concrete blocks, the three-high prisms were placed in the machine with two pieces of fiberboard on the loading surfaces. The compressive load was applied concentrically through a self-levelling metal piece.
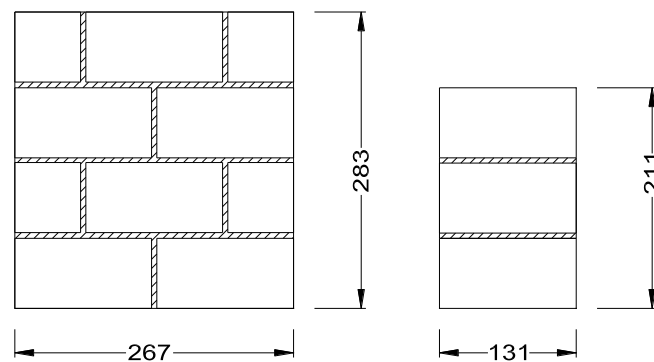
Figure 3.18. Three-high and square prisms (dimensions in mm)

Twenty seven four-high square prisms were also cast and cured. The square prisms were tested to determine the effect of the loading direction on the compressive strength of masonry and to determine modulus of elasticity and stress-strain relationship of masonry in compression. Nine hollow, nine partially grouted, and nine fully grouted square prisms

were loaded in vertical, horizontal and diagonal directions. Prisms loaded in vertical, horizontal, and diagonal directions are shown in Figures 3.19b, 3.19c, and 3.19d, respectively. LVDTs were mounted at the front and the back of all the square prisms to obtain deformation readings. The gauge lengths of the LVDTs were kept at approximately 200 mm. Horizontal and vertical specimens had a similar testing procedure to the three-high prisms. For testing in diagonal direction, two custom-made supports were used for the loaded corners as shown in Figure 3.20. Each support was a V-shaped joint inside a rectangular box designed to encase the corners and provide a straight surface for testing.

a) Three-high prism
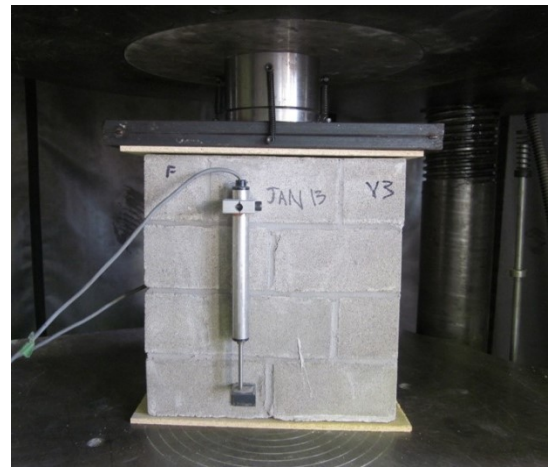
b) Square prism loaded vertically

c) Square prism loaded horizontally
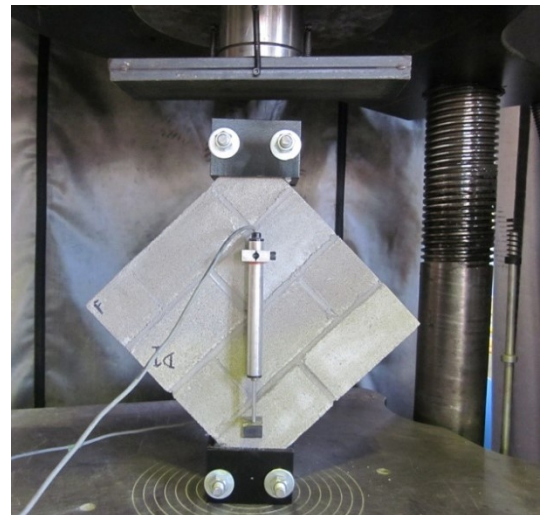
d) Square prism loaded diagonally

Figure 3.19. Compressive testing of different types of prisms

Figure 3.20. Testing shoe for diagonally loaded prisms

3.3.3 Reinforcing Steel

Three randomly selected 6 mm nominal diameter threaded rebars were tested in tension using the Instron universal testing machine (Figure 3.21) in accordance with ASTM E8/E8M (2008). Custom-made brackets with set screws were used to hold the rebar in place and avoid slippage. The average yield strength of steel was found to be 600.6 MPa and the average modulus of elasticity was 196.3 GPa. The stress-strain relationship curve is presented in Chapter 4.

Figure 3.21. Reinforcing steel in tension

CHAPTER 4   RESULTS AND DISCUSSION

4.1 RESULTS OF AUXILIARY TESTS

4.1.1 Physical Properties

Physical properties include the dimension, net area, density, 24-hour absorption rate, and moisture content of masonry blocks. Six stretcher blocks, three end blocks, and three half blocks were randomly selected and their surface dimensions were measured using a digital calliper. Table 4.1 presents detailed dimensions and Table 4.2 contains information on density, 24-hour absorption, and moisture content of blocks. In the tables, "S" designates a stretcher block; "E" designates an end block; and "H" designates a half block. The mean net cross-sectional area of a stretcher block, an end block, and a half block were determined to be 4395.4, 4344.9, and 2471.2 mm^2, respectively. Sketches of the three types of blocks are shown in Figure 4.1.

a) Stretcher block
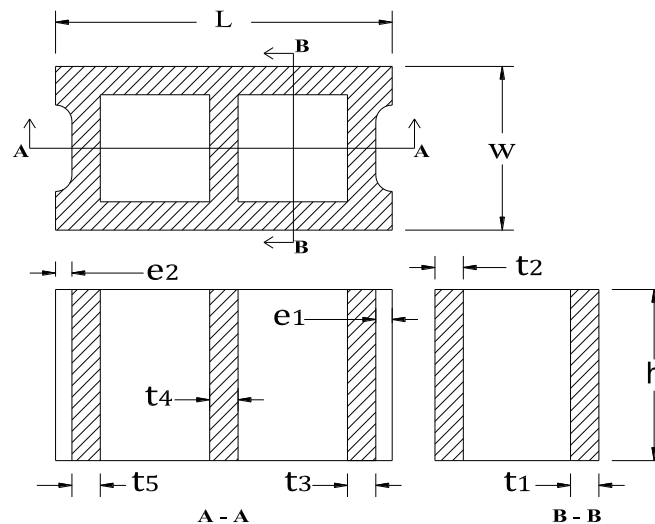
b) End block   c) Half block
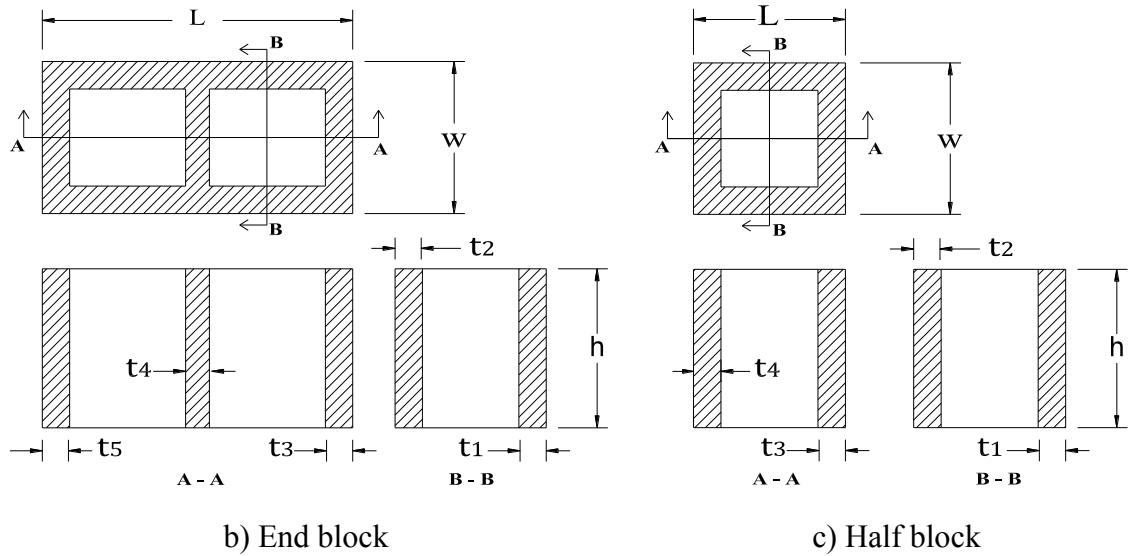
Figure 4.1. Schematic of the three types of blocks

Table 4.1. Dimensions of three types of blocks in mm and net areas in mm^2

No.	L	w	h	t_1	t_2	t_3	t_4	t_5	e_1	e_2	Net Area
S_1	130.5	63.9	66.4	11.5	11.2	10.3	11.0	10.8	6.0	5.8	4428.9
S_2	130.5	63.6	66.5	11.8	10.6	11.2	11.0	10.4	6.4	6.1	4410.3
S_3	130.7	63.5	66.7	11.0	10.9	11.1	10.8	10.1	5.5	6.4	4337.5
S_4	130.6	63.4	66.8	11.4	10.8	10.5	11.1	11.3	6.0	6.0	4398.8
S_5	130.6	63.5	67.1	11.0	11.3	10.9	10.9	11.0	5.4	6.3	4407.7
S_6	130.5	63.6	66.7	11.6	10.5	11.4	10.5	10.9	5.9	6.0	4389.3
E_1	130.4	64.0	66.5	11.5	11.6	11.2	9.7	11.8	-	-	4349.7
E_2	130.6	63.4	66.6	11.7	11.6	11.4	9.5	11.3	-	-	4334.2
E_3	130.7	63.5	66.9	11.5	11.5	12.0	9.6	11.6	-	-	4350.7
H_1	64.0	63.6	67.3	12.0	12.3	12.1	12.1	-	-	-	2506.3
H_2	63.9	63.8	67.2	11.9	11.7	11.9	12.0	-	-	-	2468.8
H_3	63.6	63.5	66.7	11.7	11.8	12.2	11.4	-	-	-	2438.6

The 24-hour absorption rate was determined for three samples from each type of blocks based on ASTM C1585 Standard Test Method for Measurement of Rate of Absorption of Water by Hydraulic-Cement Concretes (2004). The blocks were first oven dried in 100°C for 48 hours and followed by submersion in water for 24 hours. The blocks were then removed from the water and the surface water was blotted with cloth. The difference

between the saturated mass (M_s), the oven-dried mass (M_d), and the initial mass (M_i) was used to calculate the 24-hour absorption rate and moisture content using Equations [4.1] and [4.2].

$$24\text{-Hour Absorption Rate} = \frac{M_s - M_d}{M_d} \times 100\% \qquad [4.1]$$

$$\text{Moisture Content} = \frac{M_i - M_d}{M_s - M_d} \times 100\% \qquad [4.2]$$

According to the classification by CSA A165.1 Standard for Concrete Block Masonry Units, 24-hour absorption capacity of hollow concrete blocks with density of 1800-2000 kg/m^3 (Type B) should be smaller than 200 kg/m^3 and smaller than 175 kg/m^3 for concrete blocks with density of greater than 2000 (Type A).

Table 4.2. Physical properties of masonry blocks

No.	Net Area (mm^2)	Mass (g)	Density (kg/m^3)	24-Hour Absorption		Absorption CSA A165.1 (kg/m^3)	Moisture Content %
				(% by Mass)	kg/m^3		
S_1	4428.9	566.0	1924.7	9.7%	184.0	<200	12.0
S_2	4410.3	587.6	2003.5	8.1%	161.3	<175	13.7
S_3	4337.5	583.4	2016.5	8.0%	160.4	<175	14.4
S_4	4398.8	581.7	1995.0	-	-	-	-
S_5	4407.7	586.2	1975.3	-	-	-	-
S_6	4389.3	584.2	1986.9	-	-	-	-
Avg.	4395.4	581.5	1983.6	8.6	168.6	-	13.4
E_1	4349.7	571.6	1976.1	8.2%	160.4	<200	14.4
E_2	4334.2	567.5	1966.0	7.9%	154.2	<200	15.7
E_3	4350.7	578.0	1985.8	8.6%	168.7	<200	14.3
Avg.	4344.9	572.4	1976.0	8.3	161.1	-	14.8
H_1	2506.3	323.8	1919.7	8.8%	166.6	<200	13.9
H_2	2468.8	333.2	2008.4	7.8%	155.5	<175	14.7
H_3	2438.6	327.1	2011.0	8.1%	160.5	<175	14.2
Avg.	2471.2	328.0	1979.7	8.2	160.9	-	14.3

4.1.2 Mechanical Properties

The mechanical properties of blocks, mortar, grout, prisms, and reinforcing steel were determined in accordance with CSA and ASTM standard as described in Chapter 3. CSA S304 (2004) suggests that the test of five randomly selected specimens is sufficient provided that the coefficient of variation (COV) is less than 15%. If COV is greater than 15%, a minimum of ten specimens should be tested.

4.1.2.1 Masonry blocks

Compressive strength values of five randomly selected stretcher blocks, five end blocks, and five half blocks are presented in Tables 4.3 and 4.4. The ultimate load obtained from the compressive test divided by the net area of each type of block was used to calculate the compressive strength. The results show good correlation between the scaled blocks and standard 200 mm blocks. The compressive strength at 28 days of standard 200 mm CMUs in the market is commonly around 20 MPa.

Table 4.3. Compressive strength of stretcher blocks

No.	Ultimate Load (kN)	Compressive Strength (MPa)
1	74.2	18.0
2	86.2	22.8
3	118.4	22.3
4	69.7	19.6
5	79.3	21.4
Avg		20.8
COV(%)		9.6

Table 4.4. Compressive strength of end and half blocks

No.	Ultimate Load (kN)	Compressive Strength (MPa)	No.	Ultimate Load (kN)	Compressive Strength (MPa)
EB1	91.5	21.1	HB1	46.9	19.0
EB2	84.8	19.5	HB2	49.4	20.0
EB3	75.0	17.3	HB3	54.9	22.2
EB4	92.9	21.4	HB4	52.8	21.4
EB5	91.2	21.0	HB5	53.9	21.8
Avg		20.1	Avg		20.9
COV(%)		8.5	COV(%).		6.4

In summary, the compressive strength of masonry block unit is approximately 20.6 MPa.

4.1.2.2 Mortar and grout

Mortar and grout cubes were sampled and tested as described in Chapter 3. They were tested in Instron universal testing machine as shown in Figures 4.2 and 4.3. Batch 1 was sampled during the first stage of construction and batch 2 was sampled during the second stage of construction of the walls. Table 4.5 presents a summary of 28-day compressive strength of mortar cubes. The batch 2 showed 18.8% higher strength than the batch 1. The low COV suggests consistent mixes of mortar during construction within each batch.

Figure 4.2. Mortar cube in compression   Figure 4.3. Grout cube in compression

Table 4.5. Compressive strength of mortar

	Batch 1			Batch 2	
No.	Compressive Strength (MPa)	No.	Compressive Strength (MPa)	No.	Compressive Strength (MPa)
M_1	15.3	M_6	16.3	M_{11}	18.4
M_2	17.2	M_7	15.3	M_{12}	20.7
M_3	17.9	M_8	17.1	M_{13}	17.2
M_4	15.1	M_9	16.6	M_{14}	19.6
M_5	17.1	M_{10}	16.6	M_{15}	21.5
Avg			16.5		19.5
COV(%)			5.7		8.9

Table 4.6 is a summary of 28-day compressive strength of grout cubes. The grout cubes were sampled using a custom-made mould as described in Chapter 3. Similar to mortar cubes, two batches of grout cubes were also made using standard of practice. Note that the second batch of grout had a 30% higher compressive strength than the first batch. Figure 4.4 shows the failure of a grout cube in compression. Both mortar and grout cubes showed vertical splitting extending to the full specimen height at failure. This failure is attributed to the large lateral expansion due to high Poisson's ratio inherent in both masonry mortar and grout.

Table 4.6. Compressive strength of grout

	Batch 1		Batch 2	
No.	Compressive Strength (MPa)	No.	Compressive Strength (MPa)	
G_1	14.1	G_6	23.1	
G_2	13.8	G_7	20.6	
G_3	17.0	G_8	19.4	
G_4	18.1	G_9	19.0	
G_5	17.0	G_{10}	22.9	
Avg	16.0		21.0	
COV(%)	12.0		9.1	

4.1.3 Prisms

4.1.3.1 Three-High Prisms

Ten grouted and three hollow three-high prisms were tested in compression. The effective cross sectional area, A_e, was used to calculate the compressive strength of these prisms. Defined by CSA S304 (2004), A_e is the area that includes the mortar bedded area and the area of voids filled with grout. The effective area of the hollow prisms is shown as shaded area in Figure 4.4 where the center web area was not included since no mortar was applied in this area. The A_e for fully grouted prisms is the sum of the mortar bedded area (shaded area in Figure 4.5) and the area of two grouted cells. In this study, the effective areas of the grouted and hollow prisms were calculated to be 7500 mm^2 and 3933 mm^2, respectively. Tables 4.7 and 4.8 provide a summary of the results.
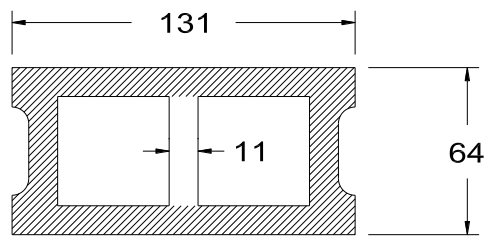
Figure 4.4. Effective area of a hollow three-high prism

For hollow prisms, the average compressive strength is determined to be 12.5 MPa with a COV of 7.5%

Table 4.7. Compressive strength of hollow prisms

No.	Ultimate Load (*kN*)	A_e (*mm^2*)	Compressive Strength (*MPa*)
PH$_1$	53.4	3,933	13.6
PH$_2$	48.0	3,933	12.2
PH$_3$	46.3	3,933	11.8
Avg			12.5
COV(%)			7.5

Table 4.8. Compressive strength of grouted prisms

Batch 1			Batch 2		
No.	Ultimate Load (kN)	Compressive Strength (*MPa*)	No.	Ultimate Load (kN)	Compressive Strength (*MPa*)
A_1	59.5	7.9	B_1	79.0	10.5
A_2	71.4	9.5	B_2	103.9	13.9
A_3	59.7	8.0	B_3	96.4	12.9
A_4	62.1	8.3	B_4	78.6	10.5
A_5	62.8	8.4	B_5	97.8	13.0
Avg		8.4	Avg		12.2
COV(%)		7.7	COV(%)		12.7

Average compressive strength of the second batch of grouted prisms is about 40% higher than the first batch. The second batch was cast using the mortar and grouted from second batch. The higher strength of mortar and grout in second batch is believed to attribute to the higher strength of second batch of prisms. Hollow three-high prisms are on a par with the second batch of grouted prisms and have higher compressive strength than the first batch. The hollow prisms were cast alongside the second batch of grouted prisms.

4.1.3.2 Four-High Square Prisms

A total of twenty-seven four-high square prisms consisting of nine fully grouted, nine partially grouted and nine hollow prisms were tested in three different loading directions. The effective area used in the calculation of compressive strength is defined as follows for these prisms. In the case of prisms with loading applied perpendicularly to the bed joint, they were referred to as "vertically loaded" in this study (V). The effective area in this case for hollow prisms consists of the bed joint and the head joint as shown in Figure 4.5 in shaded area. For the partially grouted and the fully grouted prisms, the area of the grouted cells was added to the shaded area. Therefore, fully grouted, partially grouted, and hollow prisms had the area of 14930, 11390, 7870 mm^2, respectively. All of these prisms were constructed using the second batch of mortar and grout.
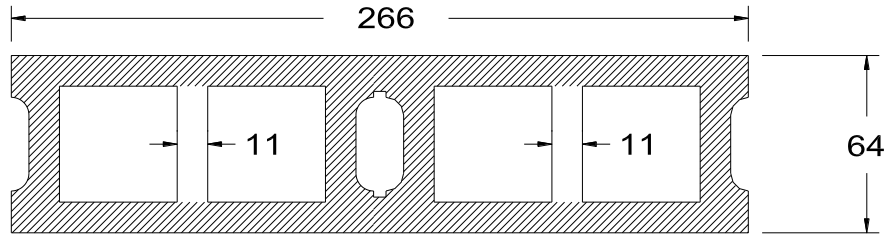
Figure 4.5. Effective area of hollow vertically loaded square prisms

In the case of specimens with loading applied parallel to the bed joint, they were referred to as "horizontally loaded" in this study (H). They are assumed to have the same effective area as their vertical counterparts due to the square shape of the prisms. This provided a basis to compare the two cases.

In the case of prisms loaded diagonally (D), the effective area of fully grouted diagonal prisms was taken as the rectangular cross section encased by the shoe. This is the cross sectional area of the rectangular shape hatched in Figure 4.6. The effective area of hollow diagonal prisms was taken as the face shell area of the same rectangular cross section. The effective area of partially grouted prisms was the average of fully grouted and hollow prisms.
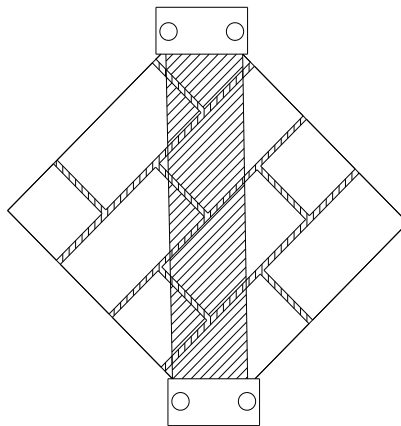
Figure 4.6. Area considered for calculation of compressive strength

The average readings obtained from LVDTs mounted on the front and the back of the prisms were used to obtain the strain values during the compression tests. By plotting the stress-strain curves for each prism, modulus of elasticity was calculated as the initial

slope of the stress-strain curve. The compressive strength and modulus of elasticity are presented in Tables 4.9, 4.10, and 4.11 for fully grouted, partially grouted, and hollow four-high square prisms respectively.

Table 4.9. Properties of the fully grouted four-high prisms

No.	Ultimate Load (kN)	Area (mm^2)	Compressive Strength (MPa)	Modulus of Elasticity (MPa)
V_1	175.2	14,930	11.7	12920
V_2	143.0	14,930	9.6	13350
V_3	133.4	14,930	8.9	12870
	Avg		10.1	13050 (1292 f'_m)
	COV(%)		14.5	2.0
H_1	78.0	14,930	5.2	9520
H_2	81.3	14,930	5.4	6740
H_3	77.3	14,930	5.2	9300
	Avg		5.3	8520
	COV(%)		2.7	1.7*
D_1	28.4	5,123	5.5	13010
D_2	28.9	5,123	5.6	13560
D_3	29.7	5,123	5.8	14220
	Avg		5.7	13600
	COV(%)		2.3	4.5

*Excluding H_2

As shown in Table 4.9, the mean compressive strength of the fully grouted horizontally loaded prisms is about 50% of the vertically loaded prisms. Despite the higher compressive strength than its counterparts, prism H_2 showed unusually low modulus of elasticity. H_2 was considered an anamoly and excluded from COV calculation. The mean compressive strength of the diagonal prisms is close to the horizontal prisms. However, diagonal prisms show significantly higher modulus of elasticity than the horizontal prisms and slightly higher than the vertical prisms. It is a common practice in design to express the modulus of elasticity in terms of compressive strength obtained from the vertical loading. It is noted that for fully grouted prisms, the average modulus of elasticity

was found to be $1292\,f'_m$, which is 60% higher than $850\,f'_m$ as suggested by CSA S304.1 (2004).

Table 4.10. Properties of the partially grouted four-high prisms

No.	Ultimate Load (kN)	Area (mm^2)	Compressive Strength (MPa)	Modulus of Elasticity (MPa)
V$_4$	106.6	11,390	9.4	14330
V$_5$	108.0	11,390	9.5	15430
V$_6$	104.5	11,390	9.2	13740
	Avg		9.4	14500 ($1543\,f'_m$)
	COV(%)		1.6	5.9
H$_4$	NA	11,390	NA	NA
H$_5$	57.1	11,390	5.0	10700
H$_6$	42.2	11,390	3.7	8140
	Avg		4.4	9420
	COV(%)		-	-
D$_4$	19.8	3,442	5.8	13300
D$_5$	25.1	3,442	7.3	17320
D$_6$	22.9	3,442	6.7	15480
	Avg		6.6	15370
	COV(%)		11.4	13.1

As shown in Table 4.10 for partially grouted prisms, the compressive strength as affected by loading directions showed a similar general trend as in the case of the fully grouted prisms. The mean compressive strength of the horizontally loaded prisms is about 50% that of the vertically loaded prisms whereas diagonally loaded specimens attained compressive strength which is 70% of the vertically loaded specimens. Diagonal prisms have the highest modulus of elasticity and the horizontal prisms have the lowest modulus of elasticity. The modulus of vertically loaded prisms was found to be $1543\,f'_m$, which is also greater than $850\,f'_m$.

Table 4.11. Properties of the hollow four-high prisms

No.	Ultimate Load (kN)	Area (mm^2)	Compressive Strength (MPa)	Modulus of Elasticity
V$_7$	78.1	7,870	9.9	NA
V$_8$	80.5	7,870	10.2	11550
V$_9$	67.1	7,870	8.5	11950
	Avg		9.5	11750 (1237 f'_m)
	COV(%)		9.5	-
H$_7$	31.2	7,870	4.0	6400
H$_8$	NA	7,870	NA	NA
H$_9$	42.0	7,870	5.3	7600
	Avg		4.7	7000
	COV(%)		-	-
D$_7$	9.4	1,760	5.3	14600
D$_8$	16.0	1,760	9.1	NA
D$_9$	14.8	1,760	8.4	17400
	Avg		7.6	16000
	COV(%)		26.6	-

For hollow prisms as seen in Table 4.11, the diagonal prisms have the highest modulus of elasticity; more than twice the modulus of elasticity of the horizontal prisms. The mean compressive strength of the horizontally loaded and diagonally loaded prisms are about 50% and 80% that of the vertical prisms, respectively. The average modulus of elasticity for hollow prisms was found to be 1237 f'_m.

In summary, for both grouted and hollow prisms, the vertically loaded ones showed the highest compressive strength followed by diagonally loaded ones and the horizontally loaded prisms attained the lowest strength, which is approximately 50% of the vertically loaded prisms. The average modulus of elasticity of prisms ranged from 1200 to 1600 f'_m with an average of 1360 f'_m, which is greater than the value specified in CSA S304.1 (2004). Also note that the vertically loaded squared prisms had lower strengths than the one-wide prisms. This can be attributed to the fact that square prisms incorporated head

joints and more bed joints. This led to more potential for failure due to complex stress state existent in the prism.

Figure 4.7 shows the stress-strain relationship of prisms loaded in vertical direction. "FG", "PG", and "Hollow" represent fully grouted, partially grouted and hollow prisms. The values of modulus of elasticity for differently grouted prisms are close and show a good consistency. This suggests that it is valid to use the same modulus of elasticity expression in terms of compressive strength regardless of the type of the prisms. However, the multiplier needs to be re-evaluated. The strain reached at the maximum load was about 0.001 for most prisms and the ultimate strain attained varied between 0.0025 and 0.003.
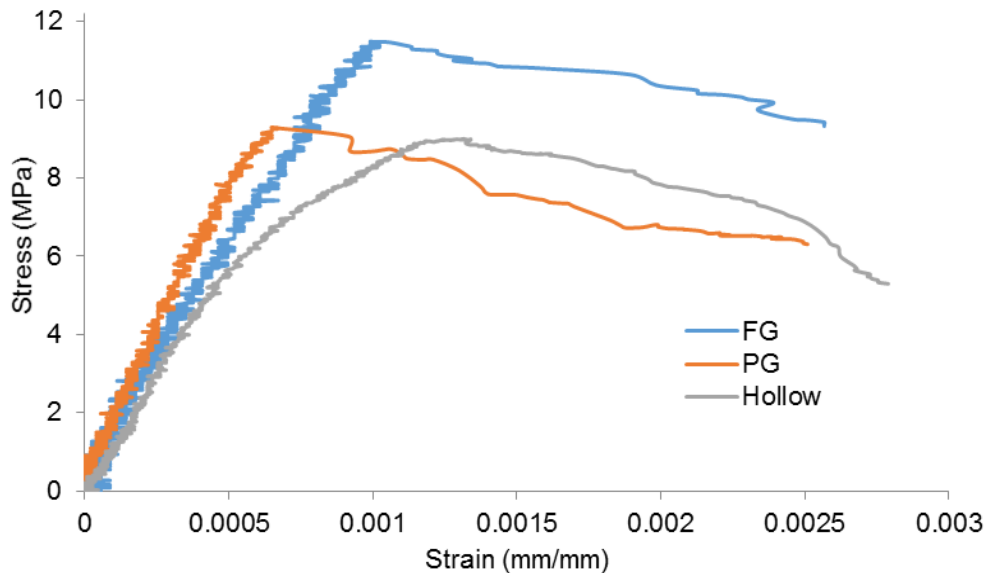
Figure 4.7. Stress-strain relationship of vertical prisms

Figure 4.8 shows the different types of prisms loaded in horizontal direction. Similar to the vertically loaded prisms, the average values of modulus of elasticity for different types of prisms are relatively consistent. The strain reached at the maximum load was less than 0.001 and the ultimate strain attained varied between 0.002 and 0.0025.
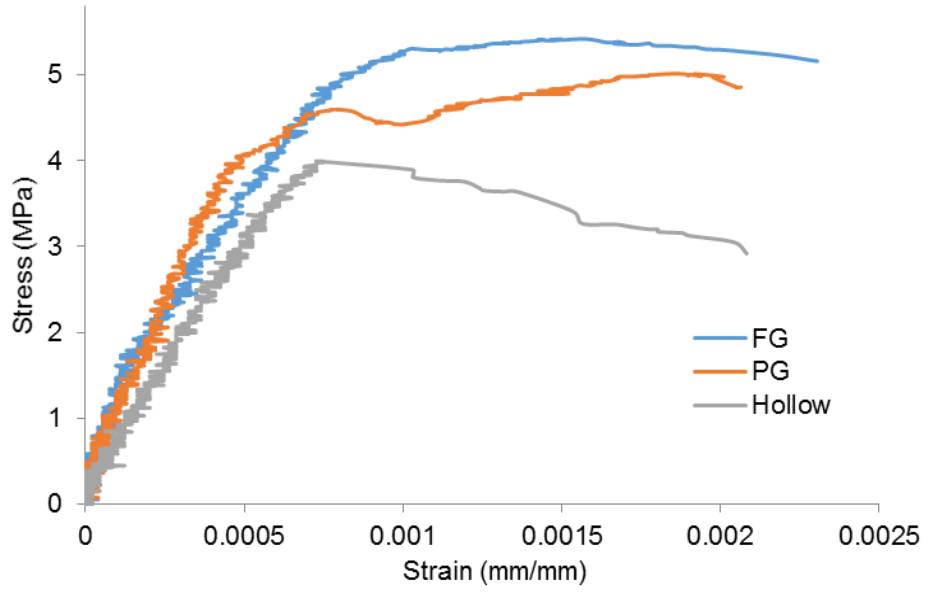
Figure 4.8. Stress-strain relationship of horizontal prisms

Figure 4.9 shows the stress-strain relationships of prisms loaded diagonally. Diagonally loaded prisms of different type also show consistent results. The strain reached at the maximum load was about 0.0006 mm/mm, the smallest comparing with the above-mentioned two cases. The ultimate strain for grouted prisms was less than 0.002 while the hollow one showed an unusually high strain.
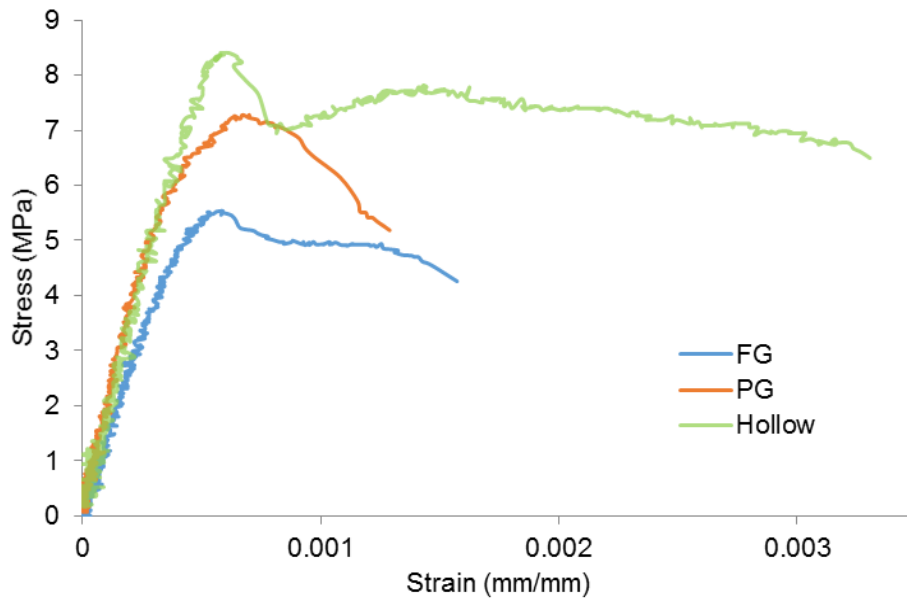
Figure 4.9. Stress-strain relationship of diagonal prisms

4.1.3.3 Failure pattern of prisms

The most common failure mode among the vertically loaded prisms (both three-high and four-high) was "splitting failure" which is marked by the development of vertical cracks (Figures 4.10 and 4.11). For prisms loaded horizontally, in addition to vertical cracks, some inclined cracks were also developed through the face shell of the prism (Figure 4.12) and one horizontal prism failed in "corner crushing" as shown in Figure 4.13.

| a) Front view | b) Side view |

Figure 4.10. Splitting failure in a 3-high prism (B_1)

| a) Front view | b) Side view |

Figure 4.11. Splitting failure in 4-high prisms (V_7)
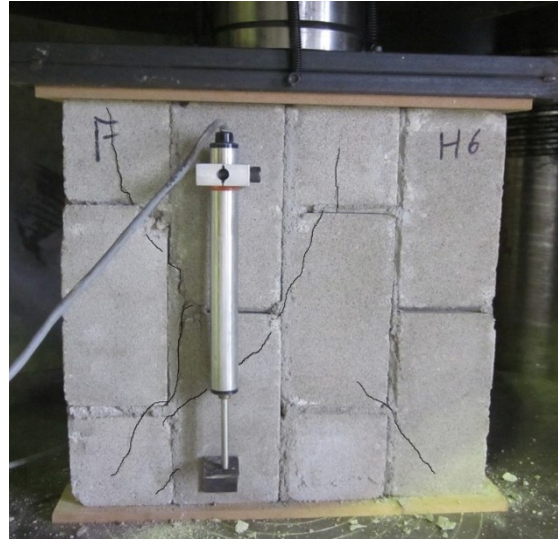
Figure 4.12. Failure of a horizontally loaded prism (H_6)

Figure 4.13. Corner crushing failure in a horizontally loaded specimen (H_7)

Most prisms loaded diagonally failed showed signs of "stepped cracking" as shown in Figure 4.14. Significant diagonal cracking also occurred in most prisms as shown in Figure 4.15.
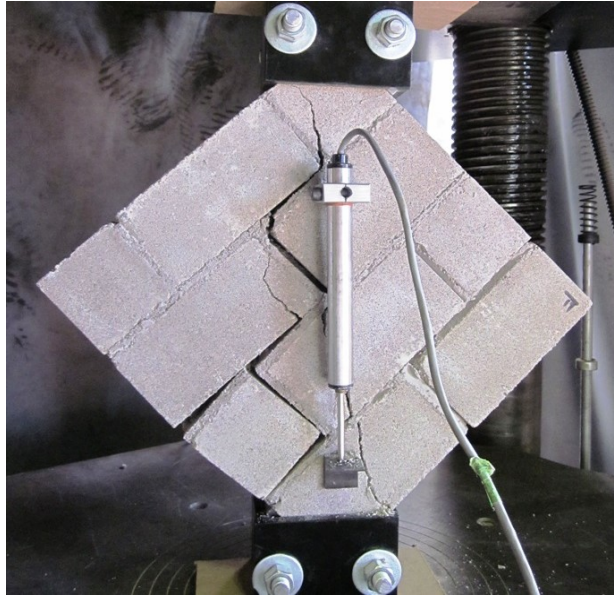
Figure 4.14. Stepped cracking failure of a diagonal prism (D_7)
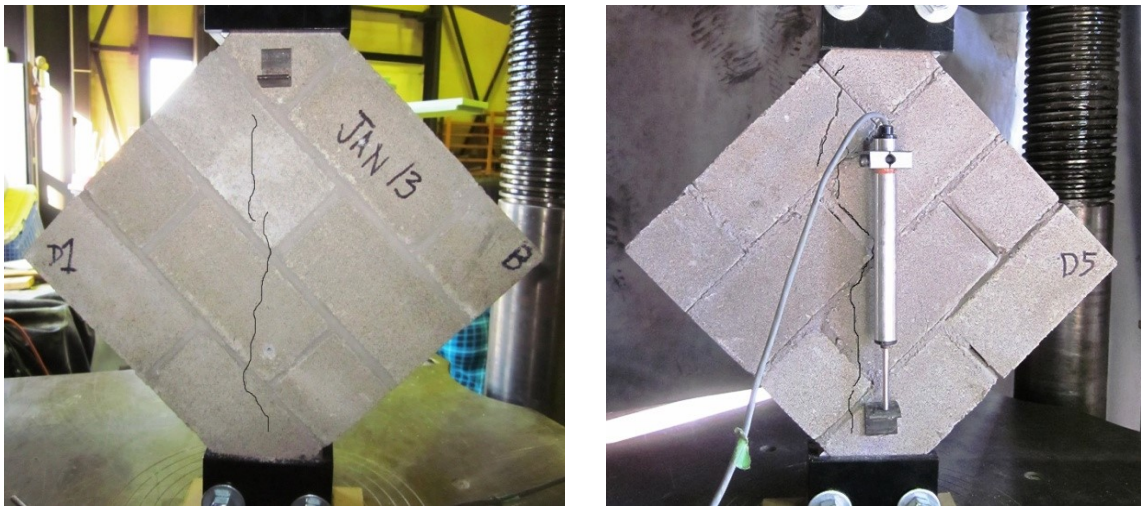
Figure 4.15. Diagonal cracks in D_1 and D_5

4.1.4 Reinforcing Steel

Table 4.12 provides the results of three tensile coupons. The average ultimate tensile strength and the yield strength were determined to be 631.8 and 600.6 MPa, respectively. Since the exact point where yielding begins is not evident, the yield strength is taken using the 0.2% offset method. The offset line for specimen 1 is shown in Figure 4.16.

Table 4.12. Properties of reinforcing steel

No.	Diameter (mm)	Ultimate Tensile Strength (MPa)	Yield Strength (MPa)	Young's Modulus (MPa)
1	5.54	651.6	618.0	200,000
2	5.77	587.4	556.0	183,980
3	5.44	656.5	627.8	205,015
Avg		631.8	600.6	196,332
COV(%)		6.1	6.5	5.6
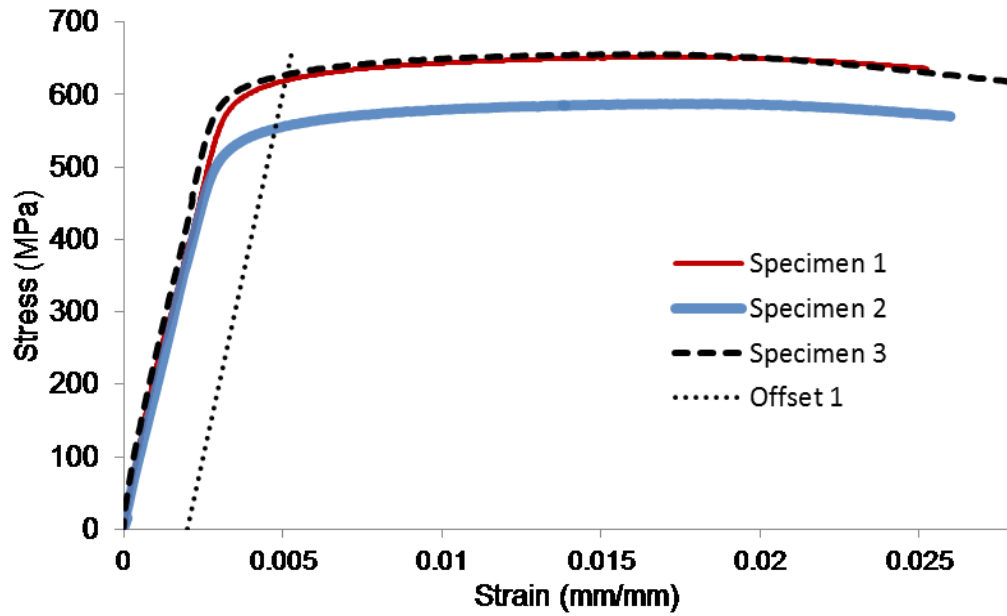
Figure 4.16. Stress-strain relationship of rebar specimens

Figure 4.17 shows the typical failure of a coupon tested in tension using the Universal Testing Machine. In two of the specimens (1 and 2), the rebar snapped at angle of about 45° and for specimen 3 rebar snapped at a horizontal angle.
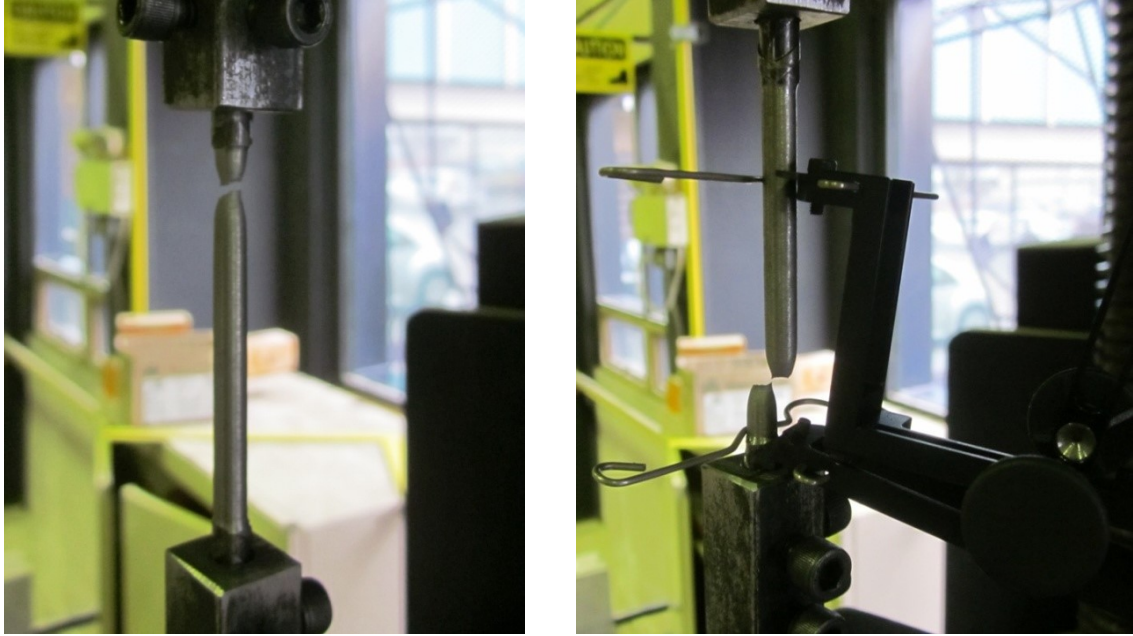
Figure 4.17. Failure of rebar

4.2 RESULTS AND DISCUSSION OF INFILL SPECIMENS

4.2.1 Crack Load and Ultimate Capacity

Table 4.13 presents a summary of results including crack load, ultimate load, deflections at both crack load and ultimate load, and the initial stiffness of the test specimens. The load at which the first visible crack appeared is referred to as "crack load" and it is accurate to ±5 kN. Ultimate load is the maximum load reached during the test. Deflections used in the table were lateral deflection calculated as the difference between readings of LVDT 2 and LVDT 1 to exclude the effect of potential translation of the entire specimen. The initial stiffness was calculated as the slope of the portion of the curve between 5% and 10% of ultimate capacity in the load vs. deflection curve of each specimen. Table 4.14 presents a brief summary of the results of infilled specimens subjected to lateral loading only.

Table 4.13. Test results of infilled specimens

No.	Specimen Designation	Crack Load (kN)	Ultimate Load (kN)	Deflection at Crack (mm)	Deflection at Ultimate (mm)	Initial Stiffness (kN/mm)	Gap (mm)
1	CF-1-1.3	165	197.7	6.4	7.5	26.4	-
2	CF-2-1.3	150	164.9	11.1	21.9	22.9	2
3	CF-3-1.3	130	151.8	10.5	29.0	24.0	-
4	CP-1-1	80	149.3	4.2	16.2	22.8	-
5	CP-1-1.3	65	126.4	4.2	12.7	19.8	2
6	CP-1-1.6	75	130.1	2.4	7.4	46.0	6
7	CPW-1-1.3	80	107.3	4.1	7.7	24.2	-
8	CPD-1-1.3	75	93.3	4.2	9.1	24.5	-

Table 4.14. Results of infilled specimens subjected to lateral load only (Soon 2011)

No.	Specimen Designation	Crack Load (kN)	Ultimate Load (kN)
9	LF-1.3	128.2	131.7
10	LP-1	91.9	111.0
11	LP-1.3	93.8	93.8
12	LP-1.6	104.2	104.2
13	LPW-1.3	52.1	89.1
14	LPD-1.3	63.8	75.3

4.2.2 Effects of Axial Load

As shown in Table 4.13 for specimens 1, 2 and 3 with axial loads of 111 kN, 80 kN, and 49 kN, an increase in the axial load resulted in increases in both the crack load and ultimate load. The effect of axial load is further illustrated in Figure 4.18 where the load vs. lateral deflection responses of specimens 1, 2 and 3 are compared. The specimen with

zero axial load was also included for comparison purpose. These four walls are all fully grouted and have an aspect ratio of 1:1.3.
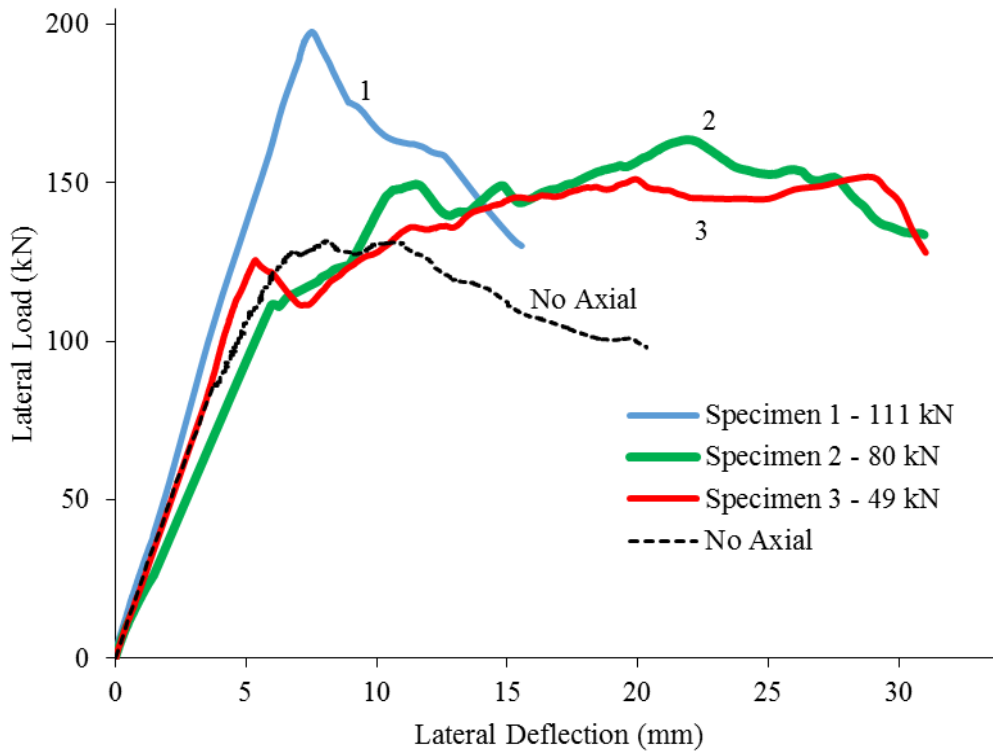
Figure 4.18. Axial load effect on the load vs. deflection behaviour

Referring to Tables 4.13 and 4.14 and Figure 4.18, as the axial load increased from 0 to 49 kN, to 80 kN, and to 111 kN, the lateral resistance increased from 132 kN by 15%, 25%, and 50%, respectively. However, in terms of ductility, the trend is opposite for specimens with axial load. A simple comparison shows the specimen with axial load of 49 kN reached around 30 mm ultimate deflection while this value is about 15 mm for the specimen with axial load of 111 kN. The ductility of specimen with 80 kN axial load lied in between. While for specimens 2 and 3 failure was gradual, specimen 1 failed suddenly. The configuration of the spreader beam for specimen 1 did not allow for rotation of the test specimen. This could be the reason for the sudden failure of the specimen. This was rectified for the other tests by installing a pivot joint that allowed a slight rotation of the test specimen.

It is also seen in Figure 4.18 that all three specimens with axial load showed similar initial stiffness at the very beginning of the loading, which is comparable to that of the specimen without axial load. As the axial load decreased, the responses showed evident development of non-linearity. In the case of specimens 2 and 3, the curves showed a "zig-zag" pattern which is of characteristic for infilled frames. A small drop of load occurred and followed by an increase of load immediately thereafter but at a lower stiffness. This pattern may repeat several times especially after the specimen reached its ultimate load. The drop of the load in the rising branch of the curve is often an indication of the development of cracking or crushing in the infill whereas the following increase of the load shows that the infill establishes alternate failure paths and maintains lateral resistance even after the damage occurred inside the infill. Figure 4.19 shows the correlation between axial load and lateral load. The data points obtained so-far seem to suggest a somewhat linear trend between the lateral load resistance and the level of axial load of up to 20% of the infill compressive capacity. More testing at different axial load levels is needed to generate a conclusive trend.
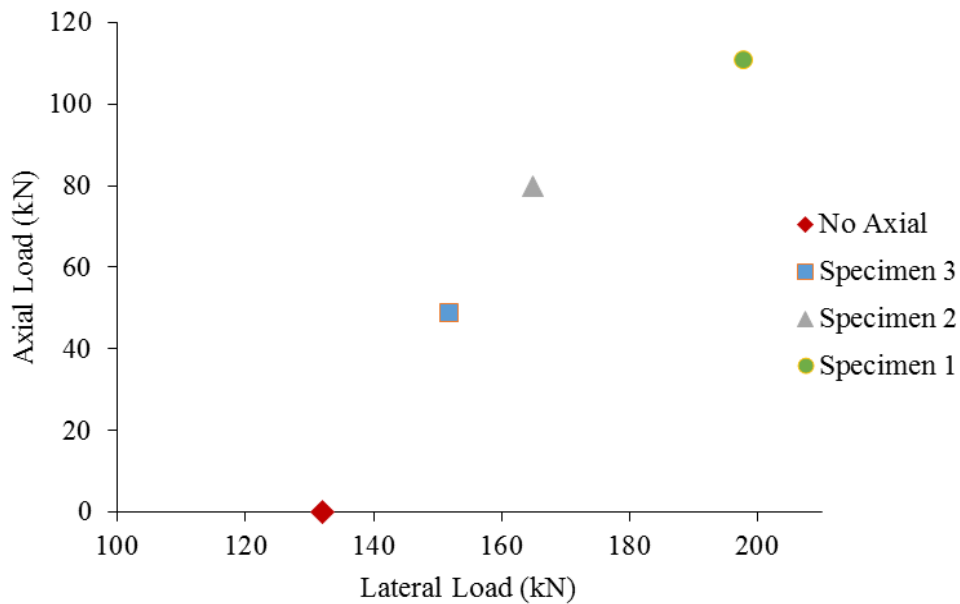
Figure 4.19. Correlation between lateral load and axial load

4.2.3 Effects of Aspect Ratio

Figure 4.20 shows the load vs. lateral deflection curves for specimens 4, 5 and 6 with height-to-length aspect ratios of 1:1, 1:1.3 and 1:1.6 respectively. The "zig-zag" characteristics are evident for all three curves. The 1:1 aspect ratio specimen had the highest ultimate capacity and the 1:1.3 exhibited the lowest ultimate capacity. The similar behaviour was observed for specimens subjected to lateral load only (Soon 2011). It is noted that both specimens 4 and 10 (lateral load only) with 1:1 aspect ratio had virtually no gap between the infill and the surrounding frame. The intimate contact enabled the development of the diagonal strut and therefore may have resulted in a higher capacity. Specimen 5 developed a small incidental gap of 1 to 3 mm between the infill and the loaded column during construction. Specimen 6 had a 6 mm gap between the infill and the top beam but shims were used to minimize the gap. The presence of gap is believed to affect the ultimate capacity of the specimen, however, quantifying the effect of the gap is beyond the scope of this work. It should be pointed out that the difference in capacity values of three specimens is not significant. From the practical point of view, it is difficult to eliminate the gap. With the given data points, the effect of aspect ratio is inconclusive
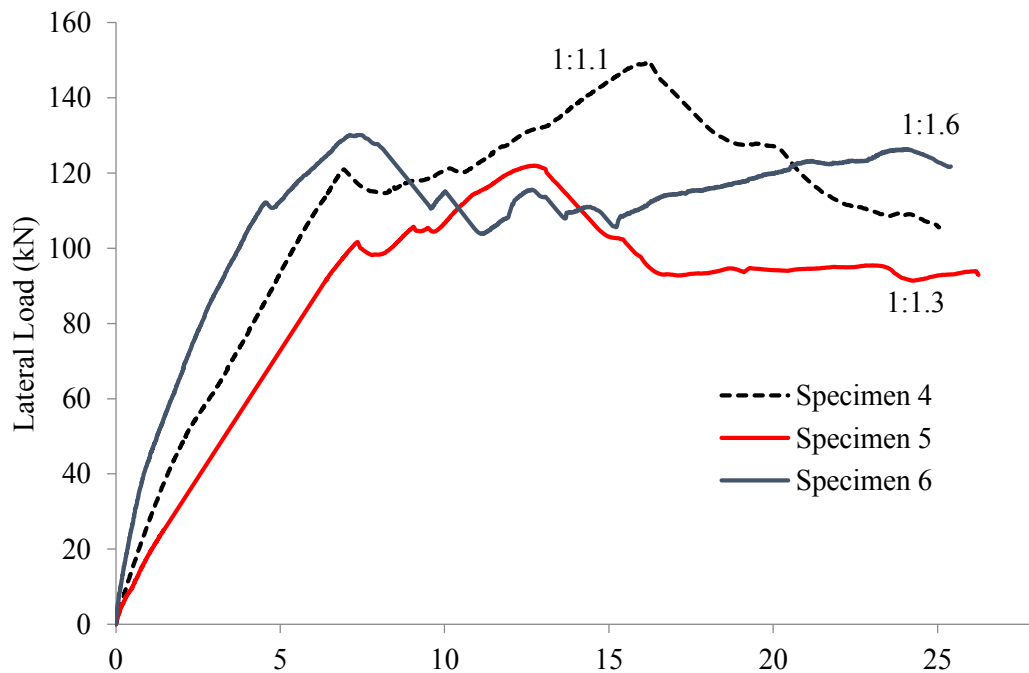
Figure 4.20. Effect of aspect ratio on the load vs. deflection behaviour

4.2.4 Effects of Opening

Specimens with openings had the lowest ultimate strength among the infilled specimens. Figure 4.21 compares the load vs. lateral deflection behaviour of specimens 5 with no opening, 7 with window opening, and 8 with door opening. They were all partially grouted and had aspect ratio of 1:1.3 and the axial load applied in this case was 111 kN.
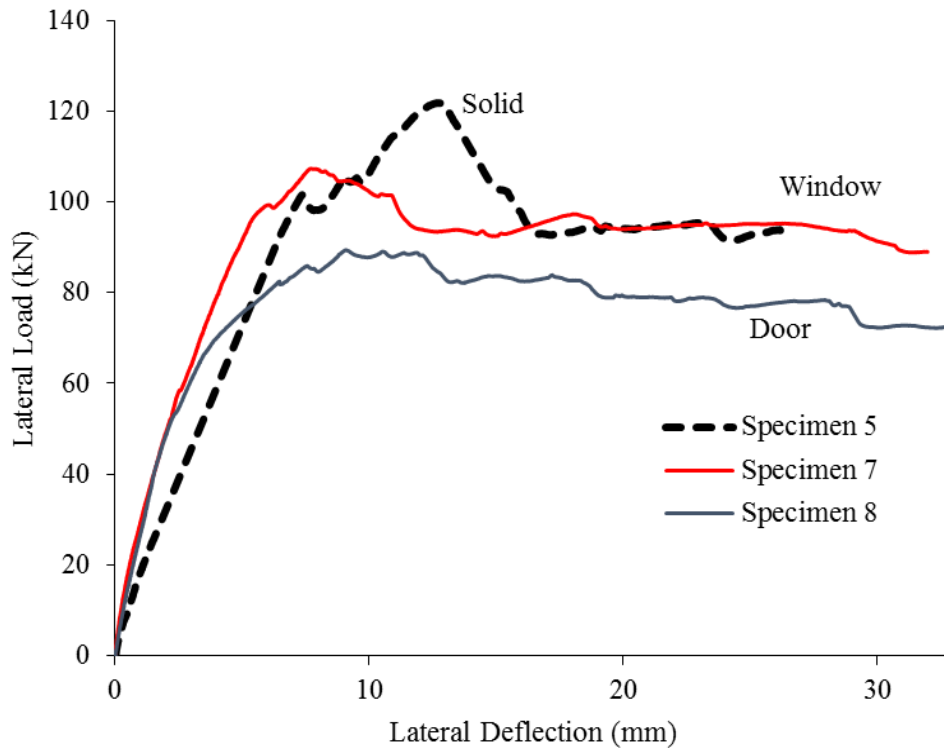
Figure 4.21. Effect of opening on the load vs. deflection behaviour

As shown in Figure 4.21, the solid specimen (specimen 5) has a higher ultimate capacity than the specimens with opening. For the given axial load, the specimen with window opening (10% of area) showed a 15.1% reduction in ultimate load than its solid counterpart whereas this reduction was 26.4% for the specimen with door opening (18% of area). It is evident that enlarging the opening decreases the ultimate capacity of the frame system but the reduction is not in proportion with the reduction in surface area. For specimens with lateral load only the reduction in ultimate strength was 5% and 20% for

the specimens with window and door opening respectively. For specimens with openings, the presence of axial load also resulted in an increase in the lateral strength. For an axial load of 111 kN, the average lateral ultimate strength of specimens with opening was about 25% higher than their counterparts with lateral load only. Overall, the specimens with opening exhibited a greater ductility while sustaining load after reaching the ultimate capacity. There was no sudden drop in the load for specimens 7 and 8. Crack load in the solid partially grouted specimens (4, 5, and 6) was about 50% of the ultimate capacity while for the specimens with opening (7 and 8), it was about 80% of ultimate. This shows that solid specimens have higher post-crack capacity in resisting lateral load. While the infills with opening still showed ability to re-establish the failure path, the opening, in comparison with the solid panel, did affect the effective development of the diagonal strut. Therefore, once cracks occur in the infill with opening, the failure is imminent.

4.2.5 Effects of Grouting

It is evident in Table 4.11 that the fully grouted specimens generally have higher ultimate capacity than the partially grouted specimens. This is largely due to the fact that the effective thickness of fully grouted specimens was about 30% higher than that of partially grouted specimens. Comparing fully grouted specimens (1, 2, 3) and partially grouted specimens (4, 5, 6), the fully grouted infills, on average, showed around 40% higher ultimate strength than partially grouted ones. Figure 4.22 shows the load vs. lateral deflection behaviour of specimens 1 and 5. They were both subjected to 111 kN axial load and had aspect ratio of 1:1.3. It is noted that the first visible crack occurred earlier in the partially grouted specimens and the partially grouted specimen seemed to exhibit a greater ductility. The ultimate strength of fully grouted specimen was about 56% higher than that of the partially grouted specimen. In the specimens with lateral load only (Soon 2011), for the same aspect ratio, the fully grouted infill had 40% higher ultimate strength than the partially grouted infill. It suggests that the presence of axial load enhances the increase in the ultimate strength due to grouting.
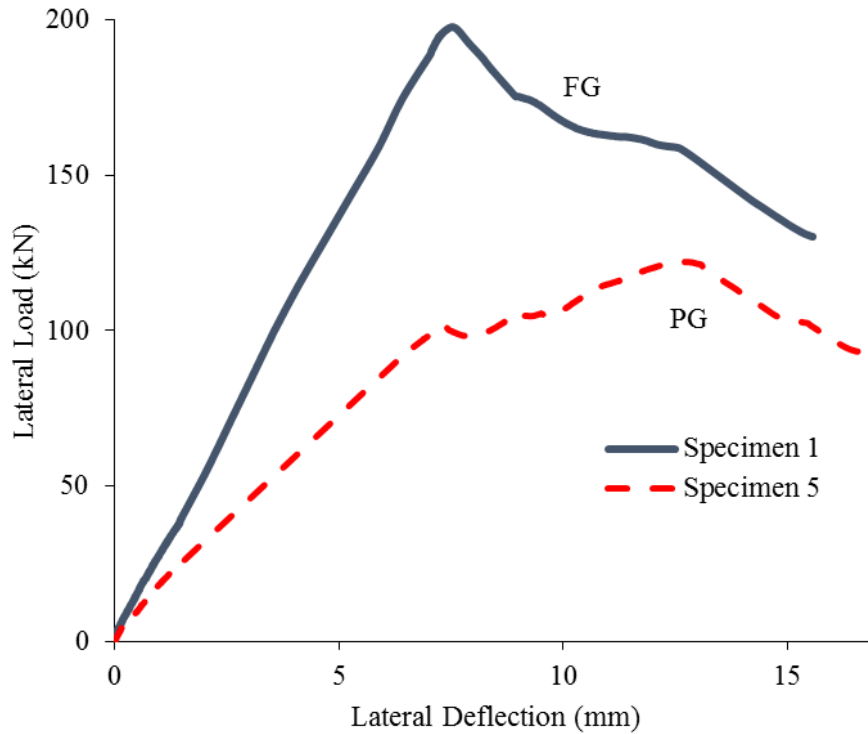
Figure 4.22. Effect of grouting

4.2.6 Failure Modes

Table 4.15 summarizes the failure modes of the infilled specimens. Corner crushing was observed as the dominant failure mode for the fully grouted specimens (Figure 4.23). All three fully grouted specimens (1, 2, and 3) failed in corner crushing mode. Specimens 1 and 2 showed no visible diagonal cracking prior to failure. A hair line crack parallel to the diagonal was observed in specimen 3 after the bottom diagonal corner was crushed as shown in Figure 4.24. The crack originated below one of the axial loading points and connected the middle of the top beam to the middle of the right column.

Table 4.15. Failure modes of specimens

No.	Specimen ID	Crack Load (kN)	Ultimate Capacity (kN)	Failure Mode
1	CF-1-1.3	165	197.7	Corner Crushing
2	CF-2-1.3	150	164.9	Corner Crushing
3	CF-3-1.3	130	151.8	Corner Crushing/Diagonal Cracking
4	CP-1-1	80	149.3	Splitting/Diagonal Cracking
5	CP-1-1.3	65	126.4	Splitting
6	CP-1-1.6	75	130.1	Corner Crushing
7	CPW-1-1.3	80	107.3	Diagonal Cracking/Splitting
8	CPD-1-1.3	75	93.3	Diagonal Cracking

a) Specimen 1, top loaded corner   b) Specimen 2, bottom loaded corner

Figure 4.23. Corner crushing failure of fully grouted specimens

Figure 4.24. Failure of specimen 3

Among the partially grouted specimens, corner crushing was only clearly visible in specimen 6. Diagonal and vertical cracks were more substantial in the partially grouted specimens and they occurred at lower loads. In specimens 4 and 5, failure occurred by development of a crack at a slight angle with the vertical axis that split the infill in two (Figure 4.25a and b). This major crack usually developed in the vicinity of the bottom compression corner and extended towards one of the axial loading point. In addition to the vertical crack, specimen 4 developed cracks parallel to the diagonal around the time of failure (Figure 4.25c). Additional post-failure cracks developed in specimen 5 after removal of the lateral load (Figure 4.25d). Failure mode is recognized as "splitting failure" for specimens 4 and 5. This failure mode is not reported in the literature for specimens subjected to lateral load only.

a) Splitting failure of specimen 4

b) Splitting failure of specimen 5

c) Additional cracks in specimen 4

d) Additional cracks in specimen 5

Figure 4.25. Splitting failure mode

Most of the damage in specimen 6 occurred close to the loaded column and especially at the bottom as shown in Figure 4.26. A 6 mm gap between the infill and the top beam developed in construction and transportation of the frame. Although attempts were made to fill the gap with shims, this unusual mode of failure may be attributed to the large gap for this specimen. Further explanation is provided in 4.2.4.

Figure 4.26. Specimen 6

For specimens with opening (7 and 8), significant diagonal and vertical cracking was evident. As shown in Figure 4.27, diagonal cracks developed throughout the solid portions of the infill. After extensive cracking and damage to specimen 8, slight crushing of the loaded corner was also observed. There was no sign of corner crushing in specimen 7. Crack patterns on specimen 7 appeared to be symmetrical on the sides of the window opening. Vertical cracks similar to those of specimens 4 and 5 were noticed in specimen 7.

a) Specimen 7   b) Specimen 8

Figure 4.27. Failure of specimens with opening

The specimens with opening showed great ability to sustain damage and achieve a high deflection without a catastrophic failure. After ultimate capacity was reached, the drop in the load was fairly gradual. This shows a degree of post-failure flexibility in the specimens with opening.

4.2.7 Diagonal Strain

The LVDTs 4, 5, and 6 were intended to monitor the strain developed in the horizontal, vertical and diagonal direction of the potential strut of the infill. The average strain is taken as the deformation divided by the gauge length of the LVDT. A typical plot of the values recorded by the internal LVDTs is presented in Figure 4.28.
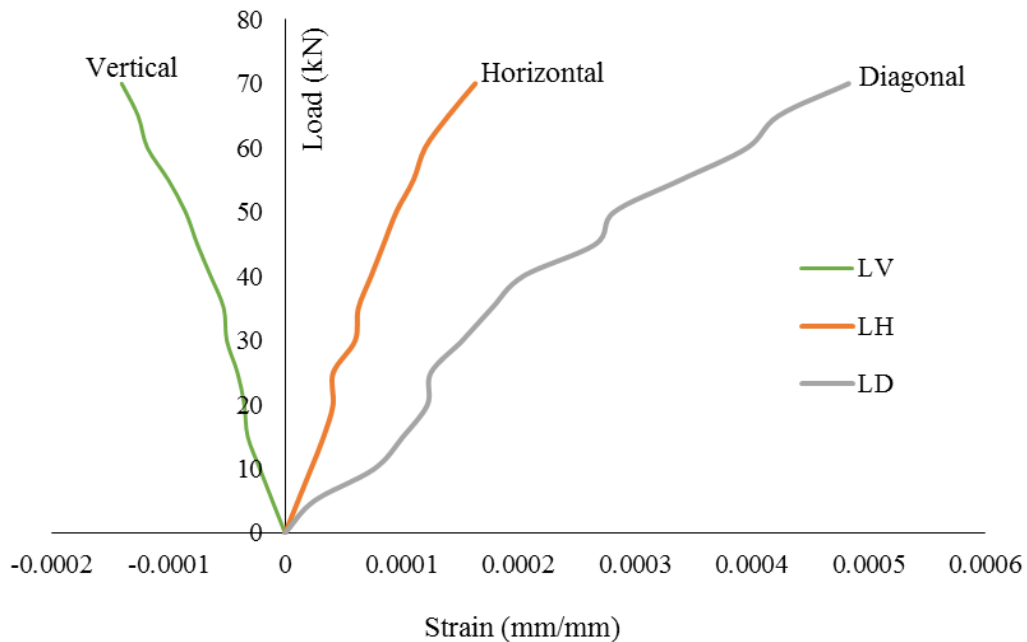
Figure 4.28. Load vs. strain from LVDTs 4, 5 and 6

It should be pointed out that cracks often developed across the length of one or two of the LVDTs (Figure 4.29). After development of such cracks, the values obtained from the LVDT were no longer representative of average strains due to the discontinuity caused by the crack. In this section, maximum principal strain, ε_1, at crack load is calculated to assess the behaviour of the specimen by observing the relationship between principal strain, crack load and failure mode.

Figure 4.29. Cracks developed across the length of LVDTs

The maximum principal strain is calculated using Equation [4.3].

$$\varepsilon_1 = \frac{\varepsilon_x + \varepsilon_y}{2} + \frac{1}{2}\sqrt{(\varepsilon_x - \varepsilon_y)^2 + \gamma_{xy}^2} \qquad [4.3]$$

where ε_x and ε_y are normal strains in x and y directions, respectively, and γ_{xy} is the shear strain. They can be calculated using the readings from three LVDTs. Table 4.16 presents the values of maximum principal strain at crack load for the test specimens.

Table 4.16. Principal strain at crack load

No.	Specimen Designation	Crack Load (kN)	Ultimate Capacity (kN)	Failure Mode	Maximum Principal Strain, ε_1 (mm/mm)
1	CF-1-1.3	165	197.7	CC	0.0004
2	CF-2-1.3	150	164.9	CC	0.0004
3	CF-3-1.3	130	151.8	CC/DC	0.0006
4	CP-1-1	80	149.3	Splitting/DC	0.0005
5	CP-1-1.3	65	126.4	Splitting	-
6	CP-1-1.6	75	130.1	CC	0.0002
7	CPW-1-1.3	80	107.3	DC/Splitting	0.0007
8	CPD-1-1.3	75	93.3	DC	0.0005

The values obtained indicate a degree of diagonal compression in all the specimens. Generally, specimens that showed some diagonal cracking have a higher principal strain than the others. Specimen 6 shows a significantly lower principal strain value which may be an indicator of the non-development of the diagonal strut. As mentioned before, the 6-mm gap between the infill and the top beam could be the reason behind the non-development of the diagonal strut.

No readings were obtained for specimen 5 due to the slippage of the diagonal LVDT during the test. The strain values obtained from the test specimens are consistent with those obtained from the prisms. Higher principal strain seems to be an indicator of the likelihood of development of diagonal and vertical cracks.

4.2.8 Stiffness

Table 4.17 presents the stiffness values of the test specimens. The initial stiffness was taken as the slope of the portion of the curve between 5% and 10% of ultimate capacity in the load vs. deflection curve. Secant stiffness at peak load was taken as the slope of the line connecting the ultimate load to the origin of the load versus deflection curve (i.e. the ultimate load divided by deflection at ultimate). Secant stiffness at crack or "cracked stiffness" was taken as the crack load divided by deflection at crack load.

Table 4.17. Initial stiffness, cracked stiffness, and secant stiffness of tested specimens

No.	Specimen Designation	Ultimate Capacity (kN)	Initial Stiffness (kN/mm)	Cracked Stiffness (kN/mm)	Secant Stiffness (kN/mm)
1	CF-1-1.3	197.7	26.4	25.8	26.1
2	CF-2-1.3	164.9	22.9	13.5	7.5
3	CF-3-1.3	151.8	24.0	12.4	5.2
4	CP-1-1	149.3	22.8	19.0	9.2
5	CP-1-1.3	126.4	19.8	15.5	9.6
6	CP-1-1.6	130.1	46.0	31.3	18.3
7	CPW-1-1.3	107.3	24.2	19.5	14.0
8	CPD-1-1.3	93.3	24.5	17.9	9.8

The values of initial stiffness are very close for most specimens. There is no significant difference in initial stiffness of fully grouted and partially grouted specimens. Past studies have suggested that cracked stiffness is a more reliable measure of experimental stiffness than initial stiffness since the initial portion of the curve can never be clearly defined. For cracked stiffness, the values for specimens 1, 2 and 3 show that the increase in the axial load resulted in an increase in the stiffness. However, the increase is not significant. With the exception of specimens 1 and 6, all cracked stiffness values are in the same order and there is no appreciable difference among specimens. Although the values for partially grouted specimens are about 20% higher than those for fully grouted specimens, this difference might be attributed to the inherent scatter of the data points and thus the observation is inconclusive. In the case of secant stiffness, values show that the secant stiffness is about 30 to 50% of the initial stiffness. Again, all secant stiffness values are similar. This stiffness comparison seems to suggest that the grouting, aspect ratio, and openings of infills do not have marked effect on the stiffness value. The presence of gap (Specimen 6), however, significantly affected the stiffness.

CHAPTER 5   COMPARISON OF EXPERIMENTAL RESULTS WITH THEORETICAL METHODS

5.1 INTRODUCTION

In this chapter, the performance of stiffness and strength equations of infills proposed in previous studies and in design codes is assessed using results obtained in this study as well as those obtained by other researchers.

5.2 STIFFNESS

5.2.1 Stiffness Evaluation Using the Theoretical Methods

Theoretical methods being evaluated in this chapter include the following:

a. The Canadian masonry design standard CSA S304.1 (2004)
b. The American masonry design code, TMS 402-11/ACI 530-11/ASCE 5-11, proposed by Masonry Standards Joint Committee (2011), hereafter referred to as MSJC (2011)
c. The method proposed by Tucker (2007)
d. The three-strut method proposed by El-Dakhakhni et al. (2003).

These four methods are selected due to the different approaches that they provide. The details of Tucker (2007) and El-Dakhakhni et al. (2003) are provided in Chapter 2 and therefore are not repeated herein. The provisions of CSA S304.1-04 and MSJC (2011) are presented in this section by Equations [5.1] to [5.5].

The Canadian masonry design standard, CSA S304.1 (2004), adopts a semi-empirical approach using the diagonal strut concept to calculate the stiffness of the infill. In this approach, the diagonal strut width, w, is defined by Equation [5.1].

$$w = \sqrt{\alpha_h^2 + \alpha_l^2} \qquad [5.1]$$

where α_h and α_l are vertical and horizontal contact lengths between the frame and diagonal strut, respectively, given by Equations [5.2] and [5.3].

$$\alpha_h = \frac{\pi}{2} \sqrt[4]{\frac{4E_f I_c h}{E_m t_e \sin 2\theta}} \qquad [5.2]$$

$$\alpha_l = \pi \sqrt[4]{\frac{4E_f I_b l}{E_m t_e \sin 2\theta}} \qquad [5.3]$$

in which h and l are the height and length of the infill wall respectively; I_c and I_b are the moments of inertia of the column and the beam of the frame, respectively; and t_e is defined as the effective thickness of the infill. Based on a suggestion by Hendry (1981), effective diagonal strut width in CSA is taken as $w/2$. The value of $w/2$ should not exceed one quarter of the diagonal length.

MSJC (2011) proposes Equation [5.4] for the diagonal strut width:

$$w = \frac{0.3}{\lambda \cos\theta} \qquad [5.4]$$

where λ is given by Equation [5.5].

$$\lambda = \sqrt[4]{\frac{E_m t_e \sin 2\theta}{4E_f I_c h}} \qquad [5.5]$$

The factor 0.3 is suggested to account for the damage characterized as "diagonal mortar joint cracking with no damage to infill units" infill may have sustained (Flanagan & Bennett 1999).

It is worth pointing out that both CSA304.1 and MSJC (2011) use the effective thickness, t_e, instead of the total thickness, t, in these equations. The equations in S304.1 were based on the value of λ developed by Stafford-Smith & Carter (1969) as outlined in Equations [2.1] and [2.2] and λ, in that case, was derived based on the total thickness of the infill, t,

since Stafford-Smith & Carter (1969) used concrete infill as opposed to masonry infill where effective thickness and total thickness are identical. In the application of masonry unit infills, the value of λ has been, historically, calculated using the total thickness in the literature (See Stafford-Smith & Carter 1969; Flangan & Bennet 2001; El-Dakhakhni 2002; Shing & Mehrabi 2002; Drysdale & Hamid 2005; Tucker 2010). However, questions may rise for this generalization considering that masonry infills are often not filled in practice. It does not seem to be correct to use the full cross-sectional thickness in this situation. The CSA S304.1 has changed the "t" in its earlier versions to "t_e" in the current version. On the other hand, MSJC (2011) equations are developed based on the work by Flanagan & Bennett (2001) who used the total thickness of infills to calibrate their formula against test results. However, in the current specification, the use of "t_e" replaced the "t". The effect of this change has not been examined since its first introduction in the code in 2011. For methods proposed by Tucker (2007) and El-Dakhakhni et al. (2003), they calibrated their equations using the total thickness of the infills regardless of whether they are hollow or grouted.

For the calculation of the theoretical stiffness using various methods, the following procedure is taken. The equivalent diagonal strut width is first obtained using the corresponding equation. The thickness of the strut is assigned corresponding to the method. A simple frame analysis using the commercial software S-Frame is then performed to determine the stiffness of the infilled system. In this study, the effective thickness is used for CSA S304.1 values, both the effective thickness and the total thickness are used in the calculation of MSJC values, and the total thickness is used for methods by Tucker (2007) and El-Dakhakhni et al. (2003).

Stiffness of a masonry infilled steel frame often decreases as the lateral load increases during a test. This is caused by the increased damage in the infill. In Chapter 4, three types of stiffness were determined: a) initial stiffness, b) cracked stiffness, and c) secant stiffness at ultimate. For the purpose of comparison, initial stiffness is not a reliable measure for two reasons: a) the initial segment of the load vs. deflection curve is never entirely linear, and b) there is no agreement in the literature as to what constitutes 'initial'

portion of the curve. Tucker (2007) suggested the use of "cracked stiffness" as a more consistent approach to compare methods and experimental results. Therefore, in this study the cracked stiffness is used for comparison purposes.

It is recognized that the number of specimens and parameters considered in this experimental study was limited. In order to have a fair assessment of these theoretical methods, it is then necessary to compare them with other experimental results available in the literature. In addition to results of the this study, results of extensive experimental programs presented by Dawe & Seah (1989) on CMU infills, Flanagan (1994) on SCT infills, Fiorato (1970), Angel (1994), Crisafulli (1997), and Al-Chaar (1998) on RC frames infilled with CMU and brick are also included in this chapter for comparison purposes.

5.2.1.1 Experimental results of scaled tests

Table 5.1 contains a summary of predicted stiffness values using various methods. For partially grouted infills, the CSA S304.1 regards them as hollow thus ignoring the contribution of grouting to the effective thickness. MSJC (2011) contains no provisions on how to consider partial grouting in the calculation of effective thickness. In the study, the effective thickness for partially grouted infills is evaluated as the effective area (*i.e.* mortar bedded area plus the area of the grouted holes) per unit length, which is 43 mm in this case. Table 5.1 presents both scenarios with and without considering the partial grouting for CSA S304.1 consideration. Tucker (2007) and El-Dakhakhni et al. (2003) used the total thickness of the infill as the basis for their proposed formulas. Therefore, their methods cannot account for the effect of grouting. It is noted that specimens 9 to 12 were subjected to in-plane lateral load only (Soon 2011). Compressive strength, f'_m is taken as 10.1 and 9.4 MPa and the modulus of elasticity is taken as 13050 and 14500 MPa for fully grouted and partially grouted infills, respectively. Specimens with opening are omitted from the comparison as none of the theoretical methods contains provisions on openings.

Table 5.1. Stiffness of the test specimens as predicted by theoretical methods

No.	Designation	Test Result	Stiffness, k (kN/mm)					
		k_{exp}	CSA[1]	CSA[2]	MSJC[3]	MSJC[4]	Tucker (2007)	El-Dakhakhni et al. (2003)
1	CF-1-1.3	25.8	104.4	104.4	38.4	41.4	36.5	60.2
2	CF-2-1.3	13.5	104.4	104.4	38.4	41.4	36.5	60.2
3	CF-3-1.3	12.4	104.4	104.4	38.4	41.4	36.5	60.2
4	CP-1-1	19.0	49.1	77.6	36.1	46.4	34.2	61.6
5	CP-1-1.3	15.5	56.5	91.9	35.3	45.8	38.3	60.2
8	CP-1-1.6	31.3	64.1	106.4	33.1	43.2	43.2	59.6
9	LF-1-1.3	22.3	104.4	104.4	38.4	41.4	36.5	60.2
10	LP-1-1	18.6	49.1	77.6	36.1	46.4	34.2	61.6
11	LP-1-1.3	22.5	56.5	91.9	35.3	45.8	38.3	60.2
12	LP-1-1.6	10.2	64.1	106.4	33.1	43.2	43.2	59.6

1. PG walls were assumed hollow and FG walls solid as suggested by CSA
2. Stiffness calculated using the actual effective thickness, t_e
3. Stiffness calculated using the actual effective thickness, t_e
4. Stiffness calculated using total thickness, t

Figure 5.1 shows the trend of the predicted stiffness values based on the aspect ratio using specimens CP-1-1, CP-1-1.3, and CP-1-1.6. MSJC (2011) and El-Dakhakhni et al. (2003) predict a higher stiffness for greater aspect ratios (shorter infill panels) whereas CSA S304.1 and Tucker (2007) predict a higher stiffness for smaller aspect ratios (longer infill panels) as evident by their proposed equations. In Equation [5.4] by MSJC (2011) and Equation [2.9] by El-Dakhakhni et al. (2003), the area of the diagonal strut is inversely proportional to $cos(\theta)$. This results in longer infilled frames having a lower stiffness. In Tucker's Equation [2.14], the width of the diagonal strut is directly proportional to the diagonal length and inversely proportional to the height of the infill. Therefore, using this method, longer infilled frames will have a higher stiffness. The width of the diagonal strut as predicted by CSA S304.1 (2004), is inversely proportional to $sin(2\theta)$ as shown in Equations [5.1 to 3]. Therefore, as long as $\theta \leq 45°$, which is the case for all the specimens presented in this chapter, this will result in longer infilled frames having a higher stiffness. In addition to that, CSA S304.1 calculates a much larger horizontal contact length, α_l, than a vertical contact length, α_h, and is, therefore, more sensitive to the length of the infill. As shown in Figure 5.1, the experimental stiffness as

affected by the aspect ratio is sporadic which might be attributed to the uncertainties inherent in the experimental testing. But it is suspected that the equations proposed by CSA S304.1 and Tucker (2007) may be more reasonable as it is reasonable to assume that for a given height, a longer infill has higher stiffness than a shorter infill. However, further experimental testing is necessary to investigate the effect of aspect ratio on the stiffness of infilled frames.
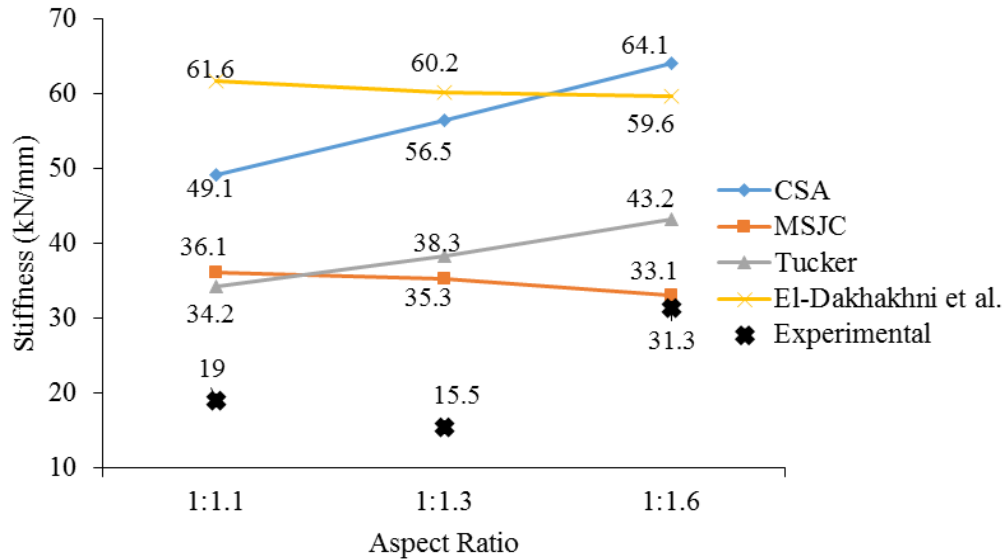
Figure 5.1. Trend of stiffness values by aspect ratio for specimens 4, 5, and 6

Table 5.2 contains the design-to-test stiffness ratios. It is clear that all four methods significantly overestimate the stiffness of the scaled masonry infilled steel frames. Among the four methods, CSA S304.1 and El-Dakhakhni et al. (2003) over-predict the stiffness by over 300% and 200% respectively while Tucker (2007) and MSJC[3] provide better results with the design-to-test stiffness around 2.0. MSJC[4] over-predicts the stiffness by 150%. The low experimental stiffness values of scaled tests contribute to this huge margin of error. This is due to the small size of frame members and CMUs. This significant overestimation is true for specimens subjected to either the lateral loading only or the combined vertical and lateral loading. In the case of MSJC, there is no significant difference using either the effective or the total thickness. In fact, due to the low experimental values, the use of total thickness led to a greater overestimation.

Table 5.2. Ratios of predicted values to test results

Specimen	Design-to-Test Ratio					
	$k_{CSA}{}^{1}/k_{exp}$	$k_{CSA}{}^{2}/k_{exp}$	$k_{MSJC}{}^{3}/k_{exp}$	$k_{MSJC}{}^{4}/k_{exp}$	K_{Tucker}/k_{exp}	K_{El-D}/k_{exp}
CF-1-1.3	4.05	4.05	1.49	1.60	1.41	2.33
CF-2-1.3	7.73	7.73	2.84	3.07	2.70	4.46
CF-3-1.3	8.42	8.42	3.10	3.34	2.94	4.85
CP-1-1	2.58	4.08	1.90	2.44	1.80	3.24
CP-1-1.3	3.65	5.93	2.28	2.95	2.47	3.88
CP-1-1.6	2.05	3.40	1.06	1.38	1.38	1.90
LF-1-1.3	4.68	4.68	1.72	1.86	1.64	2.70
LP-1-1	2.64	4.17	1.94	2.49	1.84	3.31
LP-1-1.3	2.51	4.08	1.57	2.04	1.70	2.68
LP-1-1.6	6.28	10.43	3.25	4.24	4.24	5.84
Avg	4.46	5.70	2.11	2.54	2.21	3.52
COV(%)	51.3	41.6	34.7	34.5	40.3	35.1

1. PG walls were assumed hollow and FG walls solid as suggested by CSA.
2, 3. Stiffness calculated using the actual effective thickness, t_e
4. Stiffness calculated using total thickness, t

5.2.1.2 Experimental results of Dawe & Seah

Dawe & Seah (1989) presented a summary of twenty-eight full-scale tests carried out over the years by several graduate students (McBride 1984, Yong 1984, Amos 1985, Richardson 1986) at the University of New Brunswick. Eleven of these tests are chosen for comparison with the theoretical methods. The other tests are excluded as they contained tie systems, reinforced compression diagonal, bond beams, large gaps between infill and beam, opening or hinged frames. Table 5.3 presents a summary of test results where specimens WB2, WB3, WC7, and WD7 are standard specimens and others have differing parameters as indicated in the table. The test setup and descriptions of the test specimens are presented in Chapter 2. All the specimens are constructed using standard hollow 200 mm CMUs. All frames were constructed using W250x58 and W200x46 steel sections for columns and beams, respectively. The columns were oriented in weak axis bending while the beam was oriented in strong axis bending for each test. Modulus of elasticity is taken as $700 \times f'_m$ as per Dawe & Seah's recommendation. Nominal thickness of the infills was 190 mm and the effective thickness was 64 mm as mortar was laid on face shells only and no grouting was present.

Table 5.3. Summary of test results from Dawe & Seah

Test	f'_m MPa	Crack Load (kN)	Deflection at Crack (mm)	Ultimate Load (kN)	Deflection at Ultimate (mm)	Cracked Stiffness (kN/mm)
WA1[a]	27.4	342	6.2	471	11.2	55.2
WA2[a]	27.7	356	6.8	440	13.9	52.4
WA3[a]	26.5	200	2.9	463	10.9	69.0
WA4[a]	24.4	211	3.3	476	13.2	63.9
WB1[a]	23.7	245	4.0	449	8.1	61.3
WB2	33.3	307	5.4	556	20.0	56.9
WB3	31.4	413	8.0	538	18.3	51.6
WC1[b]	31.7	270	6.6	420	20.9	40.9
WC2[b,c]	27.7	155	4.8	310	15.3	32.3
WC7	33.4	310	5.2	534	16	59.6
WD7	25.4	356	7.6	494	25.0	46.8

a) Mortar packed between column and infill
b) Polyethylene membrane between infill and frame
c) Sandy, poor quality mortar is used

Table 5.4 presents the predicted stiffness values using the four theoretical methods. Table 5.5 contains the ratios of predicted values to test results. All the theoretical methods are fairly consistent in their predictions by a COV of around 25%. MSCJ[2], Tucker (2007), and El-Dakhakhni et al. (2003) provide good predictions in the case of these large-scale CMU infilled frames. MSJC[1] performs poorly in predicting a reasonable estimate in this case as it underestimates the stiffness by about 50%. Therefore, using the total thickness for the diagonal strut of MSJC is the better option in this case. Similar to the scaled test, CSA also over-predicts the stiffness of infills of standard CMU, but only to a different degree (by 170% on average).

Table 5.4. Stiffness values of Dawe & Seah as predicted by theoretical methods

Test	Test Results	CSA (kN/mm)	MSJC[1] (kN/mm)	MSJC[2] (kN/mm)	Tucker (kN/mm)	El-Dakhakhni et al. (kN/mm)
WA1	55.2	136.6	31.8	63.2	52.2	69.2
WA2	52.4	137.5	32.0	63.6	52.6	69.0
WA3	69.0	134.1	31.2	61.9	51.2	69.7
WA4	63.9	128.0	29.6	58.7	48.7	70.9
WB1	61.3	125.9	29.1	57.7	47.9	71.4
WB2	56.9	152.1	36.0	71.4	58.7	66.7
WB3	51.6	147.3	34.7	68.8	56.7	67.7
WC1	40.9	148.1	34.9	69.2	57.0	68.8
WC2	32.3	137.5	32.0	63.6	52.6	69.0
WC7	59.6	152.3	36.0	71.5	58.8	66.7
WD7	46.8	130.9	30.4	60.2	49.9	70.1

1. Stiffness calculated using effective thickness, t_e
2. Stiffness calculated using total thickness, t

Table 5.5. Ratios of predicted values to experimental values

Specimen	Design-to-Test Ratio				
	k_{CSA}/k_{exp}	k_{MSJC}^{1}/k_{exp}	k_{MSJC}^{2}/k_{exp}	k_{Tucker}/k_{exp}	K_{El-D}/k_{exp}
WA1	2.48	0.58	1.14	0.95	1.25
WA2	2.62	0.61	1.21	1.00	1.32
WA3	1.94	0.45	0.90	0.74	1.01
WA4	2.00	0.46	0.92	0.76	1.11
WB1	2.05	0.47	0.94	0.78	1.16
WB2	2.67	0.63	1.25	1.03	1.17
WB3	2.85	0.67	1.33	1.10	1.31
WC1	3.62	0.85	1.69	1.39	1.68
WC2	4.26	0.99	1.97	1.63	2.14
WC7	2.56	0.60	1.20	0.99	1.12
WD7	2.80	0.65	1.29	1.07	1.50
Avg	2.71	0.63	1.26	1.04	1.34
COV(%)	25.7	25.9	25.9	25.8	24.1

1. Stiffness calculated using effective thickness, t_e
2. Stiffness calculated using total thickness, t

5.2.1.3 Experimental results of Flanagan (1994)

Flanagan (1994) performed large-scale tests on steel frames infilled with SCT. Five tests that used single-wythe infills are chosen and summary of results is presented in Table 5.6. Stiffness values were taken as the ratio of crack load to deflection at crack based on the values reported in Flanagan (1994). The clay tiles were laid using their cores horizontal (side-construction) with face-shell mortar only as described in Chapter 2. With the exception of specimen F9, all columns were oriented in weak axis bending. All beams were W310x52, oriented in strong axis bending. The height of all frames was 2235 mm. Modulus of elasticity and thickness of the infill were reported as 3350 MPa and 195 mm, respectively. The effective thickness was 51 mm. Table 5.7 presents the stiffness values as predicted by the four theoretical methods.

Table 5.6. Results of Flanagan (1994)

Test	Column	Aspect ratio, h/l	Crack Load (kN)	Deflection at Crack (mm)	Ultimate load (kN)	Deflection at Ultimate (mm)	Cracked Stiffness (kN/mm)
F1	W250x18	1:1	42	3.6	166	19.6	11.7
F2	W250x45	1:1	41	2.3	183	26.4	17.8
F9	W250x45*	1:1	86	3.0	221	11.2	28.7
F17	W250x45	1:1.5	98	5.3	214	31.0	18.5
F21a	W250x45	1:1.3	38	3.0	180	37.6	12.7

*Strong axis orientation

Table 5.7. Predicted stiffness values for Flanagan (1994)

Test	Test Results	CSA (kN/mm)	MSJC[1] (kN/mm)	MSJC[2] (kN/mm)	Tucker (kN/mm)	El-Dakhakhni et al. (kN/mm)
F1	11.7	19.6	3.9	9.7	6.0	14.9
F2	17.8	23.3	8.8	18.7	13.1	23.0
F9	28.7	44.4	34.4	51.3	43.3	48.5
F17	18.5	31.2	8.8	17.9	17.3	21.2
F21a	12.7	28.6	8.7	18.4	15.8	22.1

1. Stiffness calculated using effective thickness, t_e
2. Stiffness calculated using total thickness, t

Table 5.8 contains the ratios of predicted stiffness values to the test results. El-Dakhakhni et al. over-predicts the stiffness by 40% and has the lowest COV. MSJC[1] provides the worst predictions with an under-prediction of 40% and a COV of over 50%. Similar to the full-scale CMU infilled frames, MSJC[2] provides better estimates than MSJC[1] for these SCT infilled frames as it over-predicts the stiffness by 20% on average. CSA is also fairly consistent in its over-prediction of the stiffness by about 70% on average. Tucker (2007) provides the average ratio closest to unity but at a slightly higher COV of 40%.

Table 5.8. Ratios of predicted stiffness values to experimental values

Test	Design-to-Test Ratio				
	k_{CSA}/k_{exp}	$K_{MSJC}{}^{1}/k_{exp}$	$K_{MSJC}{}^{2}/k_{exp}$	K_{Tucker}/k_{exp}	K_{El-D}/k_{exp}
F1	1.68	0.33	0.83	0.51	1.27
F2	1.31	0.49	1.05	0.74	1.29
F9	1.55	1.20	1.79	1.51	1.69
F17	1.69	0.48	0.97	0.94	1.15
F21a	2.25	0.69	1.45	1.24	1.74
Avg	1.69	0.64	1.22	0.99	1.43
COV(%)	20.5	53.0	32.3	40.2	18.8

1. Stiffness calculated using effective thickness, t_e
2. Stiffness calculated using total thickness, t

5.2.1.4 Experimental results of masonry infilled RC frames

Fiorato (1970), Angel (1994), Crisafulli (1997), and Al-Chaar (1998) carried out experimental programs on masonry infilled RC frames as described in Chapter 2. Table 5.9 contains a summary of the properties of these tests. Tables 5.10 and 5.11 present the predicted stiffness values and their ratios to the test results. Fiorato (1970) only reported strength values. The three-strut method proposed by El-Dakhakhni et al. (2003) only applies to steel frames and is therefore excluded from Table 5.10.

Table 5.9. Properties of the masonry infilled RC frames

Author	ID	Type	Properties								
			h (mm)	l (mm)	t (mm)	t_e (mm)	I_c (mm^4)	I_b (mm^4)	f'$_m$ MPa	E_m MPa	E_f MPa
Fiorato (1970)	S2B	Brick	380	760	22	22	$2.8{\times}10^6$	$2.2{\times}10^7$	26.5	15850	20680
	S2H	Brick	380	760	22	22	$2.8{\times}10^6$	$2.2{\times}10^7$	26.5	15850	19300
	S2I	Brick	380	760	22	22	$2.8{\times}10^6$	$2.2{\times}10^7$	26.5	15850	19300
Angel (1994)	2a	Brick	1630	2450	45	45	$7.2{\times}10^8$	$9.6{\times}10^8$	10.9	8050	35100
	3a	Brick	1630	2450	45	45	$7.2{\times}10^8$	$9.6{\times}10^8$	10.1	5210	35100
	4a	CMU	1630	2450	90	50	$7.2{\times}10^8$	$9.6{\times}10^8$	22.9	12440	35100
	5a	CMU	1630	2450	140	50	$7.2{\times}10^8$	$9.6{\times}10^8$	21.5	11620	35100
	6a	Brick	1630	2450	50	50	$7.2{\times}10^8$	$9.6{\times}10^8$	4.6	2140	35100
	7a	Brick	1630	2450	50	50	$7.2{\times}10^8$	$9.6{\times}10^8$	11.0	2920	35100
	8a	Brick	1630	2450	190	190	$7.2{\times}10^8$	$9.6{\times}10^8$	3.5	2360	35100
Crisafulli (1997)	C1	Brick	2000	2520	75	75	$4.2{\times}10^7$	$1.0{\times}10^8$	19.3	11550	22100
Al-Chaar (1998)	AC2	CMU	1330	1830	90	40	$8.9{\times}10^7$	$8.1{\times}10^7$	22.2	18870	31860
	AC3	Brick	1330	1830	55	40	$8.9{\times}10^7$	$8.1{\times}10^7$	23.4	19890	31860

All the methods over-predict the stiffness with fairly highly COV of 35% to 55%. CSA over-predicts the stiffness by 150% but has the lowest COV. MSJC[1] and MSJC[2] over-predict the stiffness by 70% and 80%, respectively, with MSJC[2] having a slightly lower COV of 47%. Tucker (2007) over-predicts the stiffness by 80% with a COV of 50%. As discussed in Chapter 2, the stiffness of an RC frame may decrease with increase in lateral load due to the development of cracks in the columns. The over-estimation of stiffness by the theoretical methods may be due to the use of uncracked section properties. However, the amount of experimental data for masonry infilled RC frames is limited and more testing is required to establish general conclusions.

Table 5.10. Predicted stiffness values and their ratios to experimental values

Test	Test Result	CSA (kN/mm)	MSJC[1] (kN/mm)	MSJC[2] (kN/mm)	Tucker (kN/mm)
2a	46.9	156.4	120.5	120.5	123.9
3a	47.6	135.0	113.5	113.5	116.2
4a	68.3	198.8	133.1	153.8	158.8
5a	219.9	192.2	131.2	172.3	177.6
6a	38.2	113.4	105.3	105.3	107.2
7a	89.1	120.1	108.0	108.0	110.2
8a	44.5	170.6	124.9	124.9	128.6
C1	27.3	82.8	20.4	20.4	16.8
AC2	62.0	122.8	47.5	70.4	66.6
AC3	49.2	127.5	48.7	56.5	54.2

1. Stiffness calculated using effective thickness, t_e
2. Stiffness calculated using total thickness, t

Table 5.11. Ratios of predicted stiffness values to experimental values

Test	Design-to-Test Ratio			
	k_{CSA}/k_{exp}	K_{MSJC}^{1}/k_{exp}	K_{MSJC}^{2}/k_{exp}	K_{Tucker}/k_{exp}
2a	3.33	2.57	2.57	2.64
3a	2.84	2.38	2.38	2.44
4a	2.91	1.95	2.25	2.33
5a	0.87	0.60	0.78	0.81
6a	2.97	2.76	2.76	2.81
7a	1.35	1.21	1.21	1.24
8a	3.83	2.81	2.81	2.89
C1	3.03	0.75	0.75	0.62
AC2	1.98	0.77	1.14	1.07
AC3	2.59	0.99	1.15	1.10
Avg	2.57	1.68	1.78	1.79
COV(%)	35.4	53.9	47.4	50.3

5.2.2 Overview of Stiffness Methods

CSA S304.1 (2004) consistently over-predicts the stiffness by 70% to 360% for all results considered. This over-prediction is due to the large diagonal strut width calculated by

CSA. To improve the performance of the design equation, a reasonable approach is to keep the current methodology and to simply reduce the strut width by multiplying the originally determined width by a ratio less than unity. In this study, using w/6 as the width of the diagonal strut is considered. Table 5.12 provides a summary of the modified predicted stiffness values by CSA using the effective thickness of the infill and w/6 as the width of the diagonal strut. It shows that the use of w/6 in combination with the effective thickness provides more reasonable yet conservative estimates of the cracked stiffness of the test specimens presented in this chapter.

Table 5.12. Summary of modified predicted stiffness values by CSA

Spec. ID	Modified k_{CSA}	$\dfrac{k_{CSA}}{k_{exp}}$	Spec. ID	Modified k_{CSA}	$\dfrac{k_{CSA}}{k_{exp}}$	Spec. ID	Modified k_{CSA}	$\dfrac{k_{CSA}}{k_{exp}}$
WA1	56.4	1.02	CF-1-1.3	52.8	2.05	F17	21.2	1.14
WA2	56.7	1.08	CF-2-1.3	52.8	3.91	F21a	20.3	1.60
WA3	55.2	0.80	CF-3-1.3	52.8	4.26		Avg	1.30
WA4	52.4	0.82	CP-1-1	44.3	2.33		COV(%)	18.1
WB1	51.4	0.84	CP-1-1.3	48.1	3.10	2a	142.5	3.04
WB2	63.7	1.12	CP-1-1.6	50.3	1.61	3a	129.4	2.72
WB3	61.4	1.19	LF-1-1.3	52.8	2.37	4a	165.6	2.43
WC1	61.8	1.51	LP-1-1	44.3	2.38	5a	162.2	0.74
WC2	56.7	1.76	LP-1-1.3	48.1	2.14	6a	113.4	2.97
WC7	63.8	1.07	LP-1-1.6	50.3	4.93	7a	119.2	1.34
WD7	53.7	1.15		Avg	2.91	8a	150.6	3.38
	Avg	1.12		COV(%)	37.8	C1	35.3	1.29
	COV(%)	25.9	F1	14.4	1.23	AC2	65.5	1.06
			F2	17.8	1.00	AC3	67.2	1.37
			F9	39.8	1.39		Avg	2.03
							COV(%)	47.7

MSJC (2011) recommends the use of effective thickness of the equivalent diagonal strut for stiffness calculations. Comparison results show that MSJC[1] (effective thickness used in geometry of the diagonal strut) over-predicts the stiffness of the scaled specimens and masonry infilled RC frames similar to all other theoretical methods but consistently under-predicts the stiffness of all full-scale masonry infilled steel specimens by 20% to

40%. MSJC^2 (total thickness used in geometry of the diagonal strut), on the other hand, over-predicts the stiffness of almost all full scale steel specimens by 30% to 40% and the stiffness of the scaled specimens and RC specimens by 140% and 80% respectively. The consistent over-prediction and a lower COV make MSJC^2 preferable to MSJC^1 for calculating the stiffness of masonry infilled frames. As mentioned in Chapter 2, MSJC (2011) suggests that the stiffness of an infilled frame should be multiplied by 0.5 if a top gap of less than 9.5 mm is present. However, this is in contrast with the behaviour of specimen 6 that had a 6 mm top gap. Although the gap was not a controlled parameter, specimen 6 had the highest stiffness of all the specimens in this study.

El-Dakhakhni et al. (2003) over-predicts the stiffness of the scaled specimens of this study by over 200% but provides reasonable predictions for the other steel frame specimens. It predicts the stiffness of full scale CMU infilled frames accurately and over-predicts the stiffness of full-scale SCT infilled frames by 50%. This method has the lowest COV among all the theoretical methods presented in this chapter. The low COV combined with the consistent over-prediction of stiffness makes the three-strut method by El-Dakhakhni et al. (2003) the most reliable predictor of stiffness for masonry infilled steel frames. However, this method is only applicable to steel framed masonry and is more cumbersome than the single-strut methods.

Tucker (2007) provides reasonable predictions for full-scale masonry infilled steel frames with design-to-test ratios close to unity and a COV of about 30%. However, it over-predicts the stiffness of masonry infilled RC frames by 70% and a COV of over 50%. None of the above methods provides good estimates for the stiffness of the scaled specimens of this study.

5.3 STRENGTH

5.3.1 Strength Evaluation Using the Design Standards

Previous studies showed that masonry infilled frames can develop several failure mechanisms depending on the geometry and material characteristics of infill and the frame. For design purposes, CSA and MSJC provide equations to predict the strength of masonry infills according to the failure modes. CSA suggests three modes of failure: a) compressive failure, b) diagonal cracking, and c) sliding shear whereas MSJC (2011) gives equations for three failure modes which include corner crushing, in-plane lateral displacement and sliding shear. However, for infilled frames with typical geometry and material often used in practice, the diagonal strut compression failure or corner crushing has been identified as the predominant failure mode. This is the case for the experimental results used in the following comparisons. Therefore, the equation [5.7] from CSA S304.1 for diagonal strut compression failure and equation [5.8] from MSJC (2011) for corner crushing are used to calculate the design strength. Equation [5.6] from CSA 304.1 for diagonal cracking strength is used for predicting crack load.

Strength values by MSJC (2011) are calculated based on both effective thickness and total thickness. MSJC with effective thickness is referred to as MSJC[1] and with total thickness as MSJC[2] hereafter.

$$V_r = 0.16 \ (2 - \frac{M_f}{V_f d_v}) \sqrt{f'_m} t_e d_v \qquad [5.6]$$

$$P_r = 0.85 \ f'_m \ \chi \ w \ \beta_1 \ c \qquad [5.7]$$

$$V_n = (152.4 \ mm) \ t_e \ f'_m \qquad [5.8]$$

where d_v : effective depth for shear: $0.8 \times l_w$; where l_w is the wall length

                 χ : factor for direction of compressive stress = 0.5

                 w : width of the equivalent diagonal strut

β_1 : 0.8 for f'_m up to 20 MPa; minus 0.1 for every additional 10 MPa

c : distance from the fibre of maximum compressive strain to neutral axis based on a minimum eccentricity, $e = 0.1t$

t_e : effective thickness of the infill

The aforementioned equations are developed for the strength of masonry infills only. When the frame consists of members with fixed connections, a portion of the lateral load will be carried by the frame. In order to compare the design infill strength with experimental results which included the contribution of the frame, adjustment should be made to the design values using the following method.

A unit load is applied to the idealized frame as shown in Figure 5.2. Through a frame analysis using S-Frame, the compressive force in the strut (F_{AC}) can be obtained. Therefore, the portion of the lateral load resisted by the infill is $F_{AC} cos(\theta)$. In order to convert the values obtained from Equations [5.6] to [5.8] to the lateral resistance of the entire frame system, Equation [5.9] can be used.

$$ F_{MIF} = \frac{V_{ult}}{F_{AC} \cos\theta} \qquad [5.9] $$

where F_{MIF} = lateral strength of the masonry infilled frame

V_{ult} = design lateral strength of the infill panel

F_{AC} = Compressive force in the diagonal strut

θ = angle of the diagonal and the horizontal

Tucker (2007) provided formulas for crack load and ultimate strength of masonry infilled frames as described in Chapter 2. Unlike CSA and MSJC, the formulas presented in Tucker (2007) were specifically developed for the entire frame system by examining numerous experimental results in the literature. Therefore, no adjustment is required. El-Dakhakhni et al. (2003) did not provide strength equations.
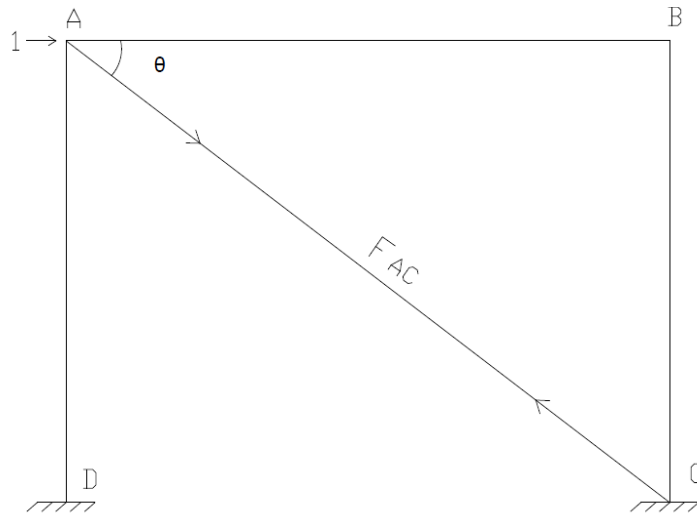
Figure 5.2. Distribution of lateral load within the frame system

5.3.1.1 Results of scaled tests

Table 5.12 presents a summary of ultimate strength predictions by CSA S304.1, MSJC (2011), and Tucker (2007) along with predicted crack load by CSA and Tucker (2007). The compressive resistance of the diagonal strut according to CSA is calculated using Equation [5.7] with a minimum eccentricity of e = 0.1t. The horizontal component of the compressive resistance of the strut is the lateral resistance of the infill panel. The compressive resistance is reduced as appropriate for secondary moment effect where the possibility of out-of-plane buckling is present. The strength of partially grouted infills in Table 5.13 is taken as the weighted average of hollow and fully grouted infills of the same size and properties.

Table 5.13. Strength predictions using the theoretical methods

Test	f'_m MPa	CSA crack (kN)	Tucker crack (kN)	CSA ultimate (kN)	MSJC[1] ultimate (kN)	MSJC[2] ultimate (kN)	Tucker ultimate (kN)
CF-1-1.3	10.1	67.6	26.3	74.2	120.2	131.3	46.1
CF-2-1.3	10.1	67.6	26.3	74.2	120.2	131.3	46.1
CF-3-1.3	10.1	67.6	26.3	74.2	120.2	131.3	46.1
CP-1-1	9.4	27.6	18.9	41.6	90.6	123.9	33.0
CP-1-1.3	9.4	33.3	23.8	49.4	89.3	123.9	41.6
CP-1-1.6	9.4	41.6	31.8	59.3	85.6	119.1	55.7
LF-1-1.3	10.1	67.6	26.3	51.1	120.2	131.3	46.1
LP-1-1	9.4	27.6	18.9	41.6	90.6	123.9	33.0
LP-1-1.3	9.4	33.3	23.8	49.4	89.3	123.9	41.6
LP-1-1.6	9.4	41.6	31.8	59.3	85.6	119.1	55.7

1. Strength calculated using effective thickness, t_e
2. Strength calculated using total thickness, t

Table 5.14 presents the ratios of predicted values to experimental values. It shows that the all methods under-predict the ultimate strength but to different degrees. For example, CSA under-predicts the ultimate strength by over 50% with a COV of 20%. Tucker (2007) under-predicts the ultimate strength of the scaled specimens by over 60% with a COV of 30%. MSJC[1] (calculate using effective thickness of infill panel) provides good predictions as it under-predicts the ultimate strength by about 25% on average with a COV of only 15%. This puts MSJC[1] slightly on the conservative side. MSJC[2] (calculated using total thickness of infill panel) provides the best predictions with ratios close to unity and a COV of 20%.

As for cracking strength, CSA under-predicts the crack load by 45% with a reasonable COV of 23%. Tucker (2007) provides poor estimates by a 70% under-prediction and a COV of 43%.

Table 5.14. Ratios of predicted crack load and ultimate strength to actual values

| Test | Test Result | | Design-to-Test Ratio | | | | | |
	P_{crack}	$P_{ultimate}$	P_{CSA}/P_{crk}	P_{Tucker}/P_{crk}	P_{CSA}/P_{ult}	P_{MSJC}^{1}/P_{ult}	P_{MSJC}^{2}/P_{ult}	P_{Tucker}/P_{ult}
CF-1-1.3	165	198	0.41	0.16	0.37	0.61	0.66	0.23
CF-2-1.3	150	165	0.45	0.18	0.45	0.73	0.80	0.28
CF-3-1.3	130	152	0.52	0.20	0.49	0.79	0.86	0.30
CP-1-1	80	149	0.35	0.24	0.28	0.61	0.83	0.22
CP-1-1.3	65	126	0.51	0.37	0.39	0.71	0.98	0.33
CP-1-1.6	75	130	0.55	0.42	0.46	0.66	0.92	0.43
LF-1-1.3	100	132	0.68	0.26	0.39	0.91	0.99	0.35
LP-1-1	45	111	0.61	0.42	0.37	0.82	1.12	0.30
LP-1-1.3	50	94	0.67	0.48	0.53	0.95	1.32	0.44
LP-1-1.6	55	104	0.76	0.58	0.57	0.82	1.15	0.54
Avg.	-		0.55	0.33	0.43	0.76	0.96	0.34
COV(%)	-		23.4	43.3	19.8	15.6	19.9	29.1

1. Strength calculated using effective thickness, t_e
2. Strength calculated using total thickness, t

5.3.1.2 Results of Dawe & Seah (1989)

Table 5.15 provides a summary of the crack load, ultimate load, and the corresponding predicted values for the full-scale hollow infill specimens by Dawe & Seah (1989). Table 5.16 presents the ratios of predicted to experimental values. Tucker (2007) provides accurate predictions for ultimate strength of these full-scale CMU infilled frames with an average ratio of 0.95 and a COV of 18%. As mentioned before, Dawe & Seah's reported tests constituted a large portion of the data against which Tucker's formulas were calibrated. Therefore, accurate estimations should be expected. Similarly, CSA provides accurate predictions for the ultimate strength of these specimens with an average ratio of 1.02 and a COV of 18%. MSJC[1] provides good predictions of the ultimate strength with a 30% under-prediction and a COV of 18%. MSJC[2], however, performs poorly in predicting the ultimate strength of these specimens as it over-predicts them on average by over 80%. Calculation of ultimate strength of "WA1" is presented in the Appendix as an example. As for cracking strength, CSA and Tucker (2007) provide accurate predictions with ratios close to unity and COV of 30% for crack load of these full-scale CMU infilled frames.

Table 5.15. Predicted crack load and ultimate strength

Test	f'_m MPa	CSA crack (kN)	Tucker crack (kN)	CSA ultimate (kN)	MSJC[1] ultimate (kN)	MSJC[2] ultimate (kN)	Tucker ultimate (kN)
WA1	27.4	257.7	242.7	451.6	296.9	809.6	424.8
WA2	27.7	259.1	244.6	459.3	300.2	818.5	428.1
WA3	26.5	253.5	237.0	444.4	287.2	783.0	414.8
WA4	24.4	243.2	223.5	417.9	267.4	728.4	391.1
WB1	23.7	242.1	218.9	413.1	262.7	714.9	383.0
WB2	33.3	284.1	278.9	526.7	353.0	974.0	488.1
WB3	31.4	275.9	267.5	504.2	336.6	927.8	468.1
WC1	31.7	277.2	269.3	507.7	339.8	936.6	471.2
WC2	27.7	259.1	244.6	459.3	300.2	818.5	428.1
WC7	33.4	284.5	279.5	527.9	354.1	976.9	489.1
WD7	25.4	248.1	230.0	430.6	278.4	758.2	402.4

1. Strength calculated using effective thickness, t_e
2. Strength calculated using total thickness, t

Table 5.16. Ratios of predicted crack load and strength values to test results

Test	Test Result P_{crack}	Test Result $P_{ultimate}$	Design-to-Test ratios P_{CSA}/P_{crk}	P_{Tucker}/P_{crk}	P_{CSA}/P_{ult}	P_{MSJC}^1/P_{ult}	P_{MSJC}^2/P_{ult}	P_{Tucker}/P_{ult}
WA1	342	471	0.75	0.71	0.96	0.63	1.72	0.90
WA2	356	440	0.73	0.69	1.04	0.68	1.86	0.97
WA3	200	463	1.27	1.19	0.96	0.62	1.69	0.90
WA4	211	476	1.15	1.06	0.88	0.56	1.53	0.82
WB1	245	449	0.99	0.89	0.92	0.59	1.59	0.85
WB2	307	556	0.93	0.91	0.95	0.63	1.75	0.88
WB3	413	538	0.67	0.65	0.94	0.63	1.72	0.87
WC1	270	420	1.03	1.00	1.21	0.81	2.23	1.12
WC2	155	310	1.67	1.58	1.48	0.97	2.64	1.38
WC7	310	534	0.92	0.90	0.99	0.66	1.83	0.92
WD7	356	494	0.70	0.65	0.87	0.56	1.53	0.81
Avg.		-	0.98	0.93	1.02	0.67	1.83	0.95
COV(%)		-	30.4	30.0	17.6	18.1	18.1	17.6

1. Strength calculated using effective thickness, t_e
2. Strength calculated using total thickness, t

5.3.1.3 Results of Flanagan (1994)

Table 5.17 presents a summary of predicted crack load and ultimate strength values. Table 5.18 presents the ratios of the predicted values to the experimental results. CSA consistently under-predicts the ultimate strength of these full-scale SCT infilled frames by about 60%. This is due to the low f'_m (5.6 MPa) and E_m (3350 MPa) of their infill panels. MSJC[1] under-predicts the ultimate strength by over 50% with a COV of 36%. MSJC[2] over-predicts the strength of these SCT infilled frames by only 10% with a COV of 15%. However, it is worth noting that if the contribution of the frame to ultimate strength is ignored, MSJC[2] will provide good predictions at 87% of experimental ultimate strength on average with a COV of 11%. Tucker (2007) provides poor predictions of ultimate strength of these full-scale SCT infilled frames by a 25% over-prediction with a COV of 30%.

As for cracking strength, CSA's and Tucker's predictions of crack load in this case are inadequate as they over-predict the crack load by 50% and 80% respectively with COV of over 35%. In fact, CSA calculates a slightly larger diagonal cracking capacity than compressive strength for these specimens. It seems that the 0.16 factor in Equation [5.6] may be too large for SCT infills.

Table 5.17. Predicted strength values from Flanagan (1994)

Test	h/l	f'_m MPa	CSA crack (kN)	Tucker crack (kN)	CSA ultimate (kN)	MSJC[1] ultimate (kN)	MSJC[2] ultimate (kN)	Tucker ultimate (kN)
F1	1:1	5.6	61.0	45.4	56.6	50.6	168.9	103.7
F2	1:1	5.6	64.3	81.6	59.6	73.8	193.0	186.5
F3	1:1	5.6	71.9	113.6	66.7	108.8	228.4	259.6
F9*	1:1	5.6	87.6	158.7	81.2	161.2	279.6	362.8
F17	1:1.5	5.6	111.9	125.2	102.2	75.0	193.0	286.3
F21a	1:1.3	5.6	92.4	107.1	85.0	73.8	193.0	244.8

*Columns in strong axis orientation
1. Strength calculated using effective thickness, t_e
2. Strength calculated using total thickness, t

Table 5.18. Ratios of predicted values to experimental results of Flanagan (1994)

Test	Test Result		Design-to-Test Ratio					
	P_{crack}	$P_{ultimate}$	P_{CSA}/P_{crk}	P_{Tucker}/P_{crk}	P_{CSA}/P_{ult}	P_{MSJC}^{1}/P_{ult}	P_{MSJC}^{2}/P_{ult}	P_{Tucker}/P_{ult}
F1	42	166	1.45	1.08	0.34	0.30	1.02	0.62
F2	41	183	1.57	1.99	0.33	0.40	1.05	1.02
F3	-	169	-	-	0.39	0.64	1.35	1.54
F9	86	221	1.02	1.85	0.37	0.73	1.27	1.64
F17	98	214	1.14	1.28	0.48	0.35	0.90	1.34
F21a	38	180	2.43	2.82	0.47	0.41	1.07	1.36
Avg.		-	1.52	1.80	0.40	0.47	1.11	1.25
COV(%)		-	36.5	37.9	16.5	36.2	15.0	29.8

5.3.1.4 Results of masonry infilled RC frames

A summary of the properties of these tests was presented in Table 5.9. Table 5.19 presents the predicted strength values.

Table 5.19. Predicted cracking and ultimate strength values

Test	f'_m MPa	CSA crack (kN)	Tucker crack (kN)	CSA ultimate (kN)	MSJC[1] ultimate (kN)	MSJC[2] ultimate (kN)	Tucker ultimate (kN)
4a	22.9	183.4	253.9	282.7	558.4	747.8	444.3
C1	19.3	189.5	63.2	264.0	245.1	245.1	110.6
AC2	22.2	88.8	103.1	155.7	214.8	406.0	180.4
AC3	23.4	59.3	125.6	94.3	212.9	280.2	238.6
S2B	26.5	24.7	33.2	48.3	206.6	206.6	63.1
S2H	26.5	25.7	32.5	50.2	216.7	216.7	61.8
S2I	26.5	25.7	32.5	50.2	216.7	216.7	61.8

Table 5.20 contains the ratios of the predicted values to the experimental values of the masonry infilled RC frames. All the theoretical methods over-predict the ultimate

strength of these infilled frames by at least 100%. MSJC[1] and MSJC[2] perform poorly by 400% and 450% over-prediction and COV of 63% and 43% respectively. Using the diagonal strut idealization explained in 5.3.1, on average, only 50% and 60% of lateral load should be taken by the infill according to MSJC[1] and MSJC[2] respectively. However, the failure of the infill much smaller loads than predicted suggests that the infill is taking a much bigger portion of the load. Both CSA and MSJC fail in estimating the strength of these infilled frames and will lead to unsafe designs. This is further discussed in 5.3.2. Even if the contribution of the frame to the strength of these infilled frames is ignored, MSJC[1], MSJC[2] and CSA will predict the ultimate strength by 150%, 200%, and 90% respectively. However, the experimental data on masonry infilled RC frames in the literature is limited and more testing is required to establish better guidelines for these frame systems.

Crisafulli (1997) (C1) reported abnormally low values for crack load and ultimate strength of the frame system. He observed an unusual mode of failure which he regarded as a consequence of the unique test setup. The structure was tested under quasistatic cyclic forces and the lateral forces, intended to simulate seismic actions, were applied to the units by pulling the top beam. They also applied coupled axial loads to the top of the columns to introduce additional overturning moment to the structure in order to simulate a multi-storey frame. Severe cracking of the upper part of the masonry panel and large elongations in the frame members led to a sliding shear failure at the top of the columns. There is no indication that the diagonal strut played any role in transferring the lateral load to the column bases (no diagonal cracks with extensive horizontal cracking at the top of the infill and the RC column). Equivalent diagonal strut idealization seems inapplicable in this case. C1 is excluded from COV calculations.

Despite the 130% over-prediction of ultimate strength values, Tucker (2007) provides the best predictions by a COV of 20% in the case of masonry infilled RC frames.

In the case of cracking strength, Tucker (2007) and CSA over-predict the crack load by 100% and 160% and reasonable COVs of 15% and 25% respectively.

Table 5.20. Ratios of predicted values to test results

| Test | Test Result | | Design-to-Test Ratios | | | | | |
	P_{crack}	$P_{ultimate}$	P_{CSA}/P_{crk}	P_{Tucker}/P_{crk}	P_{CSA}/P_{ult}	P_{MSJC}^1/P_{ult}	P_{MSJC}^2/P_{ult}	P_{Tucker}/P_{ult}
4a	116	209	1.58	2.19	1.35	2.67	3.58	2.13
C1	30	43	6.32	2.11	6.14	5.70	5.70	2.57
AC2	63	84	1.41	1.64	1.85	2.56	4.83	2.15
AC3	62	90	0.96	2.03	1.05	2.37	3.11	2.65
S2B	-	41	-	-	1.18	5.04	5.04	1.54
S2H	-	22	-	-	2.28	9.85	9.85	2.81
S2I	-	28	-	-	1.79	7.74	7.74	2.21
Avg			2.57	1.99	2.24	5.13	5.69	2.29
COV(%)			24.5	14.5	29.7	62.4	45.7	20.0

5.3.2 Overview of Strength Methods

MSJC (2011) provides overall under-estimation of the ultimate strength for all masonry infilled steel specimens considered. This underestimation ranges from 20 to 50% for the scaled specimens, the full-scale CMU infilled frames and the SCT infilled frames. Although the use of total thickness was shown to be preferable for stiffness calculations based on MSJC, the same cannot be applied to strength calculations as it would lead to a gross over-prediction of the strength in many cases. The strength calculations based on the effective thickness of the infill as defined by MSJC leads to reasonable yet conservative predictions of ultimate strength for masonry infilled steel frames. However, for masonry infilled RC frames, MSJC over-estimates the ultimate strength of these frame systems by over 400%. Ignoring the contribution of the frame to the strength of the infilled frame system will reduce this over-prediction to 150%.

CSA S304.1 under-predicts the ultimate strength of the scaled specimens and the full-scale SCT infilled frames by over 50% but compares well with full-scale CMU infilled frames. Note that the compressive strength of the scaled CMU and SCT infills were low

in comparison with full scale CMU infills, it seems to suggest that CSA does not perform well with the weak infills.

Tucker (2007) is inconsistent in its predictions of ultimate strength of the specimens discussed in this chapter. Tucker (2007) under-predicts the ultimate of the scaled specimens by about 70%. It provides accurate predictions with on average 0.96 design-to-test ratio for ultimate strength of the full-scale CMU infilled frames but over-predicts the ultimate strength of full-scale SCT infilled frames by 25%.

All methods studied provide gross over-estimation of the strength of the masonry infilled RC frames as discussed in 5.3.1.4. RC frames are generally more rigid than steel frames in standard practice. Using the diagonal strut idealization, a larger portion of the lateral load will be assigned to the frame. This may be a reason for the over-prediction of the strength of these specimens. However, even when the frame contribution is ignored, the over-prediction remains significant by all methods. It is noted that past tests that form the basis for the aforementioned methods have mainly focused on masonry infilled steel frames. Further investigation is required for better understanding of the behaviour of masonry infilled RC frames.

For design purpose, it is recommended that the frame be idealized as pin jointed so that the contribution of the frame to the strength of the masonry infilled frame is ignored. In doing so, the design of the infill will remain conservative.

5.4 CASE STUDY

As explained above, CSA S304 significantly overestimates the stiffness of a masonry infilled steel frame for all the specimens presented herein. This is also confirmed by comparative studies carried out by others (Ng'andu et al., 2005; Tucker, 2007). The significant over-prediction of stiffness by CSA S304.1 will demand a higher capacity for the infilled frame due to the fact that a stiffer frame system attracts larger forces in the event of an applied lateral load. More importantly, it may skew the lateral load distribution in the structure and may result in an unsafe design for lateral resisting elements elsewhere in the structure. To have an appreciation of this overestimation of infill stiffness on the overall load distribution of a building, a case study on the design of an idealized 8-story building for earthquake loading is presented here.

This 8-story building is idealized as a lumped mass system with equal mass and stiffness on each floor. As shown in Figure 5.3, each floor consists of two parallel masonry infilled steel frames (MISFs) on the sides to resist the lateral load along in-plane direction and is assumed to have a 200 mm concrete slab. In order to calculate the natural frequency of the building, it is assumed that the lateral forces equal to the floor weights, $w = mg$. According to Chopra (2007), the fundamental natural frequency of such a system can be estimated using Equation [5.10].

$$\omega_n^2 = \frac{g\Sigma m_j u_j}{\Sigma m_j u_j^2} \qquad [5.10]$$

where: m_j = mass of floor j
             u_j = deflection of floor j

Floor deflection values were obtained as shown in Figure 5.4. The storey drift was calculated as the ratio of storey shear over the stiffness. The floor deflection was then calculated as the sum of the lower storey drifts. Substituting floor deflection values from Figure 5.4 into Equation [5.10], natural frequency of the building can be calculated using Equation [5.11].

$$\omega_n = 0.1857\sqrt{\frac{k}{m}} \qquad [5.11]$$

where k is the floor stiffness and m is the floor mass.

Fundamental natural period of the structure can be calculated as $2\pi/\omega_n$. Using the design spectrum for Vancouver (Figure 5.5), the design spectral response acceleration, S, can be obtained.

H = 2800 mm
L_1 = 3600 mm
L_2 = 25 m

MISF   MISF

L_2 = 25 m
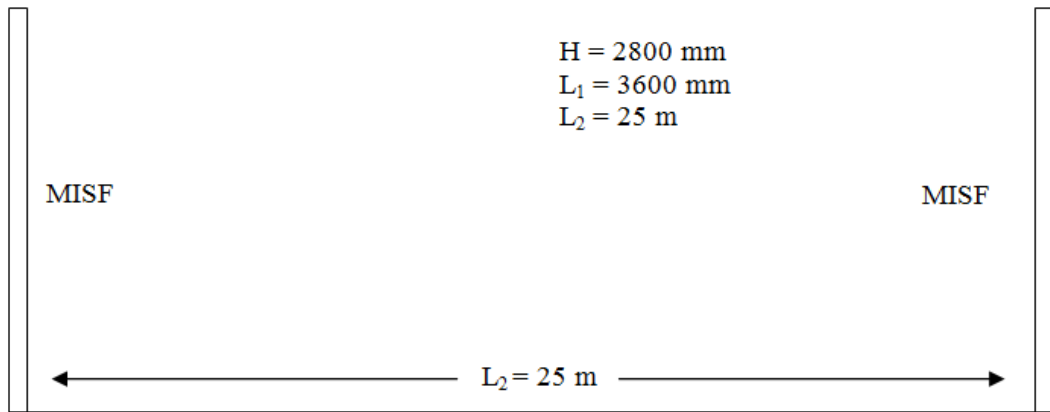
Figure 5.3. Plan view of a typical floor

	Story Shear	Story Drift	Floor Deflection
	w	w/k	36 w/k
	2w	2 w/k	35 w/k
	3w	3 w/k	33 w/k
	4w	4 w/k	30 w/k
	5w	5 w/k	26 w/k
	6w	6 w/k	21 w/k
	7w	7 w/k	15 w/k
	8w	8 w/k	8 w/k

Figure 5.4. Idealized 8-story building and calculation of floor deflection (k is floor stiffness)
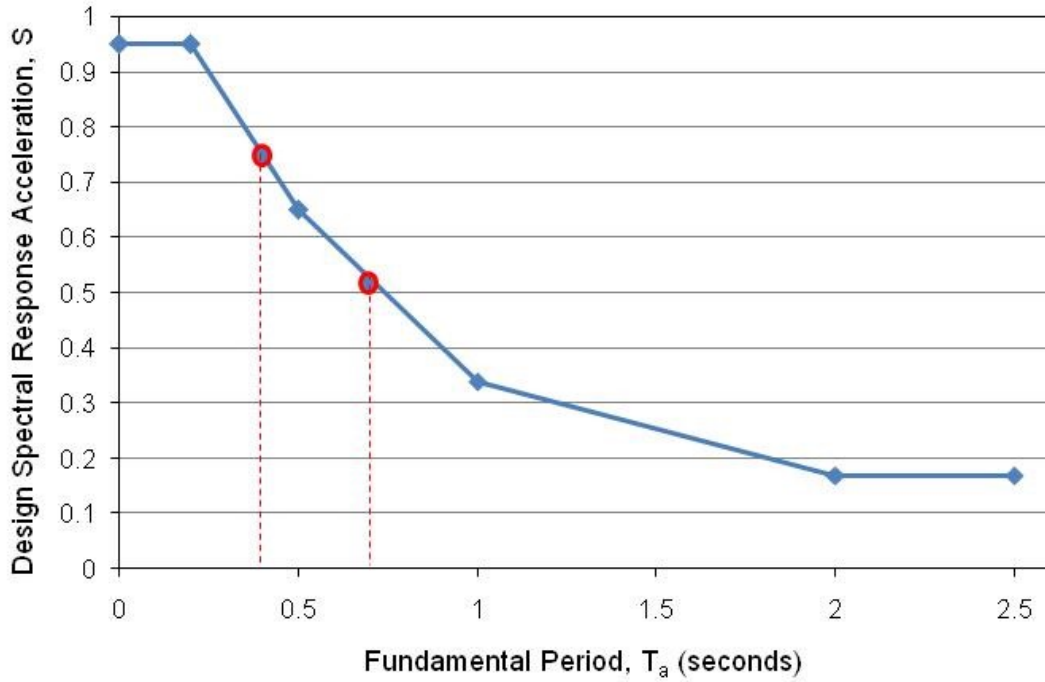
Figure 5.5. Design spectrum for Vancouver (NBCC, 2005)

A standard MISF from Dawe & Seah (WB2) is chosen for this case study. The building is analyzed in accordance to NBCC (2005) for two cases: a) using actual stiffness from experiment, and b) using predicted stiffness from CSA S304. The total lateral seismic force, *V*, is calculated using Equation [5.12] (NBCC, 2005). The total lateral seismic force is then distributed along the height of the building using Equation [5.13].

$$V = \frac{S(T_a) M_v I_E W}{R_d R_o} \qquad [5.12]$$

$$F_x = \frac{(V - F_t) W_x h_x}{\sum_{i=1}^{n} W_i h_i} \qquad [5.13]$$

where: T_a = Fundamental Period

W = Weight of building

I_E = Importance Factor; 1.0

R_d = Ductility related force modification factor; 1.5

R_o = Over-strength related force modification factor; 1.3

M_v = Factor to account for high mode effects; 1.0

S = Design Spectral Response Acceleration

F_x = Lateral force at level x

F_t = 0.07 T_aV but less than 0.25 V

W_x, W_i = Weight of floor x and i respectively

h_x, h_i = height above the base to level x and i respectively

Table 5.21 presents a summary of the calculations. Stiffness of each floor, k, is the sum of the stiffness of the two MISFs. NBCC (2005) recommends T_a to be taken as $0.1 \times N$, where N is the number of stories if T_a cannot be determined more accurately. As shown in Table 5.21, the estimated values for T_a are close to $0.1 \times N = 0.8$ seconds. Table 5.22 shows the distribution of the total lateral load to the height of the building.

Table 5.21. Summary of calculations

Type	Stiffness, k N/m	Mass, m kg	Natural Frequency, ω_n s^{-1}	Fund. Period, T_a s	Design Accel. $S(T_a)$ m.s^{-2}	Total Lateral, V kN	F_x @ top floor kN
Exp.	1.14x10^8	47x10^3	9.1	0.7	0.52	983.6	207.9
CSA	2.90x10^8	47x10^3	14.6	0.4	0.74	1399.8	302.4

Table 5.22. Distribution of the total lateral seismic force along the height of the building

Floor	F_x at top of floors, kN (*Experimental*)	F_x at top of floors, kN (*CSA S304.1*)
1	26.0	37.8
2	52.0	75.6
3	78.0	113.4
4	103.9	151.2
5	129.9	189.0
6	155.9	226.8
7	181.9	264.6
8	**207.9**	**302.4**

F_x for the top floor is calculated as 208 and 302 kN for experimental and CSA, respectively. By assigning half of the load to each frame, in the case of experimental values, 104 kN is assigned to each frame and in the case of CSA, each take 151 kN. This suggests that CSA S304.1 demands a 50% increase in the design load in this case. With the results presented herein, it is shown that in most cases, the design-to-test strength ratios obtained using CSA S304 are less than one, suggesting that CSA S304 slightly underestimate the ultimate strength. Combined with the increase in the capacity demand from the stiffness point of view, an infill design based on CSA S304 would be conservative. However, assigning a larger load to an infilled frame based on an overestimation of its stiffness may lead to an unsafe design of other load-carrying structural components in the building.

CHAPTER 6   CONCLUSIONS AND RECOMMENDATIONS

The objective of this study was to investigate some aspects of the in-plane behaviour of masonry infilled frames. Eight concrete masonry infilled steel frames were tested under combined lateral and axial loading. Five of those consisted of partially grouted infill panels and three had fully grouted infill panels. All specimens were constructed using one-third scale CMUs. The specimens were tested under a gradually increased in-plane lateral load applied at the frame top beam level in combination with constant axial load applied to the top beam to replicate gravity loads. The parameters of the study were axial load, extent of grouting, opening, and aspect ratio of the infill. The experimental results were used, along with other test results from the literature, to evaluate the efficacy of stiffness and strength predictions by some theoretical methods with a focus on Canadian and American design codes. Cracking pattern, stiffness, failure mode, crack strength, and ultimate strength of the specimens were monitored and reported.

6.1 OUTCOMES OF THE STUDY

6.1.1 Cracking Patterns and Failure Modes

All fully grouted specimens and one partially grouted specimen failed in corner crushing which is the most common failure mode in masonry infilled frames. Splitting failure was observed in two partially grouted specimens. This failure mode was characterized by the development of a major crack that extended from the vicinity of the bottom compression corner to the underside of one of the axial loading points at a slight angle with the vertical axis. Additional diagonal cracks were also observed in the specimens that exhibited splitting failure. This failure mode is unique to masonry infilled frames subjected to combined lateral and axial load. In general, partially grouted specimens often developed extensive vertical or diagonal cracking prior to failure whereas fully grouted specimens showed little visible cracks prior to failure. Specimens with opening developed extensive cracking but did not fail suddenly. They exhibited a gradual drop in lateral resistance after reaching the ultimate load.

6.1.2 Effects of Axial Load

An increase in axial load resulted in increases in both ultimate strength and crack load of the test specimens. A somewhat linear trend between the lateral resistance and the level of applied axial load was observed based on the available data points. It suggests that an increase in axial load, up to a certain point, is beneficial for the lateral performance of the infilled frame. However, further tests at higher axial load levels are needed to establish a conclusive trend. As for the ductility of the infills, the increase in the axial load results in a decrease in the ductility of the specimen. The specimen with the lowest axial load exhibited the highest ultimate deflection while the specimen with the highest axial load had the lowest ultimate deflection. Axial load did not seem to have a significant effect on the cracked stiffness of the infilled frames. Presence of axial load introduced major vertical cracks that led to splitting failure in two specimens as described in 6.1.1.

6.1.3 Effects of Opening

Specimens with opening had the lowest ultimate strength among the test specimens. Enlarging the opening decreased the ultimate capacity of the frame system but the reduction was not in proportion with the reduction in surface area. There was no marked difference between cracked stiffness of specimens with opening and their solid counterpart. Specimens with opening exhibited more ductile behaviour while sustaining load after reaching the ultimate capacity. No sudden drop in load was observed after failure in these specimens.

6.1.4 Effects of Grouting

Fully grouted specimens had significantly higher ultimate strength than partially grouted specimens. First visible crack occurred earlier in the partially grouted specimens and the partially grouted specimens exhibited more ductile behaviour failing at higher ultimate deflection than fully grouted specimens. Extent of grouting had no effect on cracked stiffness of the specimens. The increase in ultimate strength due to grouting was more pronounced in specimens with axial load.

6.1.5 Effects of Aspect Ratio

The difference in ultimate capacity of the three specimens with aspect ratios of 1:1, 1:1.3 and 1:1.6 was not significant. The square specimen had the highest ultimate capacity in the group which is followed by the specimen with 1:1.6 aspect ratio and the specimen with 1:1.3 showed the lowest strength. The square infill had the most intimate contact to the bounding frame while the other two infills had various gaps between the infill and the frame. The lower capacity of the two infills may be attributed to the existence of the gaps. Until more test results on the aspect ratio and effect of gap become available, effect of aspect ratio on stiffness and strength of the test specimens in this study was inconclusive.

6.1.6 Evaluation of Theoretical Methods

The Canadian standard CSA S304.1 significantly over-predicts the stiffness of masonry infilled frames and is deemed overly conservative. It is recommended that the width of the diagonal strut be taken as w/6 instead of w/2 to achieve more reasonable estimates of the stiffness of infilled frames. The American standard MSJC (2011) provides reasonably underestimate of the stiffness. It is recommended that total thickness of the infill instead of its effective thickness be used for stiffness calculations using MSJC (2011). Both CSA S304.1 and MSJC (2011) consistently under-predict the ultimate strength of masonry infilled steel frames. Both design standards seem to over-predict the strength of masonry infilled RC frames. It is recommended that the contribution of the frame to lateral strength of the infilled frame be neglected for strength calculations. Neither of the design codes account for the effect of the axial load, opening in the infill or the gap between the column and the infill. MSJC (2011) recommended a reduction factor of 0.5 for stiffness of masonry infilled frames with top gaps of less than 9.5 mm. This is questionable since the specimen with a 6 mm top gap showed the highest stiffness among all specimens. The Three-Strut method by El-Dakhakhni et al. (2003) provides good predictions for stiffness of masonry infilled steel frames. But it does not apply to infilled RC frames. The method by Tucker (2007) does not provide consistent predictions for infills of various materials.

6.2 LIMITATIONS OF THE STUDY

Due to the complex experimental setup required for this study, the number of specimens were limited to eight and one-third scale CMUs were used. There is currently no scaling law available for masonry infilled frames as it requires a much better understanding of the behaviour of these frame systems. Nonetheless, the use of scaled specimens can provide valuable insight into the effect of parameters. Although past tests on the reduced-scale masonry infilled frames indicate that they can capture the behaviour of full-scale masonry infilled frames, this needs to be investigated further.

6.3 RECOMMENDATIONS

6.3.1 Design and Construction

In design and construction of masonry infilled frames for in-plane loading, the possibility of the following failure modes should be eliminated: a) failure of the frame, and b) sliding shear failure of the infill. Both failure modes occur suddenly and can lead to severe damage in a seismic event. Fortunately, these failure modes are rare and easily preventable. Since the infill is confined within the frame, sliding shear failure is only possible with weak bond between blocks (El-Dakhakhni et al. 2003). Using standard mortar (i.e. type N or S as per CSA S304.1) and increasing the effective area by laying mortar on the head joints as well as the bed joints, and by grouting when possible, will reduce the chance of a sliding shear failure. Failure of a steel frame prior to the failure of infill in a masonry infilled frame is only possible with poor connection design. Proper shear reinforcement in columns can prevent sliding shear failure of RC frames (Crisafulli 1997). In designing for ultimate strength of the infilled frame, it is conservative to consider the frame as pin-jointed so to transfer the entire lateral load to the infill panel in calculations. This is to avoid over-prediction of the strength of the frame system when the frame is rigid, especially with RC frames.

6.3.2 Future Research

Effects of axial load on the behaviour of masonry infilled frames needs to be investigated further. In this study, axial load, up to 20% of axial resistance of the infill, was applied through a spreader beam to the middle of the top beam. Experimental programs with higher levels of axial load and different methods of load application, such as axial load applied to the top of the columns can broaden the understanding of the effect of this parameter on the behaviour of infilled frames.

During testing it became evident that a complete elimination of the incidental initial gap between the frame and the infill is difficult. The detrimental effect of gaps was discussed in this study as well as in past tests (Dawe and Seah 1989). Presence of initial gap reduces the contact length between the frame and the infill, and in some cases, may alter the failure mode. Future research should focus on establishing the effects of initial gap on the behaviour of infilled frames.

REFERENCES

Al-Chaar, G. (1998). *Non-ductile behaviour of reinforced concrete frames with masonry infill panels subjected to in-plane loading*. Construction Engineering Research Lab, Champaign IL. USA.

Amos, K. A. (1985). The shear strength of masonry infilled steel frames. M.Sc. Thesis. Department of Civil Engineering, University of New Brunswick, Fredericton, NB, Canada.

Angel, R. E. (1994). Behaviour of reinforced concrete frames with masonry infill walls. PhD Thesis. University of Illinois, Urbana. USA.

ASTM C1314 (2009). Standard Test Method for Compressive Strength of Masonry Prisms. ASTM International, West Conshohocken, PA. USA.

ASTM C140 (2007). Standard Test Methods for Sampling and Testing Concrete Masonry Units and Related Units. ASTM International, West Conshohocken, PA. USA.

ASTM C270 (2008). Standard Specification for Mortar for Unit Masonry. ASTM International, West Conshohocken, PA. USA.

ASTM E8/E8M (2008). Standard Test Methods for Tension Testing of Metallic Materials. ASTM International, West Conshohocken, PA. USA.

Chiou, Y. J., Tzeng, J. C., & Liou, Y. W. (1999). Experimental and analytical study of masonry infilled frames. *Journal of structural Engineering*. **125**(10). 1109-1117.

Crisafulli, F. J. (1997). Seismic behaviour of reinforced concrete structures with masonry infills. PhD Thesis. University of Canterbury, New Zealand.

CSA A179-04 (2009). Mortar and Grout for Unit Masonry. *Canadian Standards Association,* Mississauga, Canada.

CSA S304.1 (2004). Design of masonry structures. *Canadian Standards Association, Mississauga, Canada*.

Dawe, J. L., & Seah, C. K. (1989). Behaviour of masonry infilled steel frames. *Canadian Journal of Civil Engineering*. **16**(6). 865-876.

Drysdale, R.G. & Hamid, A.A. (2005). *Masonry structures: behaviour and design,* Canada Masonry Design Centre, Mississauga, Ontario, Canada.

El-Dakhakhni, W. W., Elgaaly, M., & Hamid, A. A. (2003). Three-strut model for concrete masonry-infilled steel frames. *Journal of Structural Engineering*. **129**(2). 177-185.

Fiorato, A. E., Sozen, M. A., & Gamble, W. L. (1970). *An investigation of the interaction of reinforced concrete frames with masonry filler walls*. University of Illinois, Urbana. USA.

Flanagan, R. D. (1994). Behaviour of structural clay tile infilled frames. PhD Thesis. The University of Tennessee, Knoxville, USA.

Flanagan, R. D., & Bennett, R. M. (1999). In-plane behaviour of structural clay tile infilled frames. *Journal of Structural Engineering.* **125**(6). 590-599.

Flanagan, R. D., & Bennett, R. M. (2001). In-plane analysis of masonry infill materials. *Practice Periodical on Structural Design and Construction*. **6**(4). 176-182.

Hatzinikolas, M. & Korany, Y. (2005). *Masonry design: for engineers and architects,* Canadian Masonry Publications, Edmonton, Alberta, Canada.

Hendry, A. W. (1981). *Structural Brickwork*. Wiley., New York, USA.

Holmes, M. (1961). Steel frames with brickwork and concrete infilling. *ICE Proceedings*. **19**(4). 473-478.

Liauw, T. C. & Kwan, K. H. (1983). Plastic theory of non-integral infilled frames. *Proceedings of Institution of Civil Engineers*. **75**(2). 379-396.

Mainstone, R. J. (1971). On the stiffnesses and strengths of infilled frames. *Proc. Instn. Civ. Engrs.*, supplement IV, 57–90

Maleki, M., Hamid, A. A., El-Damatty, A. A., & Drysdale, R. G. (2007). Behaviour of partially grouted reinforced concrete masonry panels under in-plane diagonal loading. *Proceedings of the Tenth North American Masonry Conference*, Jun 3-5, 2007. 1039-1050

Masonry Standard Joint Committee (2011). Building Code Requirements for Masonry Structures. ACI 530/ASCE 5/TMS 402. *American Concrete Institute, the American Society of Civil Engineers and The Masonry Society*. USA.

McBride, R. T. (1984). Behaviour of masonry-infilled steel frames subjectedto racking. M.Sc. Thesis, University of New Brunswick, Fredericton, NB, Canada.

Mehrabi, A.B., Shing, P.B., Schuller, M.P. & Noland, J.L. (1996). Experimental evaluation of masonry-infilled RC frames. *Journal of Structural Engineering.* **122**(3). 228-237.

Mosalam, K. M. A. (1996). Experimental and computational strategies for the seismic behaviour evaluation of frames with infill walls. Ph.D. Thesis, School of Civil and Environmental Engineering, Cornell University, USA.

Mosalam, K.M., White, R.N. & Gergely, P. (1997). Static response of infilled frames using quasi-static experimentation. *Journal of Structural Engineering.* **123**(11). 1462-1469.

Ng'andu, B. M., Vermeltfoort, A. T., & Martens, D. R. W. (2005). Experimental investigation into the response of steel frames infilled with calcium silicate element walls to in-plane lateral loads. *Proceedings of 10th Canadian Masonry Symposium*, Alberta, June 8 – 12, 2005. 955-964.

Polyakov, S. V. (1960). On the interaction between masonry filler walls and enclosing frame when loaded in the plane of the wall. *Translations in earthquake engineering.* Earthquake Engineering Research Institute, San Francisco, USA. 36-42.

Richardson, J. (1986). Behaviour of masonry-infilled steel frames. M.Sc. Thesis, University of New Brunswick, Fredericton, NB, Canada.

Saneinejad, A. & Hobbs, B. (1995). Inelastic design of infilled frames. *Journal of Structural Engineering.* **121**(4). 634-650.

Shing, P. B., & Mehrabi, A. B. (2002). Behaviour and analysis of masonry-infilled frames. *Prog. Struct. Engng Mater.* **4**(1). 320-331.

Simms, L. G. (1968). *The behaviour of no-fines concrete panels as the infill in reinforced concrete frames*. Building Research Station. England.

Soon, S. (2011). In-plane behavious and capacity of concrete masonry infills bounded by steel frames. M.A.Sc. Thesis. Civil & Resource Engineering Department, Dalhousie University, Halifax, NS, Canada.

Stafford Smith, B. (1967). Methods for predicting the lateral stiffness and strength of multi-storey infilled frames. *Building Science*, **2**(3), 247-257.

Stafford-Smith, B. (1968). Model test results of vertical and horizontal loading of infilled frames. *ACI Journal Proceedings.* **65**(8). 618-625.

Stafford-Smith, B., & Carter, C. (1969). A method of analysis for infilled frames. *Proceedings of the Institution of Civil Engineers*. **44**(1). 31-48.

Thomas, F. G. (1953). The strength of brickwork. *The Structural Engineer.* **31**(2). 35-46.

Tucker, C. J. (2007). Predicting the in-plane capacity of masonry infilled frames. Ph.D. Thesis, Tennessee Technological University, USA.

Wood, R. H. (1958). The stability of tall buildings. *ICE Proceedings.* **11**(1). 69-102.

Wood, R. H. (1978). Plasticity, composite action and collapse design of unreinforced shear wall panels in frames. *ICE Proceedings*, **65**(2), 381-411.

Yong, T. C. (1984). Shear strength of masonry panels in steel frames. M.Sc. Thesis. University of New Brunswick, Fredericton, NB, Canada.

APPENDIX A   Sample Calculation

Calculation of ultimate strength of "WA1" based on CSA

For the compressive capacity of the diagonal strut, from CSA S304.1 (7.13.3.4), the length of the strut for slenderness effect is

$$L_d - \frac{w}{2} = \sqrt{(2600)^2 + (3400)^2} - \frac{1907.2}{2} = 3344.6\,\text{mm}$$

where w is calculated using Equations [5.1 to 3]

$$\alpha_h = \frac{\pi}{2}\sqrt[4]{\frac{4E_f I_c h}{E_m t_e \sin 2\theta}} = \frac{\pi}{2}\sqrt[4]{\frac{4(2\times10^5).(1.88\times10^7).(2600)}{(19180).(64)\sin(74.5°)}} = 669.8\,\text{mm}$$

$$\alpha_l = \pi\sqrt[4]{\frac{4E_f I_b l}{E_m t_e \sin 2\theta}} = \pi\sqrt[4]{\frac{4(2\times10^5).(4.54\times10^7).(3400)}{(19180).(64)\sin(74.5°)}} = 1785.8\,\text{mm}$$

$$w = \sqrt{\alpha_h^2 + \alpha_l^2} = \sqrt{(669.8)^2 + (1785.8)^2} = 1907.2\,\text{mm}$$

For a minimum eccentricity of 0.1t = 0.1(190) = 19 mm, from Eq. 7.30 (Drysdale & Hamid 2005, p.377), the resistance can be calculate as

$$P_r = 0.85 f'_m \chi.b(2t_f - r) = 586.1\,\text{kN}$$

where $\chi = 0.5$, b = w/2 = 953.5 mm, f'_m = 27.4 Mpa, t_f = 32 mm flange thickness and from Eq. 7.29 (Drysdale & Hamid 2005, p.377)

$$r = \left(\frac{t}{2} + e\right) - \frac{1}{2}\sqrt{t^2 + 4te + 4e^2 - 16et_f} = 11.22\,\text{mm}$$

For slenderness effect from CSA S304.1 (7.7.6.4), the primary moment is magnified so that

$$e' = e.\left(\frac{C_m}{1 - P_r/P_{cr}}\right)$$

where C_m is taken as 1.0 for minimum eccentricity

$$P_{cr} = \frac{\pi^2 (EI)_{eff}}{(kL)^2} = \frac{\pi^2 (2.96\times10^{12})}{(0.9\times3344.6)^2} = 3224\,\text{kN}$$

where $(EI)_{eff} = 0.4 E_m I_0 = 2.96\times10^{12}\,\text{mm}^4$

$$I_0 = \frac{(953.3)(190^3 - 126^3)}{12} = 3.86 \times 10^8 \text{ mm}^4$$

Therefore $e' = 1.219e = 1.219(19) = 23.16$ mm

Replacing e with e' and recalculating, $P_r = 562.9$ kN

Therefore the lateral force that can be resisted by the infill panel is the horizontal component of this capacity: $(562.9).cos\theta = 447.1$ kN

According to the diagonal strut idealization, $F_{AC}.cos\theta = 0.99$ meaning 0.99 of the lateral force is taken by the infill. Therefore, the horizontal capacity of the frame system is:

$$\frac{447.1}{0.99} = 451.6 \text{ kN}$$